University of Nevada, Reno

A Circuit-Level Model of Hippocampal, Entorhinal and Prefrontal Dynamics Underlying Rodent Maze Navigational Learning

A dissertation submitted in partial fulfillment of the requirements for the degree of Doctor of Philosophy in Biomedical Engineering

by

Laurence C. Jayet Bray

Dr. Philip H. Goodman / Dissertation Advisor

Dr. Frederick C. Harris, Jr. / Dissertation Co-advisor

December, 2010

University of Nevada, Reno
Statewide • Worldwide

THE GRADUATE SCHOOL

We recommend that the dissertation
prepared under our supervision by

LAURENCE C. JAYET BRAY

entitled

A Circuit-Level Model of Hippocampal, Entorhinal and Prefrontal Dynamics Underlying Rodent Maze Navigational Learning

be accepted in partial fulfillment
of the requirements for the degree of

DOCTOR OF PHILOSOPHY

Philip H. Goodman, M.D., M.S., Advisor

Frederick C. Harris, Jr., Ph.D., Co-advisor

Nelson G. Publicover, Ph.D., Committee Member

Sergiu M. Dascalu, Ph.D., Committee Member

M. Sami Fadali, Ph.D., Committee Member

Tom Nickles, Ph.D., Graduate School Representative

Marsha H. Read, Ph.D., Associate Dean, Graduate School

December 2010

DEDICATION

I would like to dedicate my research and dissertation to my Ph.D. advisor, Dr. Philip Goodman, who suddenly passed away a few months ago. His guidance and contribution to my work can only be matched by the inspiration he instilled in me to work in the field of Brain Computational Neuroscience. His pioneering work in the field, coupled with his experience in mentoring students for more than 25 years, provided the perfect environment for a unique learning experience and professional growth. I am extremely grateful to him for his generous support throughout my years at the University of Nevada, Reno. Dr. Philip Goodman was a great mentor, friend, and role model, whom I will always remember.

ACKNOWLEDGEMENTS

Throughout my doctoral degree undertaking, I was fortunate to meet and work with brilliant scientists and wonderful people. Their sage advice was and will be my guiding light to my academic and professional journey. I would like to offer my deepest gratitude to my husband, Adam, for his support in difficult times, his endless patience and enlightening advice that shaped a huge part of who I am as a scientist but also as a person. I am very thankful to my co-advisor, Dr. Frederick Harris, who supported and helped me finish my research. He provided me with great guidance to successfully graduate with my Ph.D. I was fortunate to interact with and be assisted by Dr. Mathias Quoy, with whom I collaborated extensively throughout my Ph.D. I would also like to thank the students who collaborated and shared the same working space with me at the brain computational lab: Corey Thibeault, Sridhar Anumandla, Jeff Dorrity, and Mia Koci. I would also like to thank Dr. Nelson Publicover for his thoughtful suggestions as the department chair and a member of my Ph.D. committee in the Electrical and Biomedical Engineering Department, and my other committee members, Dr. Sergiu Dascalu, Dr. Tom Nickles, and Dr. Sami Fadali. I also received valuable help by the EBME administrative assistant III, Pam Jitloff. I would also like to thank Mrs. Cindy Harris for her time proofreading and editing this dissertation. I would also like to recognize Dr. Qi Wan and Dr. Nancy Horowitz for letting me use their equipment at the medical school. Last but not least my academic journey would not have been possible without the irreplaceable and never-ending support and love of my parents, Philippe and Daniele, and the rest of my family.

ABSTRACT

Interactions between the hippocampus, parahippocampal regions and the prefrontal cortex are thought to underlie the formation, consolidation, and retrieval of short term memories and play an important role in the learning processes. To date, only conceptual models have been offered to explain the potential interactions among these regions, but their connectivity and synaptic regulation remain unknown. To better understand sequential learning and decision making during spatial navigation, a large-scale biological model was needed to further guide experimental studies. The results of a putative entorhinal grid cell and hippocampal place cell circuit-level model was reported, incorporating Hebbian learning, ion channels, and asynchronous background activity in the context of recent *in vivo* findings showing specific intracellular-extracellular precession disparities and place field destabilization by entorhinal lesioning. A more complex model was then proposed by adding another hippocampal formation structure, the subiculum, in a complete recurrent loop with the prefrontal cortex. The model replicated some of the dynamics of the mammalian hippocampal-frontal loop microcircuitry, including phase synchrony of prefrontal cells to hippocampal theta oscillations. It also demonstrated short-term augmentation of navigational sequences, decision making, and learning reinforcement. To demonstrate the computational model's functionality, a graphic environment with a navigating virtual mouse was created and could be used for further real-time simulations. Finally, to refute or support the proposed mechanisms of hippocampal-entorhinal dynamics, future experimental studies were proposed to test the types of extrinsic connectivity between the entorhinal cortex and the hippocampus and the intrinsic connectivity within the subiculum.

TABLE OF CONTENTS

LIST OF FIGURES

LIST OF TABLES

CHAPTER 1: INTRODUCTION

Since the nineteenth century the research between localization and connection among brain areas has led to thinking about cortical functions. The identification and specific function of a particular brain region has become a central theme in neuroscience. This complex organ appears to adhere to fundamental principles of functional organization, integration, and specialization. The integration within and among specialized areas is mediated by connections among them, but most extrinsic and intrinsic connectivity and synaptic regulation are still unclear. One way to investigate the biological basis of information processing in the brain is to study the response of neurons to stimulation [33].

In this dissertation I try to comprehend the physiology of mammalian memory, which requires a thorough understanding of circuit-specific interactions of medial temporal neocortex and surrounding regions. A basic behavior shared by all mammals is the task of navigating in a novel environment [46], which requires reliable short-term landmark memory. During evolution, episodic and semantic memory in primates may have co-opted this hippocampal navigational system for generic short-term memory as a way-station to manipulation and long-term consolidation (and reconsolidation) in the neocortex [22, 151], and possibly even to human creativity [6] and imagination [67].

Brain dynamics can be experimentally studied using implanted electrodes to record the rates and timing of action potentials, but this invasive approach is generally difficult or not possible in humans and/or freely moving animals. Many experiments are also done on anesthetized rodents, but the activity at rest can be very different from that in an active state. Good alternatives to studying brain functions, allowing the indirect

study of neuronal activity, have been developed, such as computational neural modeling. However, to date, only conceptual models have been offered to explain the potential interactions among different brain regions.

Therefore, I propose the first two comprehensive, spike-timing, circuit-specific synaptic models: the first one of the hippocampal-entorhinal dynamics and the second one with the addition of a closed-loop with the prefrontal system. Both may explain some of the interactions among these different brain structures. The models suggest essential mechanisms during computer-simulated rodent maze navigation, demonstrating subthreshold brain dynamics consistent with recent *in vivo* recordings. They utilize recent theoretical microcircuitry dynamics and established and achieved performance criteria, based on the reported awake-behaving intracellular recordings and lesioning studies. These circuit-specific mechanistic models are also framed so that predictions can be biologically represented and experimentally tested.

The dissertation is structured as follows: Chapter 2 presents the relevance of this research and background information on the field of neuroscience and computational modeling, including a related literature review. Chapter 3 presents the body of a manuscript published in the *Journal of Frontiers of Neural Circuits* in October 2010, which describes hippocampal place cells and the associated entorhinal grid cell firing during rodent maze computational navigation. Chapter 4 presents another manuscript that is in the process of submission, which adds a hippocampal formation structure, the subiculum, in a complete recurrent loop with the prefrontal cortex to accomplish short-term memory and long-term consolidation of navigational sequences. Along with neural

models, related experimental studies are described in Chapter 5. Conclusions, contributions to the field and a look into future directions are presented in Chapter 6.

CHAPTER 2: BACKGROUND AND SIGNIFICANCE

2.1. Neuroscience

Neuroscience is the scientific study of the entire nervous system. Since the 1960s the number of neuroscientists has increased tremendously, and the scope of neuroscience has broadened to include different approaches used to study the developmental, structural, functional, evolutionary, computational, and medical aspects of the nervous system. In research, the organisms mostly used are rodents. The rat, and even the mouse, has the same basic components and major structures in its little, pecan-sized brain that we humans have in our large cantaloupe-sized brain. In general terms, what we have learned about the anatomy of its brain has been replicated by studies in higher mammals, including humans. What is particularly important is that using laboratory rodents allows us to control many variables. The related techniques have expanded enormously, from the molecular biology of individual neurons to the electrophysiology of groups of nerve cells and tissues. The study of computational neural networks has also led to recent theoretical advances in the field. These combined approaches from many disciplines have helped determine how parts of the brain actually work and how some complex processes occur within a single neuron. However, how networks of neurons produce intellectual behavior, cognition, emotion, and physiological responses is still poorly understood. Eric R. Kandel said: “The task of neural science is to explain behavior in terms of the activities of the brain. How does the brain marshal its millions of individual nerve cells to produce behavior, and how are these cells influenced by the environment … to understand the biological basis of consciousness and the mental processes by which we perceive, act,

learn, and remember?" [93]. Crucial brain areas involved in memory and learning mechanisms are at the heart of how the brain processes information [150]. A major reason for investigating these complex dynamics that underlie behavior, memory, and learning is not only to understand how the brain works, but also to have the basis for understanding and treating neurologic disorders.

2.1.1. Fundamentals

A mammalian brain consists of many complex structures of which the neocortex is of special focus in this study since it plays a key role in sensory perception, spatial navigation, memory, attention and cognition [44, 60]. The neocortex is divided into four different regions called frontal, parietal, occipital and temporal lobes, as shown in Figure 2.1, each of which contains crucial areas, which are defined to perform specific functions (Please see Section 2.1.3 for details).

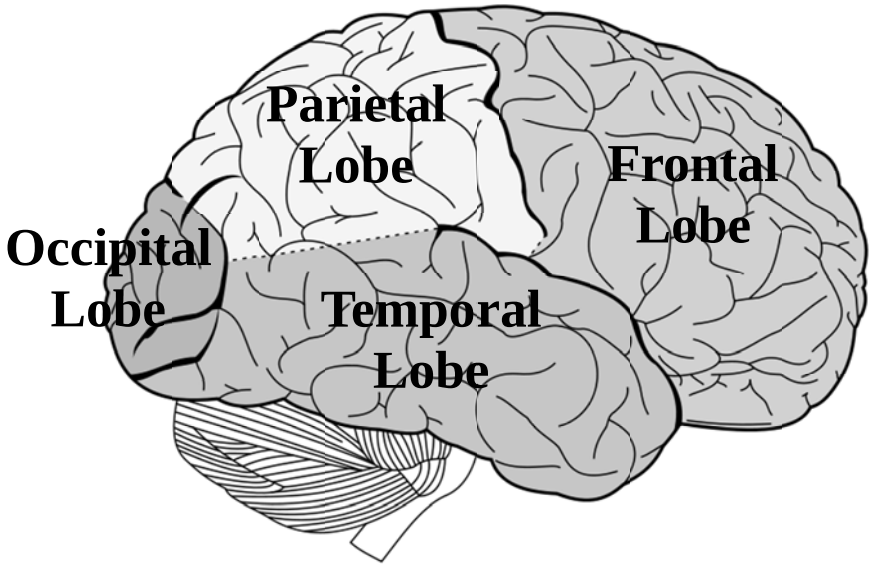

Figure 2.1: Neocortex: Lobes of the Brain (Modified from [133])

Nerve Cells or Neurons

A nerve cell or neuron is the basic component of the brain that processes and transmits long distance information in the form of electrical and chemical signals. There are three types of specialized neurons present in the brain. Afferent neurons receive excitatory sensory stimuli from sensory organs and transmit them to the central nervous system. Efferent neurons receive stimuli from the central nervous system and transmit them to effector cells like motor neurons. Interneurons have connections between neurons of the same region and most of them produce an inhibitory effect on connected neurons, which suppresses signal propagation. More than 100 billion neurons can communicate intercellularly in the brain; and these numerous, but sparse, connections result in highly complex and intelligent neural networks. This communication consists of many extensive branches called dendrites interacting with cell bodies called somas via axons. The dendrites are responsible for receiving stimuli from neighboring excitable cells, and the somas receive input from many of the dendrites. Any signals have to reach threshold and cause firing (or an action potential) for the information to be transmitted. This process is called integrate-and-fire [147], and this exchange of electrochemical information with other neurons is carried out via axon-dendrite terminals with the help of synapses.

Membrane Potential and Action Potential

A resting membrane potential of about -60mV is maintained by the ion gradient and selective permeability (or conductance). The ion concentrations directly measured in a mammalian nerve cell is such that there are many more potassium ions (K^+) inside the cell than out, and many more sodium (Na^+) and chloride (Cl^-) ions outside than in. At

rest, the negative membrane potential results from a net efflux of K^+ across neuronal membranes. K^+ concentration increases extracellularly due to a higher permeability of the membrane to that specific ion. However, when information is transmitted, Na^+ ions flow into the neuron and depolarize the membrane, which changes its permeability to these specific ions. If the depolarization reaches a certain level (threshold), an action potential, also known as a spike, will propagate from its point of initiation at the cell body to the terminus of the axon where synaptic contacts are made.

Synapses

Communication and functional contact between neurons would not be possible without synapses. Although there are many kinds of synapses within the human brain, they can be divided into two general classes: electrical and chemical synapses. Electrical synapses permit direct and passive flow of electrical current from the presynaptic element of one neuron to the postsynaptic part of another neuron via paired channels and an intracellular specialization called a gap junction. In chemical synapses, the change in membrane potential caused by the arrival of the action potential leads to the opening of voltage-gated calcium (Ca^{2+}) channels, which release neurotransmitters from the presynaptic vesicles to postsynaptic receptors. Glutamate is the most important transmitter in normal brain function. Nearly all excitatory neurons in the central nervous system are glutamatergic, and over half of all brain synapses release this agent [147]. The main types of glutamate receptors are NMDA (*N*-methyl-D-aspartate), AMPA (α-amino-3-hydroxy-5-methyl-4-isoxazole-propionate) and kainate receptors. Most inhibitory synapses in the brain use either γ-aminobutyric acid (GABA) or glycine as

neurotransmitters. As many as a third of synapses in the brain use GABA as their inhibitory neurotransmitter, which is most commonly found in local circuit interneurons [147].

Channels

Channels are crucial to the flow of ions, thereby causing the activation or the suppression of action potentials through the membrane. There are several types of channels: Ca^{2+} channels, K^{+} channels, Na^{+} channels, and Cl^{-} channels. Ca^{2+} channels are found in every excitable cell [72]. These voltage-dependent Ca^{2+} channels are involved in regulating a wide range of neuronal activities, and they control Ca^{2+} entry into cells in response to membrane potential changes. Some require a high voltage to open, and they are known as high-voltage activated (HVA) Ca^{2+} channels. This distinguishes them from low-voltage activated (LVA) Ca^{2+} channels, which open at more negative potentials, as shown in Figure 2.2.

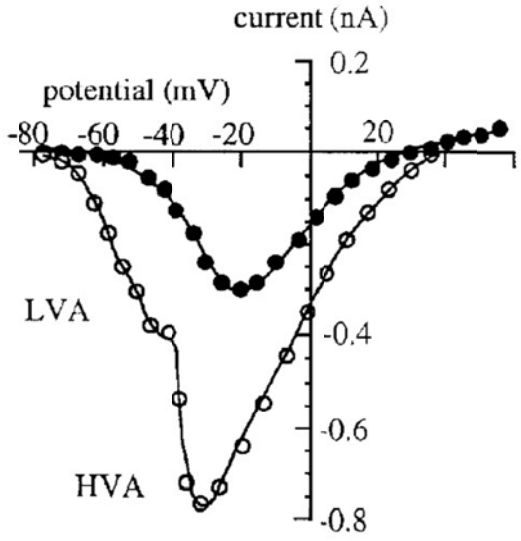

Figure 2.2: Current-Voltage Relationship of HVA and LVA Ca^{2+} Channels [39]

K^+ channels are the largest and most diverse superfamily of ion channels. They are multimeric membrane proteins that share a high selectivity for K^+. In the nervous system, Ca^{2+} activated K^+ channels (K_{Ca}) are the most common, and their activation leads to membrane hyperpolarization and cell shrinkage [165]. K_{Ca} currents were shown to underlie the after-hyperpolarization (AHP), that follows bursts or trains of action potentials in the mammalian hippocampus, known as K_{AHP} channels [2, 78, 155]. Figure 2.3 shows a decrease of neuronal excitability due K_{AHP} channels effect.

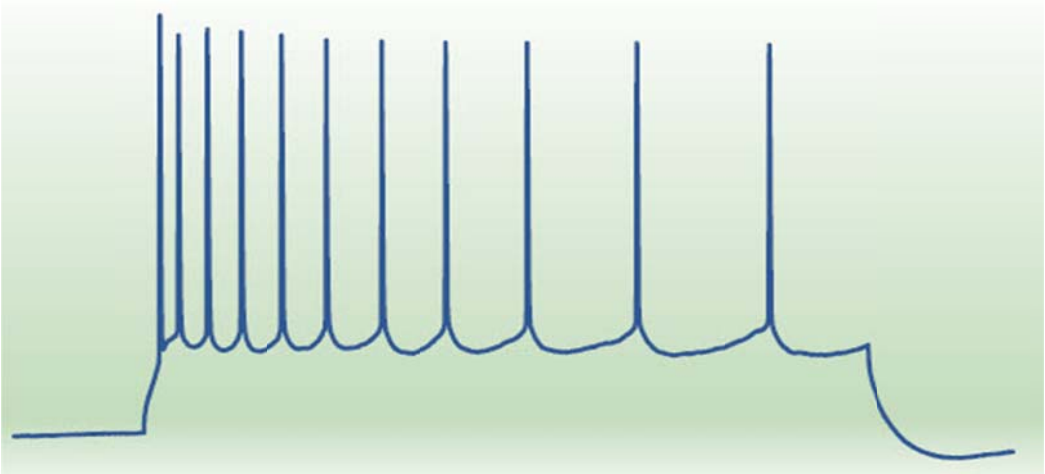

Figure 2.3: K_{AHP} Channels Effect on Hippocampal Neuron Excitability [165]

Na^+ channels, especially non-inactivating or slowly inactivating sodium current, have been found in mammalian neurons located in the neocortex, entorhinal cortex, hippocampus, and also in human neocortical neurons [28].

Finally, Cl^- channels are prominent inhibitory nerve-nerve synapses. They play major roles in intracellular pH and cell volume regulation, and in driving the secretion of fluid from secretory glands and epithelia [72].

All these different types of channels work together, but there is even more specificity in the interaction of HVA channel types with AHPs with the firing behavior of neocortical pyramidal neurons [145]. In our models, voltage-dependent Ca^{2+} channels (HVA and LVA) and Ca^{2+} activated K^{+} channels (K_{AHP}) were used. For further details on neuroscience fundamentals readers are referred to Purves *et al.* (2004) [147].

2.1.2. Memory and Navigational Learning

Memory

Memory is the ability to store, retain, and recall information based on past experiences. In recent decades, memory has become one of the principal pillars of a branch of science called cognitive neuroscience. From an information processing perspective, there are three main stages in the formation of memory: encoding, storage, and retrieval. Encoding allows the information to be received and processed. The storage in short-term memory generally allows retrieval (remembering) for a period of several seconds to a minute without rehearsal, but the memory is not retained indefinitely. By contrast, long-term memory can store much larger quantities of information for a potentially unlimited duration, up to a life span. Long-term memory is divided into declarative (explicit) and procedural (implicit) memories. Here, we concentrate more on declarative memory, especially episodic, which concerns information specific to a particular context, such as time and space. The hippocampus is essential for the consolidation of information from short-term to long-term memory, without necessarily storing information itself. On the other hand, the frontal lobe, especially the prefrontal

cortex is crucial for short-term memory. Figure 2.4 represents an abstract representation of memory.

In order to perform complex tasks such as reasoning, comprehending, and learning, another form of memory has been identified as working memory. The tasks associated are the goal-orientated active manipulation of behaviors in the face of interfering processes and distractions, such as running through a maze to reach a reward. The cognitive processes involved in working memory are the same as the executive and attention control of short-term memory, but they tend to be longer in duration (on the order of seconds). The main area of the brain responsible for this longer duration working memory, especially spatial learning, is the hippocampus-prefrontal pathway [81, 176].

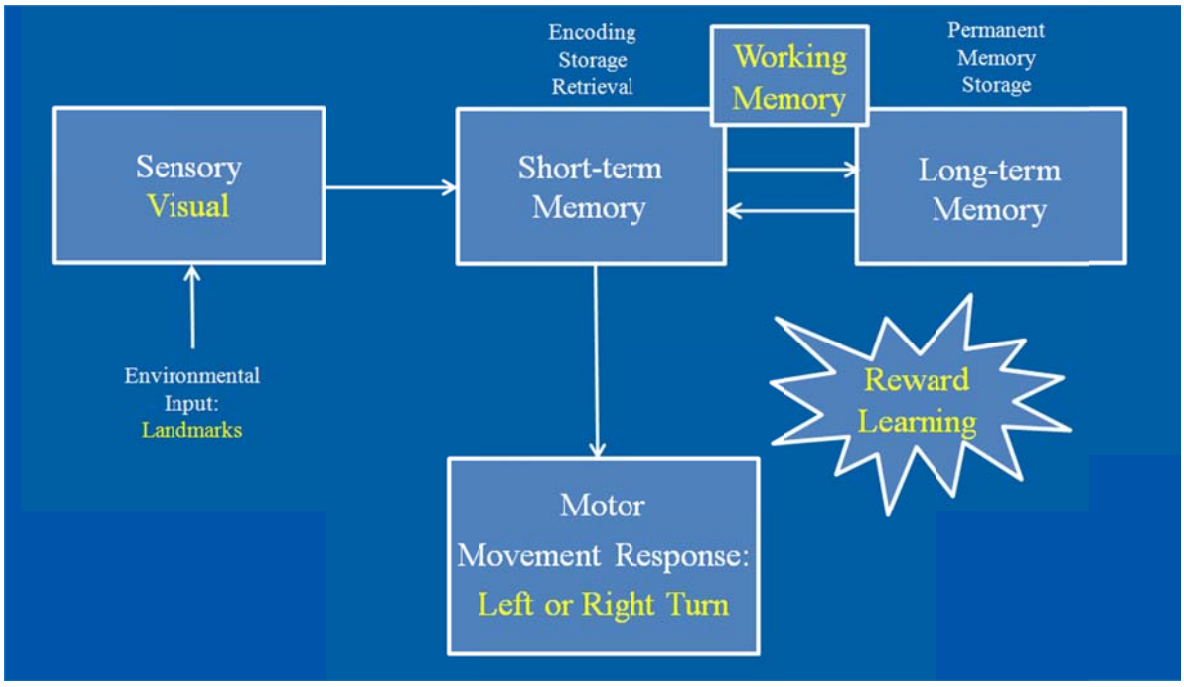

Figure 2.4: Memory Representation

Navigational Learning

Along with memory, spatial learning is navigating in an environment accurately. A person going back home and a mouse running through a maze towards a piece of cheese, both utilize visual landmarks for accurate orientation. Exploring an environment and remembering the events that occur within it are crucial cognitive abilities that have been linked to the hippocampus and parahippocampal regions [18]. In parallel, the prefrontal cortex is thought to be critical for goal-directed action and learning reinforcement [25]. Both the hippocampus and the prefrontal cortex of most organisms, especially rodents, are important for information processing, including memory [45]. This, then, poses the question: how does learning occur?

In 1949 Donald Hebb proposed that ‘‘when an axon of cell A is near enough to excite a cell B and repeatedly or persistently takes part in firing it, some growth processor metabolic change takes place in one or both cells such that A’s efficiency, as one of the cells firing B, is increased’’ [71]. This ‘neurophysiological postulate has since become a central concept in neuroscience through a series of classic experiments demonstrating Hebbian-like synaptic plasticity, including long-term potentiation (LTP) and depression (LTD) in a large variety of systems [10].

Beyond the traditional correlation-based Hebbian plasticity, spike timing dependent plasticity (STDP) opens up new avenues for understanding information coding and circuit plasticity that depend on the precise timing of neural spikes [30]. The most striking feature of STDP is the dependence on the temporal order of pre- and post-spiking. Several studies have defined the critical windows for spike timing, which are on the order of tens of milliseconds [24], as shown in Figure 2.5. In this example, each data

point represents the relative change in the amplitude of evoked postsynaptic current after repetitive application of pre- and post-synaptic spiking pairs (1 Hz for 60 s). Each fixed spike timing Δt is defined as the time interval between pre- and postsynaptic spiking within each pair. Long-term potentiation (LTP, +) and depression (LTD, –) windows are each fitted with an exponential function [10]:

—

where ΔW is the relative synaptic change, A is the spike timing window (in ms), and τ is the decay constant (in ms).

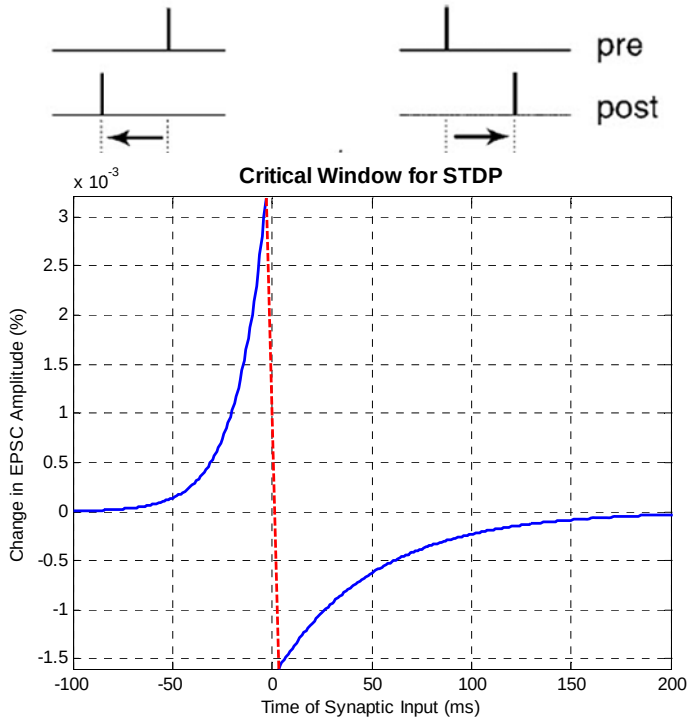

Figure 2.5: Spike-Timing-Dependent Synaptic Plasticity

Depending on when a synapse's pre-synaptic spike occurs, there can be positive learning (the synaptic strength is increased) or negative learning (the synaptic strength is

decreased). A time window is placed around the resulting post-synaptic spike of a cell. If the pre-synaptic spike occurs before the post-synaptic spike, it is in the positive learning portion. If the pre-synaptic spike occurs after the post-synaptic spike, it is in the negative learning window. Pre-synaptic spikes that occur at the same time as post-synaptic spikes or outside either window result in no change to the synaptic strength. This important concept of synaptic plasticity is known to be present in the hippocampus – prefrontal pathway [108, 168] as a candidate for physiological mechanisms in learning and memory [12].

2.1.3. Brain Areas and Functions

Many brain areas are known to play a role in short-term and long-term memory, decision making, and spatial navigation and are pathologically involved in Alzheimer's disease, schizophrenia, drug addiction, and other neurological disorders. In this study, the key is to understand some of the interactive dynamics among these different regions, especially the medial temporal lobe (Please refer to the review Squire *et al.* (2004) [162]). The visual cortex, hippocampal formation, entorhinal cortex, prefrontal cortex, and premotor cortex are key regions to this study, and they are presented below.

Visual Cortex

The primary visual cortex is located in the occipital lobe where both the dorsal and the ventral streams originate, as shown in Figure 2.6.

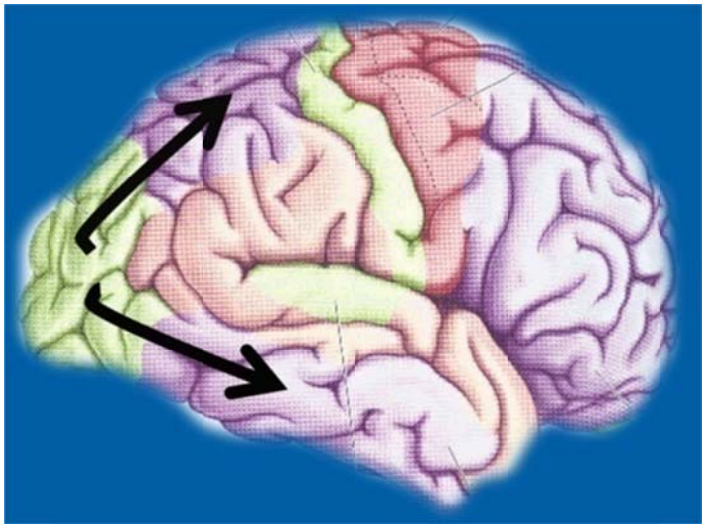

Figure 2.6: Visual Cortex Representation

The dorsal stream sends information to the posterior parietal cortex. It is sometimes called the "Where Pathway" or "How Pathway" and is associated with motion, representation of object locations, and control of the eyes and arms. On the other hand, the ventral stream transmits signals to the inferior temporal cortex. It is sometimes known as the "What Pathway" and is associated with form recognition and object representation, such as visual landmarks. It is known that rodents automatically learn the spatial disposition of objects explored in an environment [146], and it is therefore possible that this automatic spatial learning element contributes to the hippocampal activity changes [1].

Hippocampal Formation

The hippocampus is a neural structure in the medial temporal lobe, as shown in Figure 2.7 in grey.

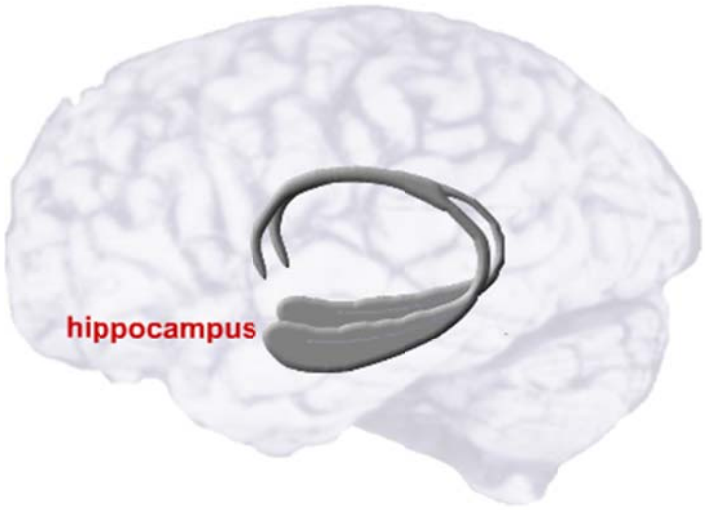

Figure 2.7: Location and Shape of Human Hippocampal Formation [38]

In rodents, the two hippocampi look similar to a pair of bananas. In primate brains, including humans, the portion of the hippocampus near the base of the temporal lobe is much broader than the part at the top, but their respective functions are comparable.

The importance of the hippocampus in spatial memory has long been recognized [141], and hippocampal damage impairs memory for all types of relations [101]. The most commonly studied relationship of navigational behavior and electrophysiology in the hippocampus relates to the phenomena of place cells [138, 140, 141]. The hippocampal formation allows for place recognition, and stores the set of places that can accessed for any given position in the environment. Figure 2.8 shows the evolution of the place fields of seven different cells as a mouse is repeatedly exposed to two different environments, square or round. Hippocampal place fields are known to encode spatial information using rate and temporal codes [139], and they strongly depend on visual input changes in a local environment [98].

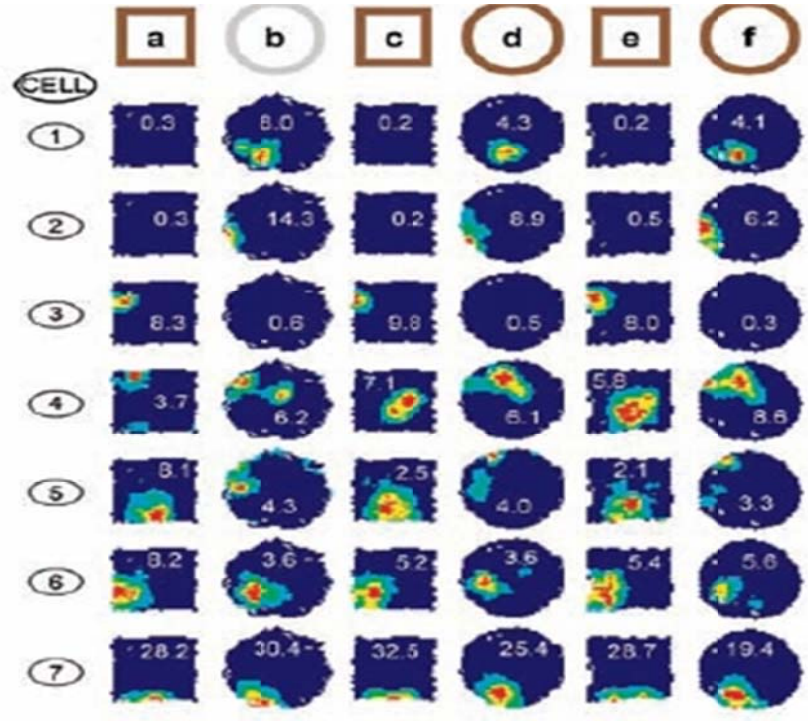

Figure 2.8: Place Cell Representation [179]

Hippocampal systems exhibit several types of oscillatory behavior at different frequencies, including theta (6-12 Hz), beta (12-30 Hz), and gamma (30-100 Hz) oscillations [4, 23, 57], where some play a functional role in memory [137]. In a freely moving rodent, these rhythms are all present and seem to be involved in memory processing [126], but theta rhythms occur more during movement through space and is crucial for temporal coding [21]. There is evidence that theta oscillations are travelling waves that propagate predominantly along the hippocampus and other neocortical regions. Therefore, time in the hippocampus, as clocked by theta oscillations, is anatomically organized in a progression of local time zones [113]. Changes in the frequency of theta activity are correlated with either the animal's speed of movement

through the environment [161] or the rapidity with which a movement is initiated [178]. However, the behavioral correlate of theta amplitude is still unclear.

Phase precession of extracellularly recorded action potential units, with respect to that theta inhibition was originally discovered by O'Keefe and Recce [142] and then later reproduced by other studies [92, 160]. Phase precession is when a neuron fires earlier with respect to the local field potential (LFP) as the animal moves toward the center of the place field. There is some evidence that an oscillation arises as interactions among cell assemblies but is not due to a cell "pacemaker effect" [41]. More realistically, some authors explain that theta phase is used as a gating mechanism for encoding and retrieving information [120] and supports remembering the order of events [119]. Harris *et al.* [65] reported an overall relationship between phase and rate in spikes recorded on a linear track, and a similar relationship was seen in Huxter *et al.* studies [79].

Hippocampal formation is divided into four areas: dentate gyrus, two cornu ammonis (CA1 and CA3), and subiculum.

Dentate gyrus, a tightly packed layer of small granule cells wrapped around the end of the hippocampus proper, is actually a separate structure. Unlike many other areas, it has not evolved by building connections with any other cortical regions [3]. Dentate gyrus granule cells exhibit place sensitivity [91], and interneurons have a higher firing rate in novel environments [135].

The CA areas are all filled with densely packed pyramidal cells similar to those found in the neocortex. These CA regions are structured in clearly defined layers: stratum oriens (SO), stratum pyramidale (SP), stratum radiatum (SR), and stratum lacunosum and stratum molecular, often known as SLM. In the SO layer, the cell bodies of inhibitory

basket cells target the proximal dendrites of pyramidal neurons. (For more detail about each layer, please refer to the review [115]). It has been proposed that the distal dendritic regions of CA1 (SLM layer) may receive rhythmic synaptic excitatory inputs [177] during theta oscillations. Whereas the somatic regions (SO and SP layers) may receive synchronous hyperpolarizing input from interneuron networks [92], which could explain the mechanisms of phase precession [105, 116]. Also, CA1 and CA3 neurons tend to fire selectively on the type of task (encoding and retrieval of memory) [61], and their intrinsic pathways can be modified by LTP during place representation [42]. Similarly, synaptic plasticity can be induced at synapses connecting place cells [80], which supports the evidence of STDP to trigger at recurrent synapses of both CA1 and CA3 networks [99]. Although most studies concentrate on LTP, LTD seems just as important in hippocampal long-term memory [118].

The subiculum is known to be the major output of the hippocampal formation and plays a role in short-term memory and decision making. It acts as a comparator, and its task is to increase negative affective bias in all of the active and conflicting goal processing areas until only one alternative is clearly dominant, as a winner-take-all role [123, 134]. The subiculum is composed of at least two neuron types -strong bursting (SB) and regular spiking (RS)- and one type of interneuron -fast spiking (FS)- where the interconnectivity allows for local inhibition [124]. Their action potential bursting is said to be driven by a Ca^{2+} tail current [90].

These areas are crucial within the hippocampus and interact with each other, but the major pathways of the signal through the hippocampus combine to form a loop with the entorhinal and the prefrontal cortices [143].

Entorhinal Cortex

Parahippocampal regions, including the entorhinal cortex is located in the medial temporal lobe, adjacent to the hippocampus, as shown in Figure 2.9 in pink.

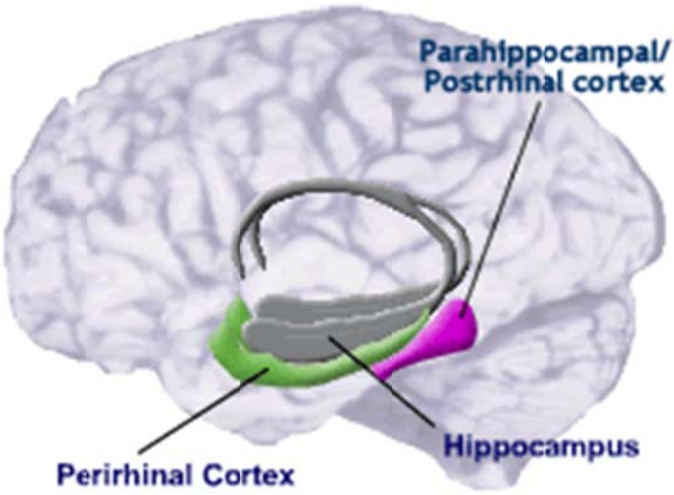

Figure 2.9: Location and Shape of Human Entorhinal Cortex [38]

The important role of the entorhinal cortex in memory and navigation has long been understood, with two main superficial layers, II and III. Recently, entorhinal grid cells were reported as part of a generalized path-integration-based map of the spatial environment in rats [63, 153]. Their firing pattern spans the environment in a remarkably regular triangular or hexagonal pattern [51] and is thought to play a crucial function on the spatially confined activity of hippocampal place fields [34, 52, 63, 131, 170]. As depicted in Figure 2.10, firing fields of simultaneously recorded cells from the layer III of the entorhinal cortex are shown. Each row represents one cell, and each pair of columns represents one trial. The left side of each column shows the trajectory with superimposed spikes (red), and the right side shows the corresponding color-coded rate map (red: peak rate; blue: zero; white: regions not visited).

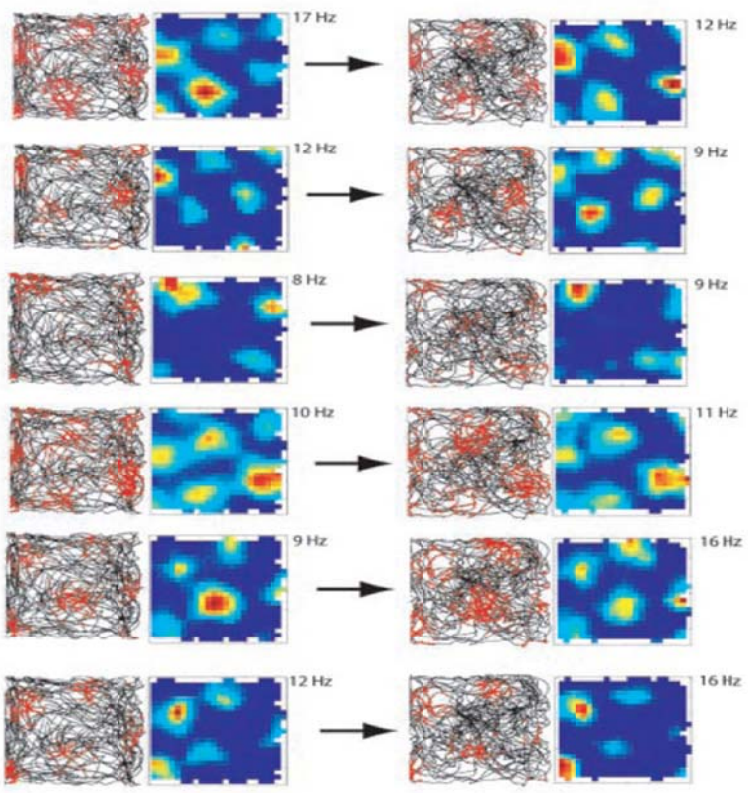

Figure 2.10: Grid Cell Firing Patterns [52]

There is also evidence for grid-cell-like representations in humans and for their implication in a specific type of neural representation in a network of regions which supports spatial cognition and also autobiographical memory [37]. These recent discoveries have described the basic properties of grid cells, but the neuronal mechanisms responsible for the formation and maintenance of the place code and the modulation of entorhinal grid cells on hippocampal place cells remain unclear [171].

Prefrontal Cortex

The prefrontal cortex is the anterior part of the frontal lobe of the brain, as shown in Figure 2.11 in cyan.

Figure 2.11: Frontal Cortex Representation

The well-known role of the prefrontal cortex is its executive functions, such as working toward a defined goal, the prediction of outcomes, and more specifically, spatial working memory [32]. Learning-induced changes in functional activity in prefrontal neurons provide crucial evidence for the notion that memories are stored in the brain by altering patterns of synaptic strengths (short-term augmentation) among coactivated neurons [5]. Also, LTP can be induced in the medial prefrontal cortex through stimulation of hippocampal CA regions, especially CA1 [84, 107, 108]. Furthermore, studies have shown cooperativity between hippocampal-prefrontal short-term and long-term plasticity [40, 94].

Premotor Cortex

The premotor cortex is an area of the motor cortex lying within the frontal lobe of the brain (Figure 2.11 in yellow) between the prefrontal cortex (cyan) and the primary motor cortex (pink), which serves as the posterior border for the prefrontal cortex. Any activity within this region is critical to the sensory guidance of movement and control of proximal and trunk muscles of the body.

Projections to and from these structures and their respective connectivity of neurons are well studied. Even though there are still a lot of unknowns, any new anatomical and physiological information is crucial to the field.

2.1.4. Recent *In Vivo* and Lesioning Studies

In information processing, sequential activity of cortical networks may allow for serial execution of multiple steps [114]. When rapid, one-trial, learning of a novel place is required, the hippocampus is essential for effective performance but the hippocampus is not absolutely required after incremental learning even if the tasks are performed much more slowly [7]. This suggests that the need of interactions from other neocortical regions, such as the entorhinal cortex and/or the prefrontal cortex, is necessary for comparable performance.

Lesions of CA1 and CA3 regions of the hippocampus, especially dorsal portions seem to disturb temporal pattern of spatial sequence processes [75, 109]. Within CA regions, the proximal portions of CA1 pyramidal neurons (the soma) receive a rhythmic 5–10 Hz input from the inhibitory basket cell and axo-axonic cell network. In parallel, the dendrites receive a relatively sparse, but nevertheless potentially effective, input from the bistratified and O-LM (oriens-lacunosum moleculare) interneuron populations that is 180° out of phase with the axo-axonic and basket cell input [97]. Figure 2.12 (a) shows somatic recording (red) obtained as a 10 Hz sine wave was injected in the soma (blue), and a random pattern of EPSC-shaped currents of increasing intensity was simultaneously injected through a dendritic electrode (b).

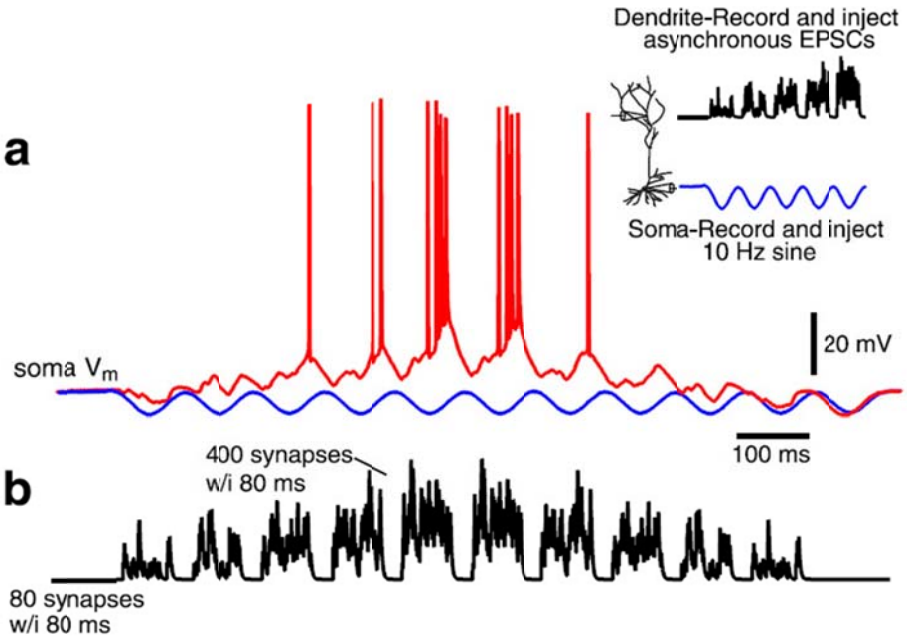

Figure 2.12: Simultaneous Somatic-Dendritic Recordings [54]

Several studies have suggested a direct entorhinal-hippocampal circuitry during spatial recognition tasks [16], representing spatial-memory processes [132], especially long-term consolidation [149]. Figure 2.13 shows direct projections from entorhinal layer II to CA3, and from layer III and perforant path (PP) to CA1, which are responsible for hippocampal spatial firing [15].

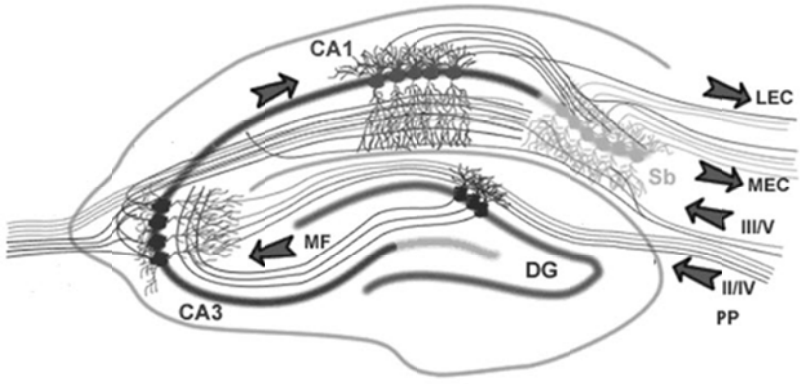

Figure 2.13: Hippocampal-Entorhinal Pathways (Modified from [38])

Insight into this relationship was provided by subsequent lesioning results of Van Cauter *et al.* (2008) [170], demonstrating that entorhinal cell populations are responsible for stabilizing place fields in several ways via layer-specific direct projections to hippocampal CA regions, as shown in Figure 2.14. Figure 2.14 on the left gives the areas of the brain that were lesioned. CONT rats were the control groups, which showed the activity of hippocampal cells stabilized in one area. On the other, ENTO rats were the animals which underwent entorhinal lesioning. In this case, hippocampal cells tended to fire at random areas. The table in Figure 2.14 summarized the number of active cells and the in-field mean firing rate in Hz of both the CONT and ENTO groups. CONT rats had a lower number of active cells, which had higher firing rates; ENTO rats had a higher number of active cells, but lower firing rates.

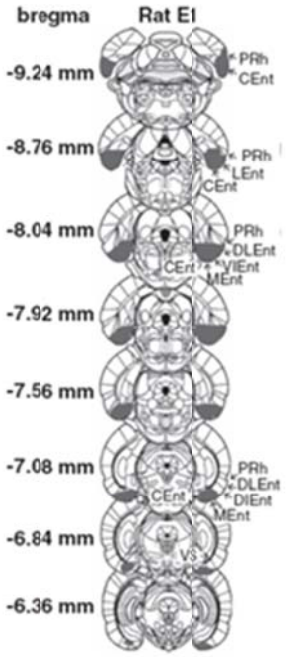

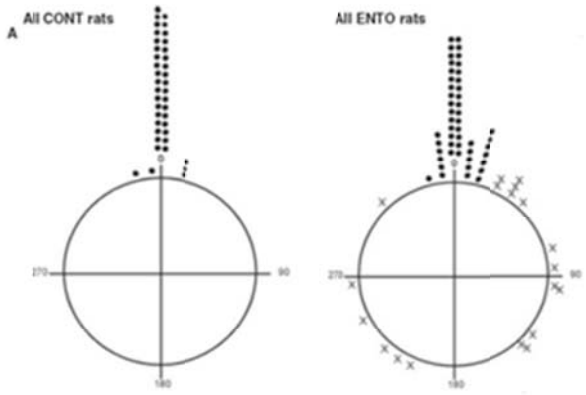

	Number of cells	In-field mean firing rate (Hz)
CONT	40	2.64 ± 0.41*
ENTO	85	1.70 ± 0.15

Figure 2.14: Hippocampal Place Fields Modulated by the Entorhinal Cortex (Modified from [170])

In parallel to these lesion studies, the first recordings done in freely moving animals were achieved by Harvey *et al.* (2009) [66]. This most recent and relevant awake-behaving measurements correlated extracellular with intracellular CA1 neuronal physiology during navigation. This confirmed extracellularly measured theta phase precession but showed that precession does not occur with respect to intracellular theta. Figure 2.15 shows raw (left) and filtered (6–10 Hz, right) membrane potential and LFP traces in the place field from a simultaneous LFP and whole-cell recording. The times of LFP theta peaks (vertical grey lines), intracellular theta peaks (circles), and spikes (crosses) are shown to illustrate the phase precession of spikes and intracellular theta relative to LFP theta oscillations and the absence of phase precession of spikes relative to intracellular theta oscillations. Rather, higher frequency of intracellular theta toward the center of the place fields explains this disparity. These authors also observed asymmetric subthreshold, ramp-like depolarization but could not explain this behavior using their proposed model.

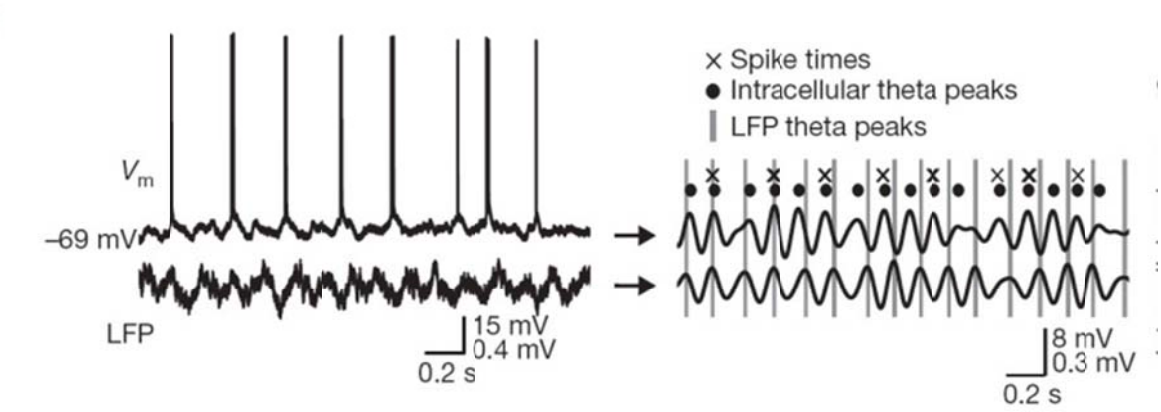

Figure 2.15: Membrane Potential Theta Oscillations in Place Cells [66]

Along with this hippocampal-entorhinal relationship, the medial prefrontal cortex receives profuse projections from the hippocampus [83] to mediate the formation of executive matter. These connections are important for spatial awareness, working memory and motivation [77], and goal-based memory task [110]. During reward expectation, the anticipatory activity in the prefrontal cortex is dependent on similar activity in the hippocampus [19]. Similarly, lesions in the prefrontal cortex show a change in sensitivity in hippocampal place cell firing [106]. There is also evidence of a feedback loop between the two structures, which seems to play a role in synaptic plasticity, and consequently memory [176] and dynamic goal-directed behavior [53]. Therefore, both the hippocampus and the prefrontal cortex are necessary for a biconditional paired-associate task [111]. Also, the main connective flow departs from prefrontal areas and proceeds through premotor cortex toward a primary motor processing area [50].

Finally, the comparison of hippocampal theta amplitude, phase, and frequency (synchronization) to prefrontal theta rhythms has been examined during the performance of a task requiring working memory [159]. Signals are processed and transmitted to other areas, possibly supported by the emergence of highly synchronized activations of cell groups or cell assemblies representing an effective input from afferent structures [49]. Within individual brain areas, oscillations can synchronize neurons and create coherent cell assemblies [64]. For instance, human medial prefrontal oscillations have been linked to decision making [26], and hippocampal theta can synchronize medial prefrontal activity during learning [144, 158], depending on task demands [88]. Overall, there is evidence of a strong coherence between hippocampal and prefrontal thetas during

learning [9, 156, 159], but the mechanism is not known by which this form of learning-related coherence or cell assemblies is tightly synchronized.

Experimental studies are essential to the research in neuroscience. For a detailed review on lesion and neuroimaging evidence on the role of the hippocampus, and other structures in relation with episodic, semantic and spatial memory, please refer to Moscovitch *et al.* (2005) [129]. Experimentally, cognitive processing that involves signal propagation through multiple regions and the activation of large numbers of specific neurons cannot always be researched. Therefore, computational approaches are useful for studying the nature and mechanisms of this phenomenon.

2.2. Computational Neural Modeling

Computational neuroscience is the study of brain function in terms of information processing properties, and it emphasizes descriptions of functional and biologically realistic neurons (and neural systems) and their physiology and dynamics. These models capture the essential features of the biological system at multiple spatial-temporal scales, from membrane currents and protein and chemical coupling to network oscillations, columnar and topographic architecture, and learning and memory. To date, the growing experimental evidence that spike timing may be important to explain neural computations has motivated the use of spiking neuron models, rather than the traditional rate-based models [14].

2.2.1. Different Types of Networks of Spiking Neurons

Although spiking neural models have encountered problems due to large numbers of active neurons they still propose important mechanisms that generally provide a

theoretical understanding relating brain to behavior. They often require the use of detailed biophysical representations of the neurons, which can be accomplished by conductance-based (COBA) models, such as the Hodgkin and Huxley type or current-based (CUBA), as shown in Figure 2.16.

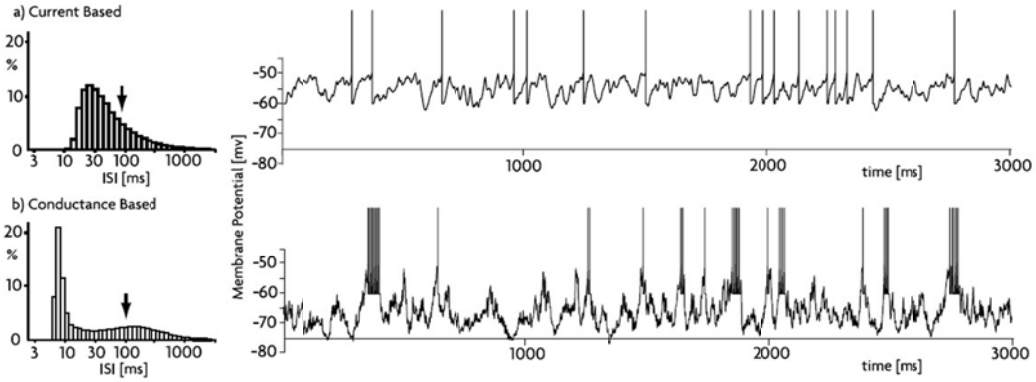

Figure 2.16: Difference of Activity of the CUBA and COBA Models [174]

These computational models include the relation of voltage-dependent ion channels to the propagation of action potentials [76]. In other cases, if the realistic capture of the spike generating mechanisms is not needed, simpler models, such as the integrate-and-fire model, are sufficient. These models are also fast to simulate and are particularly attractive for large-scale network simulations. Some models can combine more than one strategy, which can make the simulation more efficient. A large number of different tools have been developed to allow the simulation of spiking neural networks.

2.2.2. Simulation Tools

In computational modeling of spiking neurons, there are a variety of well-known existing tools. We review the main available tools in this section.

NEURON

The development of NEURON was started by John W. Moore and Michael Hines at Duke University [73]. NEURON is a nerve simulation program used for modeling single neurons in high levels of detail by implementing the concept of sections. It has been applied to the study of large networks of neurons, in which cable properties of cells play an important role, possibly including extracellular potential close to the membrane, and where cell membrane properties are complex, involving many ion-specific channels and ion accumulation [74].

GENESIS (General Neural Simulation System)

The GENESIS project began at California Institute of Technology by James M. Bower. It was originally utilized for the simulation of large networks for the realistic modeling of neural and biological systems. This simulator provides modelers the ability to change and reuse discrete components without having to change unassociated code. GENESIS also offers a parallel simulation environment allowing to model over networked workstations, a parallel cluster or supercomputer [13].

NEST (Neural Simulation Tool)

NEST was created by Markus Diesmann and Mark D. Gewaltig to help extend neural simulator development. It is ideally suited for simulations of large networks consisting of point neurons and architecture with minimal compartments, and is employed in studies interested in the dynamics of neural structures [36]. The development of efficient parallelization methods and integration techniques, such as the

efficient incorporation of precise spike times in globally time-driven simulations, is achieved by a combination of multi-threading and message passing [35].

2.2.3. NeoCortical Simulator (NCS)

Because parallel architectures and the degree of neuronal compartmental simplification required for reasonable performance times had not been achieved yet, the NCS was developed at the Brain Computation Lab at the University of Nevada, Reno to optimize the modeling of the horizontally dispersed, vertically layered distribution of neuron parameters of the mammalian neocortex with detailed synaptic plasticity and connectivity.

In this study, all simulations were performed using NCS [14, 43, 95, 180, 184] on a shared-memory three 16-processor Sun 4600. All models included leaky integrate-and-fire neurons with conductance-based synapses with a sampling frequency of 1,000 Hz per second, where each integrate-and-fire neuron is characterized by a membrane time constant of 20 ms, a membrane resistance of 100 MΩ, and a resting membrane potential of -60 mV. Whenever the membrane potential crosses the spiking threshold of -50 mV, an action potential is generated, and the membrane potential is reset to the resting potential where it remains clamped for a 5 ms refractory period. At a single cell level NCS solves a limited and slightly reordered form of the Hodgkin-Huxley model that is similar to the following equation. However, during the numerical integration a constant membrane leak is added.

$$C_N \frac{dV}{dt} - I_M - I_K - I_{AHP} - I_{input} - I_{syn} - I_{leak} = 0 \qquad (2)$$

Both I_M and I_{AHP} contribute to the membrane voltage by controlling spike-frequency adaptation. These are small ionic currents that have long period of activity when the membrane voltage is between rest and threshold. I_K is the transient outward potassium current. In this study, I_{AHP} is the current provided by small spike-adaptation contributing channel. These represent voltage independent K^+ channels that are regulated by internal Ca^{2+}, where the charge delivered after each time step is updated as:

$$I_{AHP} = g_{AHP} S m^P (E_{AHP} - V) \quad (3)$$

where S is a non-dimensional strength variable added to NCS and P is the power that the activation variable m is raised to. This K_{AHP} m particle is modeled as:

$$\frac{dm}{dt} = \frac{m_\infty - m}{\tau_m} \quad (4)$$

$$\tau_m = \frac{\epsilon}{f(Ca) + b} \quad (5)$$

$$m_\infty = \frac{f(Ca)}{f(Ca) + b} \quad (6)$$

where ϵ is the scale factor, b is the backwards rate constant, and $f(Ca)$ is the forward rate constant defined by:

$$f(Ca) = k[Ca]_i^\alpha \quad (7)$$

where α is the exponential factor.

NCS can calculate internal Ca^{2+} concentrations at the compartment level. Physiologically, the concentration inside a cell increases when an action potential fires. After the action potential has ended the internal concentration of Ca^{2+} will diffuse through the cell where

it is taken up by numerous physiological buffers. In NCS, this diffusion/buffering phenomenon is modeled by a simple decay equation defined by:

$$[Ca]_i(t+1) = [Ca]_i(t)\left(1 - \frac{dt}{\tau_{Ca}}\right) \quad (8)$$

where *dt* is the stimulation time step, and τ_{Ca} is the defined time constant for the Ca decay.

The synaptic currents are calculated by:

$$I_{syn} = g_{syn}PSG(t)\left(E_{syn} - V\right) \quad (9)$$

The leakage current is voltage-independent and is modeled by:

$$I_{leak} = g_{leak}(V - E_{leak}) \quad (10)$$

The leakage current is subtracted in the membrane voltage equation rather than added, as seen in the traditional membrane voltage equations.

I_{input} is injected from external input at times appropriate for igniting networks, and I_{syn} includes excitatory and inhibitory afferents neurons. Reversal potentials are E_{AHP} = -80 mV, E_{syn} = 0 mV for excitatory and -80 mV for inhibitory synapses, and E_{rest} = -60 mV (resting membrane). Synaptic conductances (*g*) are modeled as:

$$\tau_s \frac{dg}{dt} = -g \quad (11)$$

$$g \leftarrow g + w_i \text{ upon spike arriving at synapse i}$$

with post-synaptic conductance time constants of 5 ms (excitatory) and 10 ms (inhibitory) [14]. W_i represents the synaptic weight that arrives at synapse i.

In vivo mammalian recordings, a self-sustaining non-Poissonian bimodal firing is observed [127]. NCS is able to simulate this asynchronous background activity using the baseline parameters including the inhibition of the inhibition, sparse connectivity (3% among all cells) among an approximately 4:1 ratio of excitatory to inhibitory neurons with 10-fold greater inhibitory than excitatory conductance [17, 56, 102, 172, 174]. Self-sustained firing activity is achieved by a brief irregular external input. The resultant firing pattern of any given cell is irregular, with periods of higher firing rates separated by generally longer periods of low inactivity. Because the cells fire asynchronously with respect to one another, we refer to this as "recurrent asynchronous irregular non- linear" (RAIN) activity, as shown in Figure 2.17. This RAIN network uses 1,300 excitatory cells for 300 inhibitory cells with 3% connectivity and synaptic conductances G_{exc} and G_{inh} (Figure 2.17 A) where a sample of the activity is shown in Figure 2.17 B. (Membrane potential: green; mean rate: blue). The corresponding supra-Poissonian coefficient of variation (typically 30-50% greater than a Poisson spiking process), the wide range of RAIN firing rates of 2-60 Hz with mean rate of 14.8 Hz, and the bimodal distribution of firing (n = 50 cells) are represented in Figure 2.17 C-E.

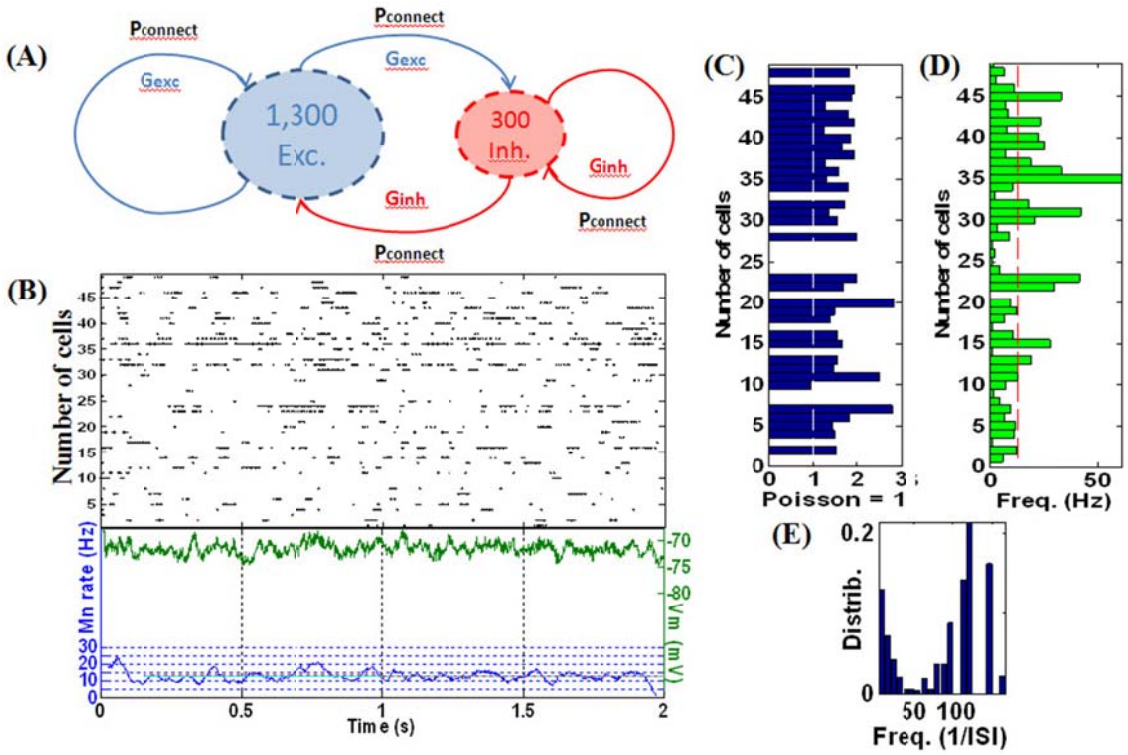

Figure 2.17: Recurrent Asynchronous Irregular Non-linear (RAIN) Activity

NCS can use two kinds of learning, Hebbian and synaptic facilitation depression (SFD). Here, Hebbian learning is considered for a long-term learning where SFD is more replicating short-term learning, which decay over time.

2.2.4. Theoretical Models

The use of computational models has been invaluable for exploring the link between neurons and behavior, enabling hypothetical mechanisms to be defined precisely and examined quantitatively [4]. Some models have focused on the hippocampal area, especially CA1 and CA3. Menschik and Finkel (1998) [125] advanced a network model of hippocampal CA3 region dynamics inspired by Buzsaki's two-stage memory model [20]. Lisman and colleagues concentrated more on gamma cycles embedded within theta

rhythm [112]. Kunec *et al.* (2005) [103] modeled a detailed CA3 representation using the major type of pyramidal cells and two types of interneurons, and Cutsuridis *et al.* (2009) [29] recently advanced a far more detailed biophysical model of the CA1 microcircuit. Wu *et al.* (2010) [182] worked on the coupling of dendritic with the soma–axonal action potential initiation zone of CA1 pyramidal cells. Finally, an integrate-and-fire model of short buffering was used to simulate performance in hippocampus-dependent spatial navigation tasks [69, 100].

Other models have proposed an explanation for grid cell interference [11] and grid cell firing phenomena [57, 58, 68], but most classes of theoretical models have been offered to explain place cells and grid cell effects. McNaughton *et al.* (2006) [122] proposed a topographically arranged network that serves as a tutor to train medial entorhinal cortex cell modules. Other local-network models, Gaussier *et al.* (2007) [55] and Samu *et al.* (2009) [152] proposed that stabilization of hippocampal place cells is due to the combination of modulo projections from entorhinal grid cells and visual place cells. Another class of models is based on the hypothesis that path integration occurs at the single cell level and is related to phase precession [130]. In particular, Tsodyks *et al.* (1996) [169] proposed a neural network model based on integrate-and-fire neurons that accounts for phase precession.

A rich set of experimental data has been gathered from computational models on the neural representation of spatial behavior found in and around the hippocampus. However, the interactions between place cells and grid cells, their individual and interactive mechanisms, their significance for memory storage, and their dynamics with representations in other cortical regions remain to be determined [130]. Also, the

complete hippocampal-entorhinal-prefrontal loop has yet to be successfully modeled to provide more understanding of these microcircuitry dynamics.

Therefore, the first model presented in this study (covered in Chapter 3) was used to understand hippocampal and entorhinal cell interactions, specific intracellular-extracellular precession disparities and place field destabilization by entorhinal lesioning. The corresponding input files used are summarized in Appendix A. The second model (covered in Chapter 4) completed the loop with the prefrontal cortex, replicating phase synchrony of prefrontal cells to hippocampal theta oscillations, and demonstrating short-term memory of navigational sequences, decision making, and learning reinforcement. The corresponding input files used are summarized in Appendix B. Ultimately, these computational models are used to frame hypotheses that can be directly tested by future biological experiments. The corresponding fundamentals in brain slice experiments are presented in Chapter 5, and future recording experiments are suggested as future work in Chapter 6.

2.3. Relevant Experimental Studies

After important hypotheses are defined through computational modeling, there are several assumptions that could be tested in experimental studies. For instance, the mechanisms of hippocampal dynamics modulating influences of entorhinal cortex could lead to interesting findings in the field. Experiments may include exploring the types of extrinsic connectivity between the two structures, or the intrinsic connectivity within the hippocampus, especially in the subiculum. A hippocampal slice study presented fast synaptic activation of hippocampal interneurons by afferents subcortical neurons [173].

Few other studies have tried to combine *in vitro* hippocampal and parahippocampal slices [8, 148, 163, 166, 167, 175] in rats. However, such studies on mice are not available due to the difficulty of preparing a smaller brain, slicing it accordingly, and getting relevant recording data. Our experiments have revealed fundamental procedures to make studies on mice more feasible.

2.3.1. Brain Removal

The fastest and easiest way of animal execution is by decapitation, although alternatively halothane (for anesthesia) or CO_2 (suffocation) could be employed. These last two methods are not recommended because they take more time and could produce some neuronal damage prior to the brain removal. Once the animal is decapitated, the skull is removed with scissors, cutting along the sagital axis from the caudal (posterior) to the rostral (anterior) part and then opening the two skull pieces laterally. For shelling out the brain, slide the forceps or the scissors in the caudal part, and remove the whole organ backwards. The process of brain removal should be gently accomplished, but as fast as possible [157]. Once the brain is removed from the skull, place it rapidly into oxygenated ice-cold (4°C, 95% O_2 - 5% CO_2) artificial cerebrospinal fluid (ACSF) containing KCl, NaCl, $NaHCO_3$, glucose, $MgCl_2$, and $CaCl_2$ (Please see specific concentrations in Section 5.1.1). This solution should be sufficiently cold that it contains a few ice crystals, and the container should be sitting on ice to maintain this low temperature. Immediately after a short incubation time in cold ACSF, the brain is ready for slicing [104].

2.3.2. Brain Slice

To reduce damage of the tissue and to minimize the metabolic activity, it is particularly important to keep the brain immersed in iced-cold ACSF during the whole slicing process. Despite the many different procedures employed for brain slicing, the main goal is to prepare a slice of tissue where the neurons, fibers, and synapses that are important to the experiment are in a viable condition.

The slicing is usually done using a vibratome. The vibration frequency (usually near the maximum of 85 Hz) and the slicing speed of the blade should be adjusted to prevent the tissue from being pushed while cutting the slices. The angle is critical to obtaining the right brain regions that are important to the study [89]. Slicing should be accomplished in less than 10 minutes. The brain slices are carefully taken using a cut and fire polished Pasteur pipette filled with the ice-cold solution. The slices are then incubated at a temperature of around 36ºC for at least 1 hour. Oxygenation and normal pH are maintained by bubbling the ACSF with 95% O_2 - 5% CO_2. This allows the tissue to recover from the damage imposed by the preparation and adjust to the new extra cellular milieu as well as to change metabolic activity before recordings.

The animals used in preparing slices are most often small rodents. Young animals have some advantages for the slice preparation: their skulls are soft, and therefore easier to remove, and their brain is smaller and cools more rapidly when placed in ice-cold solution. On the other hand, older animals' tissue is more susceptible to anoxia, and the neuronal damage is higher as time goes by. More myelination and the presence of more connective tissue may result in more damage to the cells. Slices can vary from 400 μm to 1-2 mm in thickness, but thin slices allow a greater optical resolution due to smaller

effect from light scattering. Thicker slices exhibit centrally-located necrotic cells that are suggestive of hypoxic damage. A standard slice is cut at 300-400 μm thickness.

2.3.3. Patch Clamp Recording

The cells and parts of the dendrites can be visualized using a 40 X high numerical aperture, long working distance water immersion objective. There are different types of patch clamping, such as multiple electrodes, whole-cell or cell-attached recordings. The chosen method and the assessment of electrical parameters of slices depend on the type of experiments and the characteristics of the particular cells within the tissue, respectively. The basic indicators include resting membrane potential, input resistance, and amplitude of the action potential. More sensitive measures include the ability of the cells to produce a regular, rhythmic train of action potentials after the injection of a small current. Damaged neurons will often respond with a single action potential at the onset of the current pulse. In addition to direct cellular parameters, amplitudes of extracellular fields reflect the synaptic action and are convenient for assessing the overall state of a slice or at least of small regions within a slice [164]. Table 1 describes the advantages and disadvantages of brain slice experiments.

Advantages	**Disadvantages**
Direct visualization	Loss of connectivity
Technical accessibility	Damage of neurons
Mechanical stability	Tissue debris mixed with healthy cells
Ease of use	Altered metabolic state
Control of extracellular medium	Slow release of ions from damaged cells

Table 2.1: Advantages and Disadvantages of Brain Slice Experiments

Despite these few studies and guidelines regarding hippocampal-entorhinal brain slices, there is still a lot to discover about optimal slicing and recording techniques and the interconnectivity between and within brain regions.

CHAPTER 3: HIPPOCAMPAL PLACE FIELD DYNAMICS MODULATED BY ENTORHINAL GRID AND SUPPRESSION-GENERATING CELLS

This model represents hippocampal-entorhinal dynamics during spatial navigation on a linear track, passing visual landmarks (VL). A summary of the input files used are located in Appendix A.

3.1. Material and Methods

3.1.1. Navigational Paradigm

To replicate the virtual linear maze of Harvey *et al.* (2009) [66], we developed a computational system representing a navigating rodent (Figure 3.1). The animal is assumed to have been trained to run with minimal hesitation along a 180-centimeter linear track, passing *en route* five visual landmarks demarcating an environment we refer to as VL1 to VL5. Each VL represents potential place field activity (45 centimeters long), modeled as a two-second Gaussian distribution of spike probability along an assumed occipital-parietal-temporal axonal pathway terminating in CA regions of the hippocampus. Consistent with the experimental findings [66], VL overlap is 37%, the total duration of the run is eight seconds, and the average speed of the animal is 22.5 cm/s. Three consecutive passes through the maze were analyzed for each experimental condition (an additional fourth pass was simulated, but no changes in dynamics were observed beyond three passes).

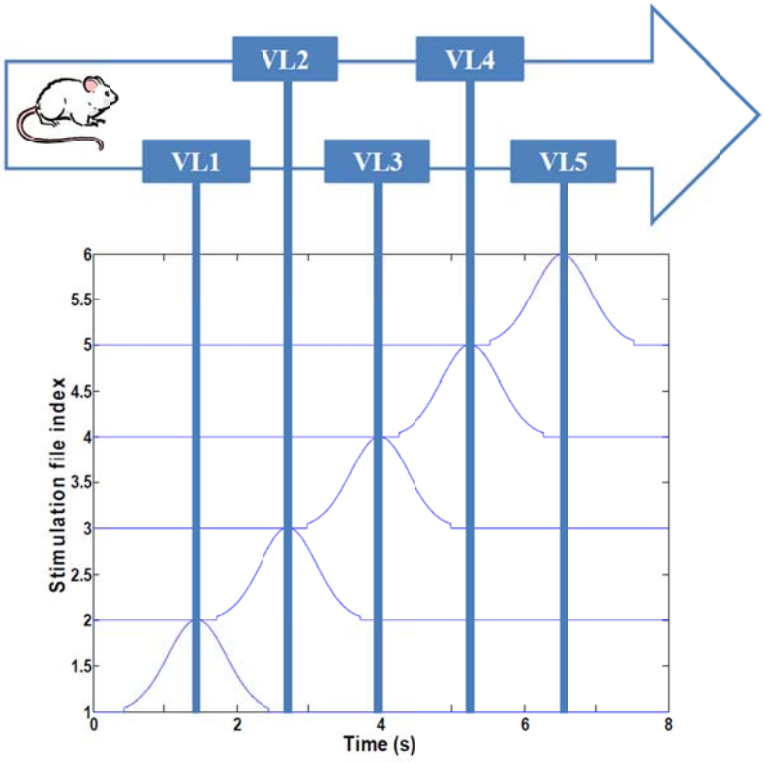

Figure 3.1: Simulated Navigational Environment

3.1.2. Computational Brain Model Implementation

The hippocampal model included a total of 37,500 leaky integrate-and-fire neurons. Pyramidal cells were represented as quasi-bicompartmental [82] neurons by the inclusion of a population of single-compartment apical tuft cells that connect to the pyramidal somatic compartment. In the soma, each of five place-field RAIN subnetworks included 3,200 neurons, comprised of 2,600 pyramidal and 600 single-compartment interneurons. We hypothesized that grid cell activation at place-field boundaries followed by visual-parietal input should trigger self-sustained, asynchronous background activity limited to the place field, which was achieved by a 300 ms irregular input into these RAIN networks. To generate theta activity, a 1,600-cell RAIN network was weakly

connected (0.23%, one E to E group) to a 1,600-cell RAIN network whose excitatory cells contain K_{AHP} channel activity the latter oscillates at 6-10 Hertz oscillation with variability that appears biologically plausible (Figure 3.2). These oscillating networks represented synchronized BC activity, with connections to pyramidal and OLM cells as described in Section 3.2.1.1., allowing us to mix incoming VL excitatory activity with anti-phase theta inhibitory activity in the distal tuft, independent of somatic currents.

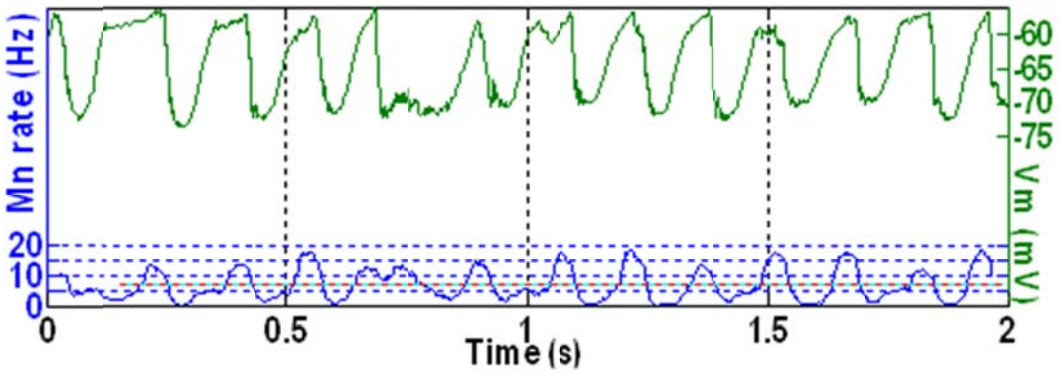

Figure 3.2: Biological-Like Theta Activity

Excitatory synapses among pyramidal cells (CA RAIN networks) included K_{AHP} channels and underwent STDP (See Sections 2.1.1 and 2.1.2). K_{AHP} channels had a scale factor of $\epsilon = 0.000125$, an exponential factor of $\alpha = 2$, a half-min of $b = 2.5$, a tau scale factor of 0.01, and a unitary channel strength of 0.00044. STDP had positive and negative fractional changes in synaptic strength (ΔW) of 0.003, with positive window ($+A$) of 50 ms and negative window ($-A$) of 90 ms, and with positive decay constant ($+\tau$) of 15 ms and negative decay constant ($-\tau$) of 30 ms [30]. External inputs were injected at times appropriate for igniting the RAIN networks and activating grid cells and VL pathways (Figure 3.3).

3.1.3. Analytic and Statistical Methods

We established specific performance criteria with respect to the published awake-behaving intracellular recordings of Harvey *et al.* (H) and the entorhinal cortical lesions of Van Cauter *et al.* (V):

H1: Intracellular theta oscillations increase in amplitude toward the center of the place field.

H2: Asymmetric ramp-like depolarization of the DC-filtered baseline membrane potential occurs.

H3: Spike precession relative to extracellular LFP theta is associated with increased frequency of intracellular theta.

V1: Entorhinal cells regulate the location of place fields.

V2: Entorhinal lesions reduce place cell discharge firing rates by about a fourth and approximately double the number of active place cells responding in a given place field.

Frequency of Intracellular Theta

We filtered inhibitory LFP and somatic Vm using Matlab fir1 (finite impulse response) notch-filtering from 6 to 10 Hz (Figure 3.5 A). Extracellular LFP theta was measured two seconds before entering and during each place field. To determine whether our findings were consistent with the rising intracellular theta frequency reported by Harvey *et al.* (2009) [66], we fit the sequence of filtered intracellular inter-theta peak intervals using locally weighted least squares regression (LOWESS) (Figure 3.5 B) for display purposes and statistically compared the mean frequency of theta oscillations during the central third with the first and last thirds of each field (Figure 3.5 C).

Spectral Analysis of Intracellular Membrane Potential

We analyzed theta power spectra for epochs inside and outside of the place field using multi-taper spectral analysis methods (function mtspecgramc from the Chronux toolbox, http://chronux.org, Figure 3.6 A). We also calculated the ratio of power during epochs inside to outside the place field for bands from 6-10 Hz (Figure 3.6 B).

Membrane Potential Depolarization Inside Place Fields

We obtained low frequency Vm during the place field tracings using notch-filtering from 1 to 2 Hz (Figure 3.7 B). We defined the baseline membrane potential as the low frequency mean just prior to entering the place field and subtracted this from the in-field membrane potential values to derive the ramp ΔV. From this, we computed the magnitude and, to estimate asymmetry, the timing of the peak ramp ΔV with respect to its location in the place field (Figure 3.7 C).

Spike Precession with respect to LFP

To analyze phase precession, we computed spike timing with respect to LFP theta phase within the place field (Figure 3.8 A). All cells with increasing mean ramp ΔV in the place field were included. For the phase versus position distribution, we first computed its outer hull; to that curve we fit a non-linear parabolic curve to obtain parameters estimating the phase and timing of the phase of greatest precession (Figure 3.8 B). From this, we computed the magnitude and, to estimate asymmetry, the timing of the trough (maximal precession) with respect to theta (Figure 3.8 D).

Entorhinal Cortex Lesioning

To analyze the effect of putative entorhinal suppression, we compared the population sizes and firing rates of active place cells in both control and lesioned groups (Figure 3.9). Place field stabilization by the entorhinal cortex was explored by comparing place field activation during full 8-second runs in the control versus lesioned groups (Figure 3.10).

Statistics

To assess reproducibility, we ran the entire simulation under ten different pseudo-random seeds. Because firing pattern means and variances did not differ statistically by 1-way ANOVA comparisons, in the subsequent analyses we combined the passes through the track and then compared the results of 30 runs of the entorhinal-lesioned group with 30 runs of the control group. All runs included K_{AHP} channels in CA pyramidal cell somas. Group means were compared using the appropriate paired or unpaired student *t*-test or one-way ANOVA, and medians compared by the SIGNRANK test.

3.2. Results

3.2.1. Model Description

Hippocampal Place Field and Entorhinal Cell Representation

Integrate-and-fire neuronal simulations are increasingly being used to represent interacting cortical and subcortical interactions [47]. Here, we represented CA pyramidal neurons as bicompartmental cells with a soma in the stratum pyramidale and apical dendritic tuft in the stratum lacunosum moleculare, as shown in Figure 3.3. Pyramidal

cells are arranged into subnetworks, receiving inputs from (1) sensory parietal-temporal axonal pathways responding to VL, (2) entorhinal cell populations, (3) basket cells (BC) in the stratum oriens (SO), (4) O-LM interneurons [96], and (5) perforant pathway associated (PPA) interneurons [96]. We assume that visual neocortical activity, along with entorhinal cell activity passes through the perforant pathway to activate the distal tufts of hippocampal CA networks. VL may or may not synapse in the entorhinal cortex specifically, but fibers could pass through the entorhinal cortex or parahippocampal regions en passant to hippocampus. We also assume that the GC network was already formed during the development of the mouse, and is modeled as a group of simple single-cell leaky integrate and fire neurons. We program the model to inject short sequence of square-wave pulses (1 ms width, 3 nA) just as the mouse crosses the boundary of the grid between place fields (because this is a linear maze, the "grid" tiling becomes simple linear spacing, or repeating pattern at the boundaries). We modeled five such discrete networks serving as the potential basis for corresponding place-field representation. We assume that BC are activated by global CA activity and give rise to theta (6-10 Hz) phasic field activity [4], which in turn is broadcast as inhibitory input to the proximal dendritic branches of the pyramidal cells. BC also inhibit O-LM interneurons, giving rise to anti-phase inhibitory theta activity that projects to dendritic tufts in SLM [92]. To simulate the putative effects of entorhinal lesioning described by Van Cauter *et al.* (2008), we included two populations of entorhinal cells: (1) "suppression-generating" cells (notated EC SG in Figure 3.3) connecting to PPA interneurons, which in turn inhibit the pyramidal apical tufts, resulting in fewer cells responding in place fields, and (2) grid

cells (notated EC GC in Figure 3.3) connecting to the basilar dendrites, responsible for triggering activity at the boundaries of place fields [63].

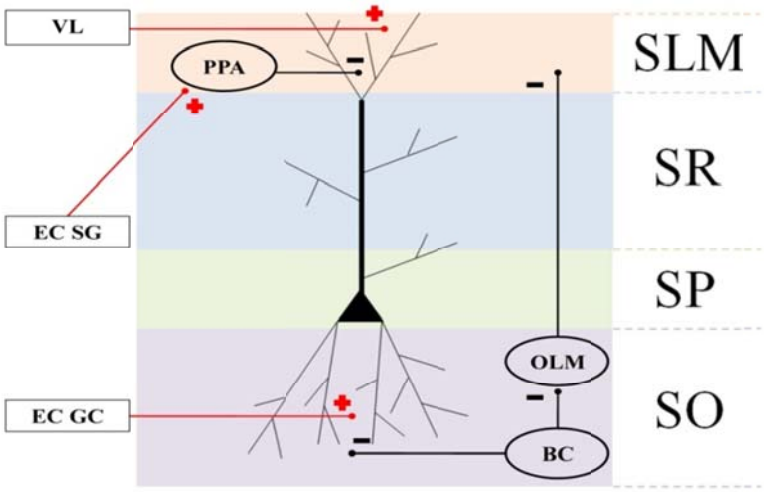

Figure 3.3: Connectivity of the Hippocampal Structures and Surrounding Regions

Hippocampal Place Field and Entorhinal Cell Modeling

The description of neuronal network models should communicate enough information for readers to comprehend and re-implement a model and to compare different models [136]. Table 3.1 gives an outline of the model, which validates its implementation (See Section 3.1.2).

A	Model Summary
Populations	Seven: CA pyramidal cells, axonal pathway (VL), entorhinal cells (2), basket cells, OLM interneurons, PPA interneurons
Neuron Model	Leaky integrate-and-fire, fixed threshold, refractory time
Plasticity	STDP
Channel Model	K_{AHP} channels
Synapse Model	Conductance-based
Measurements	Membrane Potential

B	Populations	
Name	**Elements**	**Size**
CA	5 RAIN networks	3,200 cells
VL	5 E cell groups	200 cells
EC SG	Linear positive current	N/A
EC GC	Current file based	N/A
BC (theta)	RAIN network	1,600 cells
OLM	I cell group	300 cells
PPA	Linear negative current	N/A
C	**Neuron and Synapse Model**	
Type	Leaky integrate-and-fire neurons, conductance-based synapses	
Dynamics/Spiking	See Section 2.2.3 for equations	
D	**Channel and Plasticity Model**	
K_{AHP} and STDP	See Section 2.2.3 for equations	
E	**Measurements**	
Membrane potential V of all neurons		

Table 3.1: Tabular Description of Model. The model is summarized in panel A and detailed in panels B-E.

3.2.2. Model Analysis

Analytical and Numerical Experiments

The first part of model analysis is a description of analytical and numerical data used in the model, as shown in Table 3.2.

A	Connectivity	
Type	**Probability (%)**	**Conductance strength (mS)**
RAIN - BC	3	0.004
BC - CA	3	0.003
BC - OLM	3	0.2
OLM - VL	3	0.01
VL - CA	5	0.006

B	Input
Type	**Description**
Visual cortex	2 second Gaussian distribution (5 of them)
Entorhinal cortex (SG) / PPA	Linear negative current suppressing CA networks (50%) with amplitude of -4 mA and constant duration
Entorhinal cortex (GC)	File based current exciting CA networks (100%) with amplitude of 3 mA and duration of 300 ms

Table 3.2: Tabular Analysis of Model. The description of the model connectivity is shown in panel A and the model input is given in panel B.

The second part of model analysis is a description of the results obtained. These results are designed to test hypotheses H1, H2 and H3, and V1 and V2 (See Section 3.1.3).

Hippocampal Formation Dynamics

During the first two passes, place field activity spread over most of the two-second traversal period, but after the virtual mouse ran an additional repetition through the maze, place cells localized to a narrower field, with a mean rate decrease from 33.1% (pass 1) to 27.9% (pass 2) to 24.9% (pass 3). Figure 3.4 (A-C) shows typical place field firing from the middle to the end (1 sec) during the first traversal (A), second traversal (B), and third traversal (C) through the maze for sample of 100 cells. This narrowing corresponded to a mean decrease in synaptic strength of 1.6% over the course of three passes through the track illustrated in Figure 3.4 (D-F) for a sample of 100 cells. Individual repetitions of a place field for 10 consecutive runs or different seeds showing each pass (1: blue; 2: green; 3: red) and Gaussian fit from the middle to the end of a place field (99% CI bands) for the first pass (blue), second pass (green), and third pass (red) though the maze (Figure 3.4 G,H). The peak rates (maximum, at the middle of the place

field) are statistically different from one pass to the next ($P < 0.001$). However, the decay rates or variances of the curves are not statistically different. Removing K_{AHP} channels affected these results by decreasing theta resonance.

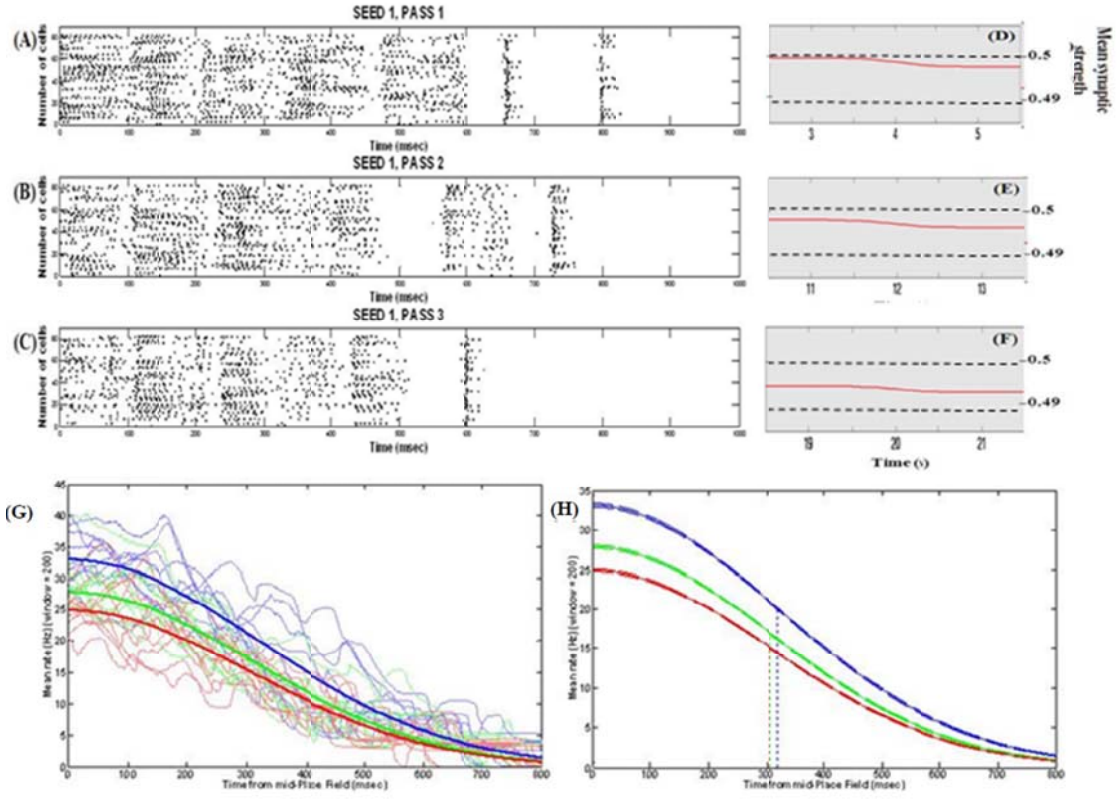

Figure 3.4: Place Field Activity during Multiple Runs through the Track

The frequency of intracellular theta gradually increased toward the center of the field (4.75 Hz, $P < 0.001$, $N = 30$ fields) and fell again toward the end of the field. This increased frequency results from interference of the signal arriving from the apical dendrites (a mixture of visual pathway and local OLM inhibitory theta) and the local BC theta effect (180 degrees out of phase with OLM, as experimentally shown by Kamondi and Buzsaki *et al.* [92]). An example of 6-10 Hz filtered mean theta within a typical place field and a corresponding moving window average of the theta oscillation period is

shown in Figure 3.5 A and B (n = 19 cells with increasing mean). Figure 3.5 C emphasizes the difference of mean frequencies during the first, middle, and last third of all fields (P < 0.001 by ANOVA, middle versus combined first and last thirds, n = 472 cells with increasing mean). Error bars are ± 1 s.e.m.

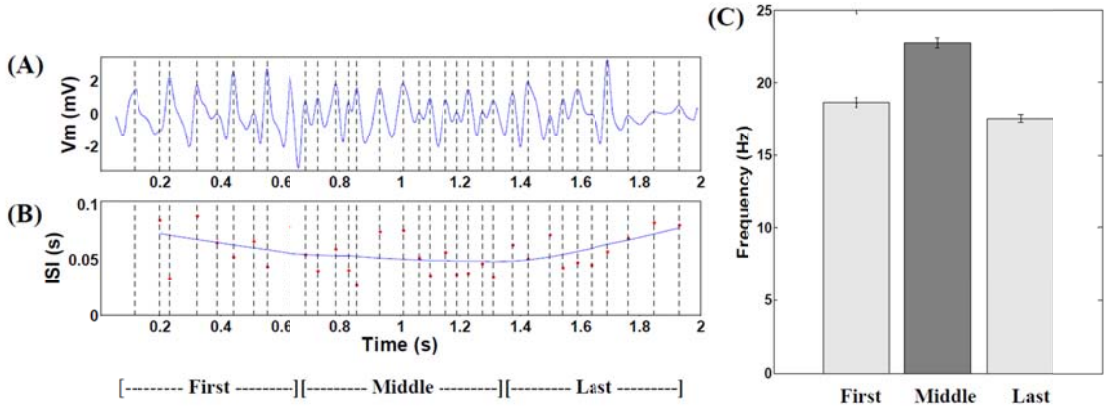

Figure 3.5: Frequency of Intracellular Theta

Power spectral analysis as a function of the mouse's position on the linear track (N = 30 fields) and theta-band (6-10 Hz) power in the membrane potential trace are shown in Figure 3.6 A. Figure 3.6 B compares the ratio of theta power inside over outside the place field of the control to the lesioned group. (*n* = 390 cells). Error bars are ± 1 s.e.m. Theta-band power of the membrane potential was significantly higher within place fields than outside (Figure 3.6 A) due to interference of local inhibitory theta with visually-driven apical dendritic input with an average ratio of power in-field to power out-of-field of 6.7 (P < 0.001; Figure 3.6 B). There were no significant differences between control and entorhinal-lesioned groups (P > 0.05).

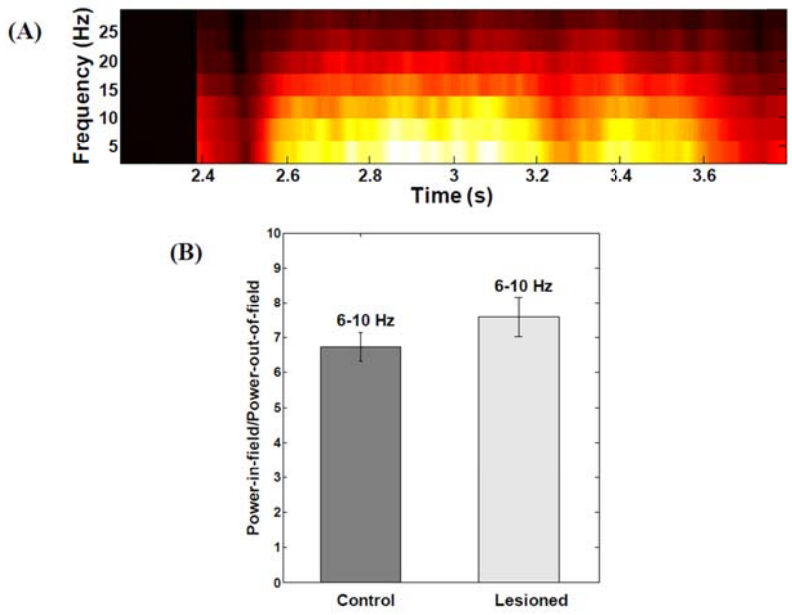

Figure 3.6: Spectral Analysis of Intracellular Membrane Potential Recordings

LFP was measured from within the soma of a CA pyramidal cell, outside (0-2 sec) and within a place field (2-4 sec), as shown in Figure 3.7 A; spike unit timing is indicated by dotted red lines. Cyan and magenta markers indicate auto-detection of 0 and 180 degree theta limits. The corresponding intracellular Vm (green line), with a superimposed 1-2 Hz filtering (dashed black line), and red dots indicating spike timing are illustrated in Figure 3.7 B (truncated, n = 1 cell as an example). Figure 3.7 C gives a representative sample of mean 1-2 Hz filtered ramps from third place field (black line: mean of all curves; black vertical dashed line: true center of place field; red vertical dashed line: mean timing of the peak of individual ramps). As the virtual mouse approached a visual landmark, the average membrane potential increased in a ramp-like manner and remained increased beyond the center of the place field (Figure 3.7 C). The ramp of depolarization often began before the start of action potential firing in the place

field. In some cases, the ramp reached a depolarization as large as 13.5 mV with an average peak depolarization of 8.2 ± 2.6 mV. On complete runs through the place field, ramps of depolarization were asymmetric, with the timing of the peak depolarization shifted toward the end of the field. The average right shift of the peak was 0.07 seconds ($P < 0.05$), and the average right skewness was 0.5 ($P < 0.001$). There were no significant differences among the five place fields (ANOVA $P > 0.05$) for these measurements. Removing K_{AHP} channels resulted in statistically symmetric ramps of depolarization ($P > 0.05$). This asymmetric ramp depolarization is attributable to the propagation delay or momentum of RAIN networks; perturbation of a RAIN network affects all other cells with delays ranging from 50 to 100 ms because both excitatory and inhibitory cells are sparsely connected and tonically inhibited, resulting in widely spaced irregular bursting. In this case, the CA RAIN networks experience an average delay of about 70 ms.

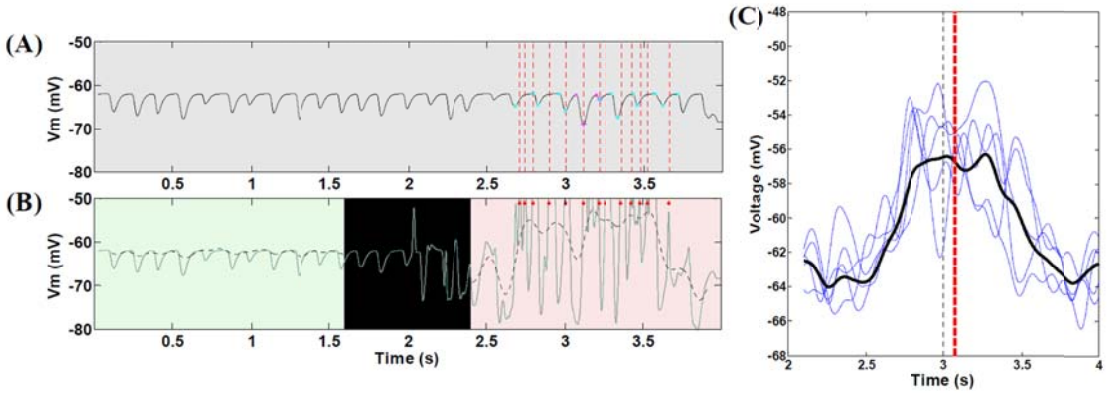

Figure 3.7: Asymmetric Ramp-Like Membrane Potential Depolarization inside Place Fields

Figure 3.8 A magnifies the first spike timing of a sample of all 19 cells with an increasing mean from a single run superimposed on extracellular theta within the third

place field. For each spike in (Figure 3.8 A), the phase with respect to LFP is represented in Figure 3.8 B with an outer hull fit. The location of spikes with respect to theta waveform is shown in Figure 3.8 C. For clarity, a representative sample of 25% of outer hull fit of precession during third place fields is compared in Figure 3.8 D (Black dashed line: true center of place field; red dashed line: mean timing of the troughs or maximal precession). Because spikes occur reliably at or near the peak of *intracellular* oscillation (there is no intracellular precession per se) and the intracellular oscillation frequency increases near the middle of the field, spike timing will appear to precess with respect to *extracellularly* measured theta LFP. Phase precession with respect to LFP theta spanned the entire range between 0 and 360 degrees (Figure 3.8 A). Figures 3.8 B and C show a typical distribution of spike timing with respect to theta phase while traversing a place field. A parabolic outer hull fit had significant ($P < 0.001$) curvature and maximal precession shifted asymmetrically toward the right half of the field (0.06 sec), as shown in Figure 3.8 D ($P < 0.001$). There were no significant differences among the five place fields (ANOVA $P > 0.05$) for these measurements.

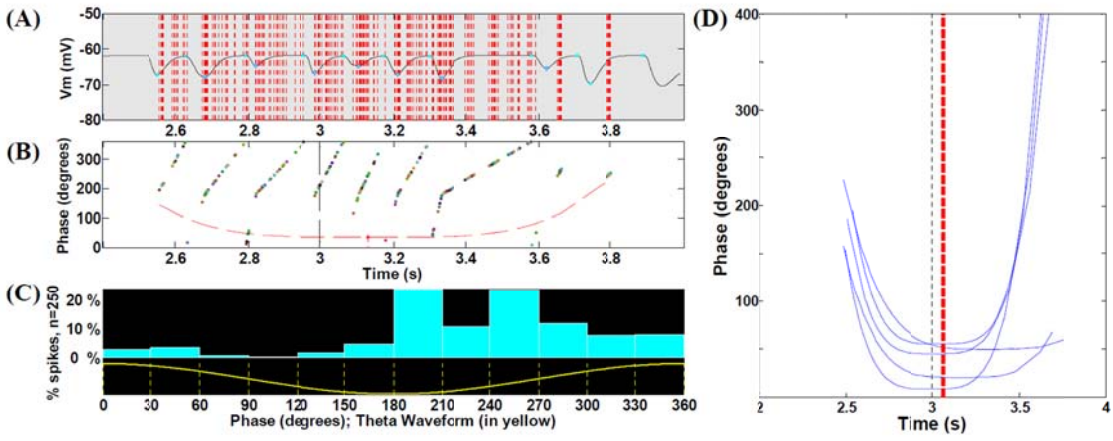

Figure 3.8: Precession with respect to LFP during Place Fields

Entorhinal Cortex Lesioning

The average number of active cells and the average firing rates within five place fields are compared between the control and lesioned groups (Figures 3.9 A and B) a sample of n = 390 cells is represented. Lesioning the putative suppressive input from the entorhinal cortex resulted in approximate doubling ($P < 0.001$) of the proportion of cells firing within a place field (Figure 3.9 A). Contrary to this *increased* population response, the actual mean firing rate *decreased* by 24.3% ($P < 0.001$, Figure 3.9 B). Removing K_{AHP} channels did not affect these results ($P > 0.05$). Tonic extrinsic inhibition (as postulated to arise from the entorhinal cortex) into CA principle cells was manually adjusted to suppress about half the population excitatory cells from firing; rather than a net decrease in firing rate among the remaining active cells, an increase of about 24% was observed, consistent with entorhinal-lesioning findings of Van Cauter *et al.* (2008) [170]. The paradoxical response is attributable within RAIN networks to an auto-regulatory increase of inhibition of inhibition (less net inhibition).

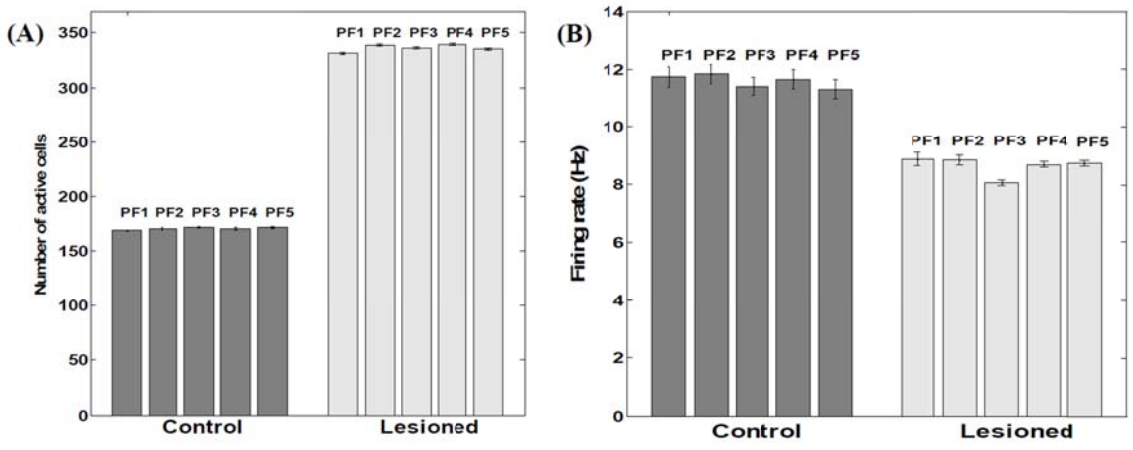

Figure 3.9: Number of Active Cells and their Firing Rates within Place Fields

Control groups (Figure 3.10 A) with the active role of entorhinal cortex grid cells contribute tonic suppression during all five place fields. Tonic entorhinal-derived inhibition mediated by PPA interneurons and EC SG is sufficient to suppress RAIN CA networks from triggering in the absence of concurrent visual pathway stimulation. On the other hand, entorhinal lesioned groups (Figure 3.10 B) in the absence of tonic suppression show random surges arising within the hippocampus can spuriously ignite the CA networks when the animal is between place fields, consistent with *in vivo* findings of Van Cauter *et al.* (2008) [170]. (One typical 8 sec run shown, n = 390 cells as a sample). The presence of entorhinal suppression stabilized the location of every place field throughout the run. As shown in Figure 3.10 A, each place field fired at its corresponding visual landmark along the track when the entorhinal cortex was intact. However, when the entorhinal cortex was lesioned, place field location varied and often triggered at anomalous locations (Figure 3.10 B).

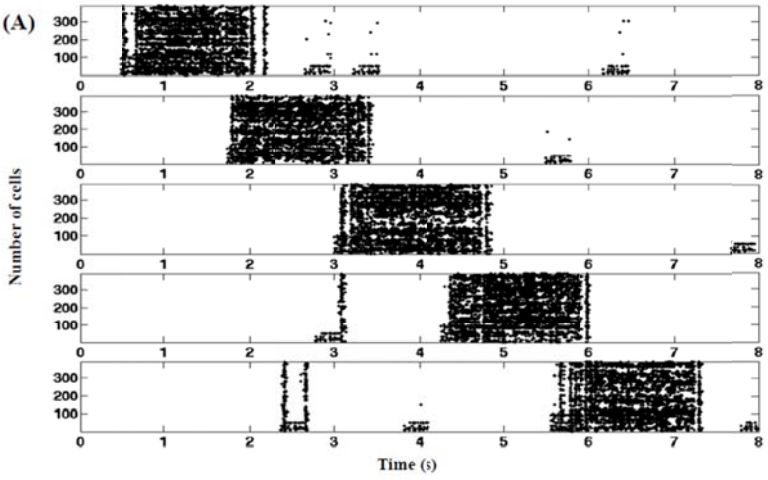

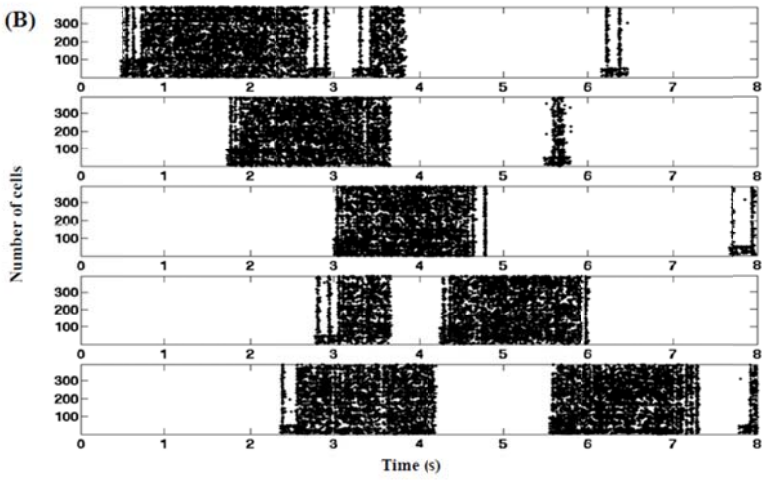

Figure 3.10: Place Fields Stabilization

3.3. Discussion

We report here two unique circuit-level network features that can explain intracellular and extracellular CA place field dynamics observed during *in vivo* spatial navigation: (1) self-sustained recurrent asynchronous irregular nonlinear (RAIN) networks underlying place cell responsiveness and (2) entorhinal neuron groups providing both transient excitatory ignition (EC GC) and tonic suppression (EC SG). In particular, RAIN networks incorporating K_{AHP} channel-like dynamics provide a mechanism for the *in vivo* asymmetry of intracellular place field ramping not explained by the models of Harvey *et al.* [66] and Gasparini and Magee [54]. Additionally, these dynamics explain the apparent population-rate discordance of the entorhinal-lesioning results of Van Cauter *et al.* (2008) [170].

RAIN networks are easily ignited by transient (50-300 ms), sparse (< 100 spikes) external stimulation, self-sustained non-Poissonian bimodal firing similar to that observed in most *in vivo* mammalian recordings [127], yet they readily shut down with

unopposed theta range inhibitory input. This bimodally distributed firing requires conduction-based synapses [174]. Interaction among RAIN networks spontaneously gives rise to biological-appearing, variable-background inhibitory theta activity. Several studies have shown that networks of sparsely connected current-based synaptic spiking model neurons can produce highly irregular, chaotic activity without any external source of noise [17, 172]. Conductance-based synaptic models exhibiting asynchronous irregular firing patterns have been proposed as the basis for prefrontal working memory [27], but to our knowledge this is the first such application to the hippocampal formation.

Simulated hippocampal place-cell activity was consistent with that reported by Harvey *et al.* (2009) [66]. Our model showed increased theta power (H1, as defined in Section 3.1.3.) toward the middle of a place field. This resulted from a net increase in the theta-modulated signal arriving from apical dendrites, which overrides the relatively constant anti-phase interference of the local BC theta inhibition onto the principal cells [92]. Asymmetric ramp-like depolarization (H2) during place field traversals is attributable to the propagation delay or momentum of RAIN networks; perturbation of a RAIN network affects all other cells with delays ranging from 50 to 100 ms, because both excitatory and inhibitory cells are sparsely connected and tonically inhibited, resulting in widely spaced irregular bursting. In this case, the CA RAIN networks experience an average delay of about 70 ms. Of note, the model proposed by Harvey *et al.* could not explain this asymmetry [66]. Our model also confirmed an increased frequency of intracellular theta oscillations toward the middle of place fields (H3), which explains phase precession of spikes with respect to extracellular LFP theta activity. Spikes occurred reliably at or near the peak of *intracellular* oscillation, but the intracellular

oscillation frequency increased near the middle of the field, which made spike timing appear to precess with respect to *extracellularly* measured theta LFP. The increased frequency results from interference of the signal arriving from the apical dendrites, mixture of visual pathway and local OLM inhibitory theta. The local BC theta effect, which is 180 degrees out of phase with OLM [54] was experimentally consistent with Kamondi and Buzsaki *et al.* (1998) [92].

Our incorporation of STDP in the excitatory connections within the place cell networks and K_{AHP} dynamics in the RAIN theta networks resulted in stabilization of place field response generally by the third pass through the track, consistent with such delays reported by Wilson and McNaughton (1993) [181] and Frank *et al.* (2004) [48].

To test our hypotheses about the mechanism of the entorhinal cortex regulation of CA place field behavior, we simulated the lesioning experiments of Van Cauter *et al.* (2008) [170]. Our results support dual roles for entorhinal cell populations projecting to CA regions: triggering place-specific pyramidal cell firing and, mediated by local CA interneurons, suppressing sporadic place cell activation of established place fields (V1). It is the self-regulating characteristic of RAIN networks that accounts for the seemingly discordant entorhinal lesioning results, where an increased number of active place cells is associated with reduced, rather than increased, overall place cell firing rates (V2). If CA networks did not have the inhibition of the inhibition feature of RAIN activity, tonic inhibition of the principle cells would lead to a decrease in the firing rate rather than an increase and also to the destabilization of place field activity [170].

We speculate that transient activation of neural architectures consistent with RAIN-like networks may subserve hippocampal CA place field dynamics. This insight is

important to better understand not only mammalian navigation but more complex episodic and semantic short-term memory and mechanisms of long-term memory consolidation and reconsolidation.

CHAPTER 4: A CIRCUIT-LEVEL MODEL OF HIPPOCAMPAL, ENTORHINAL, AND PREFRONTAL DYNAMICS DURING SEQUENTIAL LEARNING

This model represents hippocampal-entorhinal-prefrontal dynamics during spatial navigation on a three binary decision sequential maze, passing visual landmarks. A summary of the input files used are located in Appendix B.

4.1. Material and Methods

4.1.1. Navigational Paradigm

To study sequential learning, we developed a computational system representing a navigating rodent (Figure 4.1). The animal is assumed to have been trained to run with minimal hesitation in a correct sequence of three turns needed to receive a reward. In any scenarios, he is passing *en route* six visual landmarks demarcating an environment we refer to as VL. Each VL represents potential half of a place field activity, modeled as a Gaussian distribution of spike probability along an assumed occipital-parietal-temporal axonal pathway terminating in CA regions of the hippocampus. The correct sequence to get to the reward is a right turn, followed by a left turn, and finally a right turn (right-left-right or VL1-VL4-VL5). The total duration of one full run is nine seconds, including one second to reposition the animal to the beginning of the maze. The average speed of the animal is 22.5 cm/s for nine consecutive passes through the maze, which were analyzed. During the first pass, the animal made a right-left-left (VL1-VL4-VL6) sequence and did not get a reward. During the second trial, the animal was forced to make the correct sequence (right-left-right) and did get a reward, but it was considered not to have learned fully yet. After making the wrong sequence during the third pass, the rodent was again

biased to make the correct sequence during the fourth trial. During passes five through nine, the animal went directly to the reward showing its learning performance without any biasing, which means it took about four trials for the animal to fully learn a sequence of three decisions.

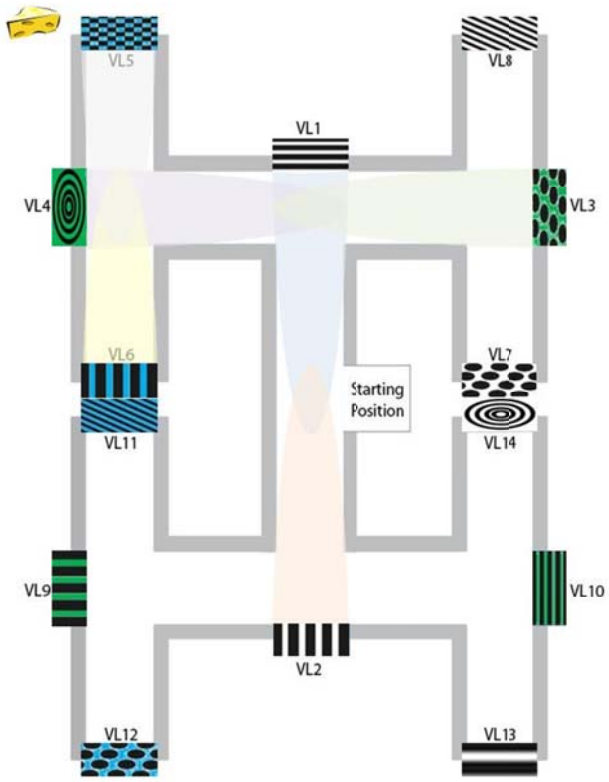

Figure 4.1: Simulated Navigational Environment

4.2.2. Computational Brain Model Implementation

This model included a total of 64760 leaky integrate-and-fire neurons arranged in 214 clusters. CA pyramidal cells were represented as quasi-bicompartmental (Izhikevich *et al.*, 2004) neurons by the inclusion of a population of single-compartment apical tuft cells that connect to the pyramidal somatic compartment. Entorhinal grid cell activation

at place-field boundaries followed by visual-parietal input triggered self-sustained, asynchronous background activity (RAIN networks) limited to the place field. For more details on our first model, please refer to Chapter 3 or Jayet Bray *et al.* (2010) [85].

From our previous model (chapter 3), we used additional variations of RAIN networks. To represent the prefrontal columns, 1600-cell RAIN subnetworks that included reward learning, represented each decision to turn left or right in the maze. Two types of learning were tried within the E-E connection of the prefrontal cortex: the first type of learning was STDP (Hebbian), which is a long-term learning that does not decay over time as much as the second type, synaptic facilitation depression (SFD), which is a short-term learning type. Subicular pyramidal neurons (SB and RS) and fast spiking interneurons (FS) were represented using K_{AHP} and HVA / LVA channels in the subiculum. The firing pattern of both SB and RS neurons are shown in Figure 4.2.

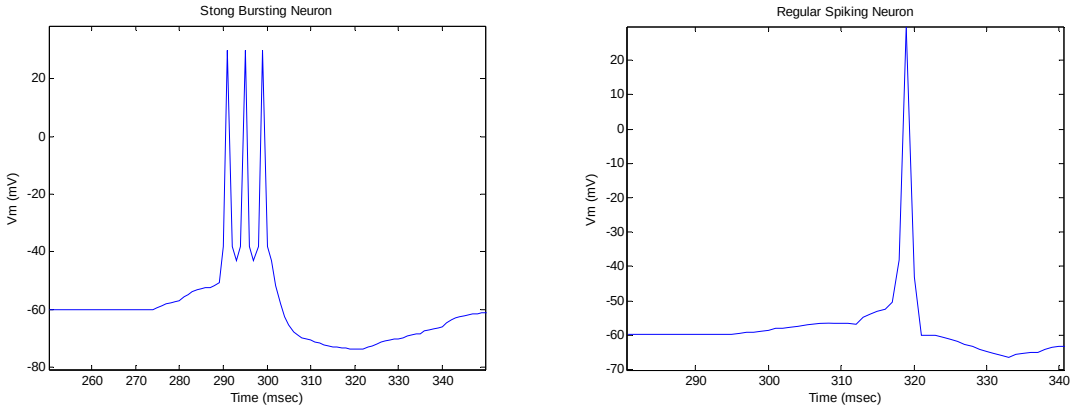

Figure 4.2: Subicular Pyramidal Neurons (SB and RS) Firing

Premotor cortex was modeled as a group of cells showing a left or right turn motion depending on the decision at any given time in the maze. Oscillating networks were used to represent theta activity in both the hippocampus and the prefrontal cortex.

4.1.3. Analytical and Statistical Methods

Spectral Analysis of Hippocampal and Prefrontal Theta Synchrony

We analyzed power spectra for both hippocampus and prefrontal oscillating LFP using multi-taper spectral analysis methods (mtspecgramc function from the Chronux toolbox, http://chronux.org, Figure). We also compared the coherence between the two rhythms using multi-taper spectral analysis methods (mtcohergramc function from the Chronux toolbox, http://chronux.org, Figure). Both analyses used custom written MATLAB-based programs, and they concerned periods starting when the animal entered the maze until it reached the end of the maze. The coherence was compared during the second decision in the maze, during trial 3 and trial 9 and also analyzed during decision time versus turning time.

Statistics

To assess reproducibility, we ran the entire simulation under ten different pseudo-random seeds. Firing pattern means and variances did not differ statistically from one run to the next.

4.2. Results

4.2.1. Model Description

Hippocampal, Entorhinal, and Prefrontal Loop Representation

Here, we represent a hippocampal-entorhinal-prefrontal microcircuitry loop. In chapter 3, hippocampal pyramidal cells were arranged into subnetworks, receiving inputs from sensory parietal-temporal axonal pathways responding to VL, entorhinal cell

populations, basket cells (BC) in the stratum oriens (SO), O-LM interneurons [96], and perforant pathway associated (PPA) interneurons [96]. We assumed that BC were activated by global CA activity and gave rise to theta (6-10 Hz) phasic field activity [4], which in turn was broadcast as inhibitory input to the proximal dendritic branches of the pyramidal cells. BC also inhibited O-LM interneurons, giving rise to anti-phase inhibitory theta activity that projected to dendritic tufts in SLM [92]. We also included two populations of entorhinal cells: (1) EC SG connecting to PPA interneurons, which in turn inhibited the pyramidal apical tufts, resulting in fewer cells responding in place fields, and (2) EC GC connecting to the basilar dendrites, responsible for triggering activity at the boundaries of place fields [63]. In the current model, left and right subicular pyramidal neurons were added as two groups of three subgroups of cells (SB, RS, and FS). Extrinsically, RS neurons received inputs from both CA pyramidal cells and prefrontal columns. This represented a feedback loop between the hippocampus and the prefrontal cortex, which seems to play a role in synaptic plasticity, and consequently memory [176] and dynamic goal-directed behavior [53]. Intrinsically, RS excited subicular interneurons (FS), which inhibited the opposite groups of RS and SB neurons, suppressing one turn alternative to favor the dominant choice. Prefrontal neurons were also organized in subnetworks receiving profuse projections from each hippocampal pyramidal networks [83] where each place field provided an increase in activity at a given place and time in the maze. Each subnetwork underwent learning if the correct sequence was chosen and the animal reached the reward. Finally, premotor neurons received inputs from both the subicular RS and prefrontal neurons to create the chosen

motion of the animal. The overall connectivity among regions is represented in Figure 4.3.

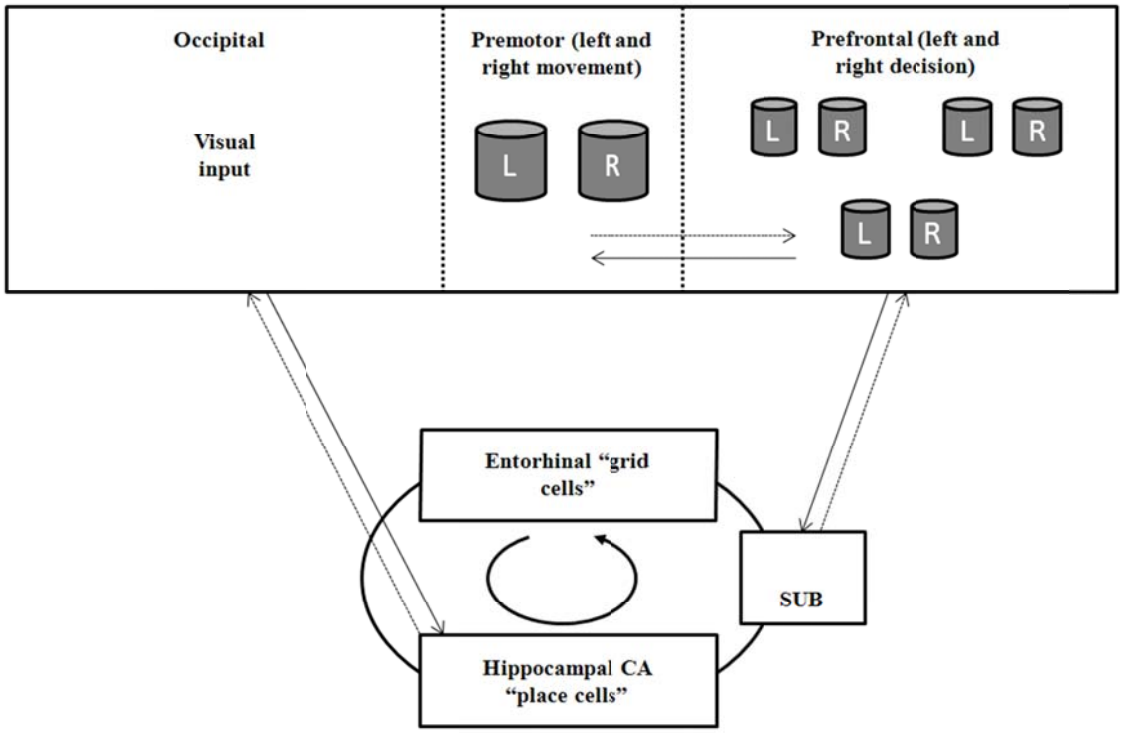

Figure 4.3: Connectivity Representation

Hippocampal, Entorhinal, and Prefrontal Modeling

The description of neuronal network models should communicate enough information for readers to comprehend and re-implement a model, and to compare different models (Nordlie *et al.,* 2009). Table 4.1 gives an outline of the model, which validates its implementation (See Section 4.1.2).

A	Model Summary	
Populations	CA pyramidal cells, axonal pathway (VL), EC cells (2 groups), basket cells (theta), OLM interneurons, PPA interneurons, subicular neurons (SB, RS, FS), prefrontal (PF) pyramidal cells (6 columns), PF theta, premotor (PM) cells (2 groups)	
Neuron Model	Leaky integrate-and-fire, fixed threshold, refractory time	
Plasticity	STDP or SFD	
Channel Model	K_{AHP}, HVA and LVA channels	
Synapse Model	Conductance-based	
Measurements	Membrane Potential	
B	**Populations**	
Name	**Elements**	**Size**
CA	5 RAIN networks	3,200 cells
VL	5 E cell groups	200 cells
EC SG	Linear positive current	N/A
EC GC	Current file based	N/A
BC (theta)	RAIN network	1,600 cells
OLM	I cell group	300 cells
PPA	Linear negative current	N/A
SB	2 E cell groups	80 cells
RS	2 E cell groups	80 cells
FS	2 I cell groups	20 cells
PF	6 RAIN networks	1,600 cells
PF (theta)	RAIN network	1,600 cells
PM	2 E cell groups	100 cells

C	Neuron and Synapse Model
Type	Leaky integrate-and-fire neurons, conductance-based synapses
Dynamics / Spiking	See Section 2.2.3 for equations
D	**Channel and Plasticity Model**
Channels / Plasticity	See Section 2.2.3 for equations
E	**Measurements**
Membrane potential V of all neurons	

Table 4.1: **Tabular Description of Model.** The model is summarized in panel A and detailed in panels B-E.

4.2.2. Model Analysis

Analytical and Numerical Experiments

The first part of model analysis is a description of analytical and numerical data used in the model, as shown in Table 4.2.

A	Extrinsic Connectivity	
Type	**Probability (%)**	**Conductance strength (mS)**
RAIN – BC	3	0.004
BC – CA	3	0.003
BC – OLM	3	0.2
OLM – VL	3	0.01
VL – CA	5	0.006
RAIN – PFt	3	0.004
PFt – PF	3	0.003
CA – PF	0.9	0.002
SB – FS	24	0.006

CA – SB	0.5	0.003
PF – SB	1	0.002
PF – PM	5	0.015
B	**Intrinsic Connectivity**	
FS – RS	20	0.008
FS – SB	20	0.008
SB – RS	10	0.006
C	**Input**	
Type	**Description**	
Visual cortex	2 second Gaussian distribution (5 of them)	
Entorhinal cortex (SG) / PPA	Linear negative current suppressing CA networks (50%) with amplitude of -4 mA and constant duration	
Entorhinal cortex (GC)	File based current exciting CA networks (100%) with amplitude of 3 mA and duration of 300 ms	
PFt suppress	Linear current suppressing PF networks (100%) with amplitude of 4 mA and duration of 1 sec	
Biasing	Pulse current biasing of 2 mA and duration of 500 ms	

Table 4.2: **Tabular Analysis of Model.** The description of the model connectivity is shown in panel A (extrinsic) and B (intrinsic) and the model input is given in panel C.

The second part of model analysis is a description of the results obtained.

Brain Loop Dynamics

The firing pattern of each brain region used in our model during nine consecutive runs through the maze is presented in Figures 4.4 a-c. In these results, STDP was used such that prefrontal activity remained continuously active once the animal had fully learned (after trial 4). STDP had positive fractional changes in synaptic strength ($+W$) of

0.0059 and negative fractional changes in synaptic strength ($-W$) of 0.003, with positive window ($+A$) of 50 ms and negative window ($-A$) of 90 ms, and with positive decay constant ($+\tau$) of 15 ms and negative decay constant ($-\tau$) of 30 ms. The hippocampal place fields (green rectangle) fire appropriately with respect to the position of the mouse in the maze. For instance, the first row represents a place field, which corresponds to VL1 where the second row represents a second place field that corresponds to VL2. When the mouse is located at a decision point, both landmarks, VL1 and VL2 are seen equally until the animal decides to go one direction towards one specific landmark. Then the place cells responsible for firing when VL1 is seen become more active. The subicular area (purple rectangle) firing shows a winner-take-all firing pattern, which corresponds to every decision the animal made. The first and third rows represent a left decision when the second and forth rows represent a right decision. The first two rows represent SB neuron firing and the last two rows show RS neuron activity. The prefrontal region (blue rectangle) is firing accordingly to the CA input. Each row represents one of the six decisions in the order of landmarks (VL1-VL6). Each column underwent STDP when the animal got a reward (R). The premotor area (red rectangle) shows a left motion (second row) followed by two right motions (first row) during the first run, for example. The field potential is shown at the top of the figure where a gamma frequency is seen at the end of every run for one second. This is the time we assumed it would take to reposition the animal at the beginning of the maze for the next run.

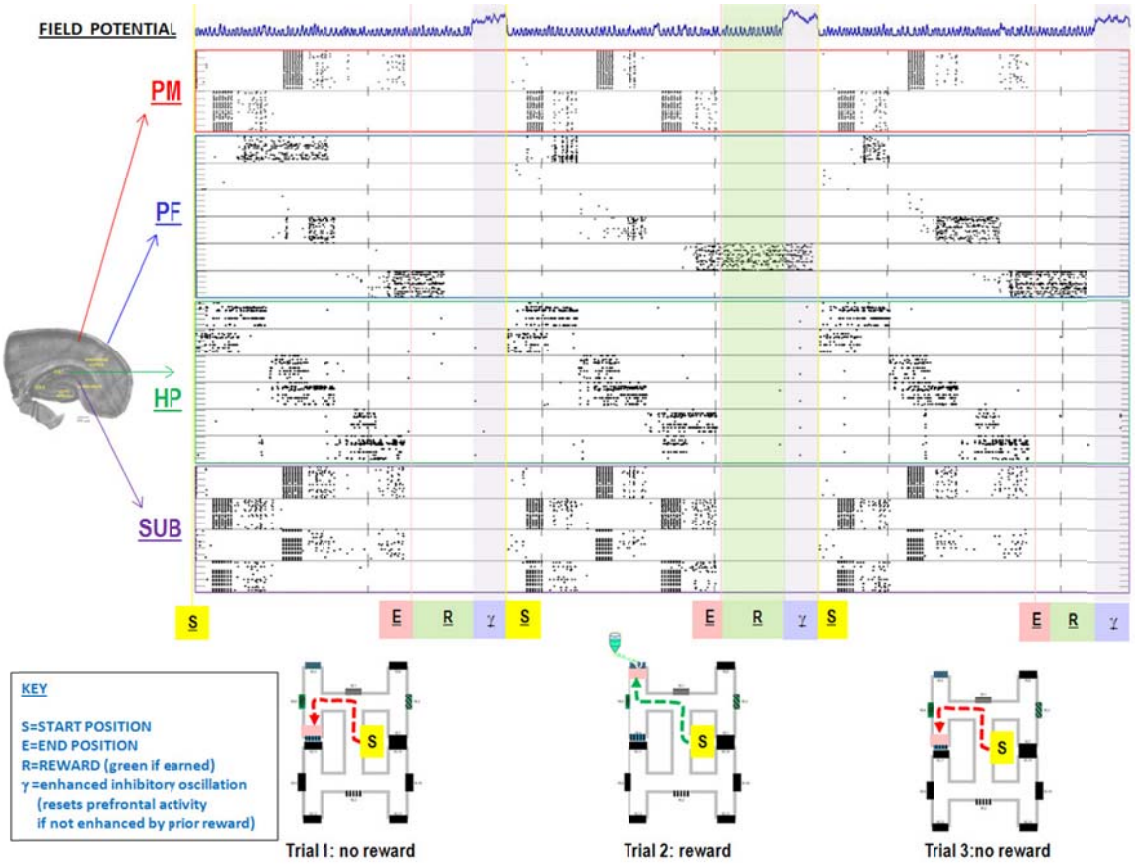

Figure 4.4a: **Brain Loop Dynamics.** Trials 1-3.

After four to five trials through the maze and biasing the sequence towards the reward, the animal seems to have fully learned. Without any biased decisions, trials 5 through 9 (Figure 4.4b-c) show the correct sequence and according firing in each of the regions. The prefrontal area remains active until the end of trial 9 to reinforce the subiculum neurons for further runs through the maze.

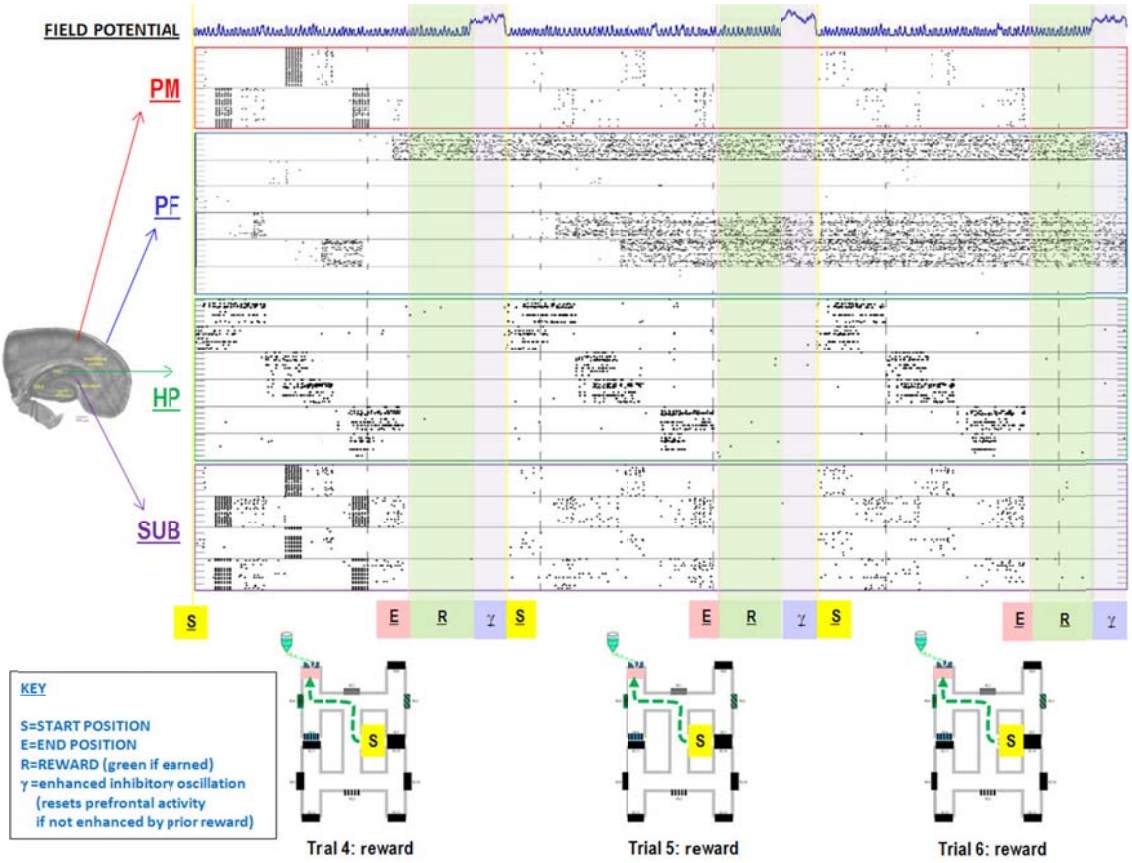

Figure 4.4b: **Brain Loop Dynamics.** Trials 4-6.

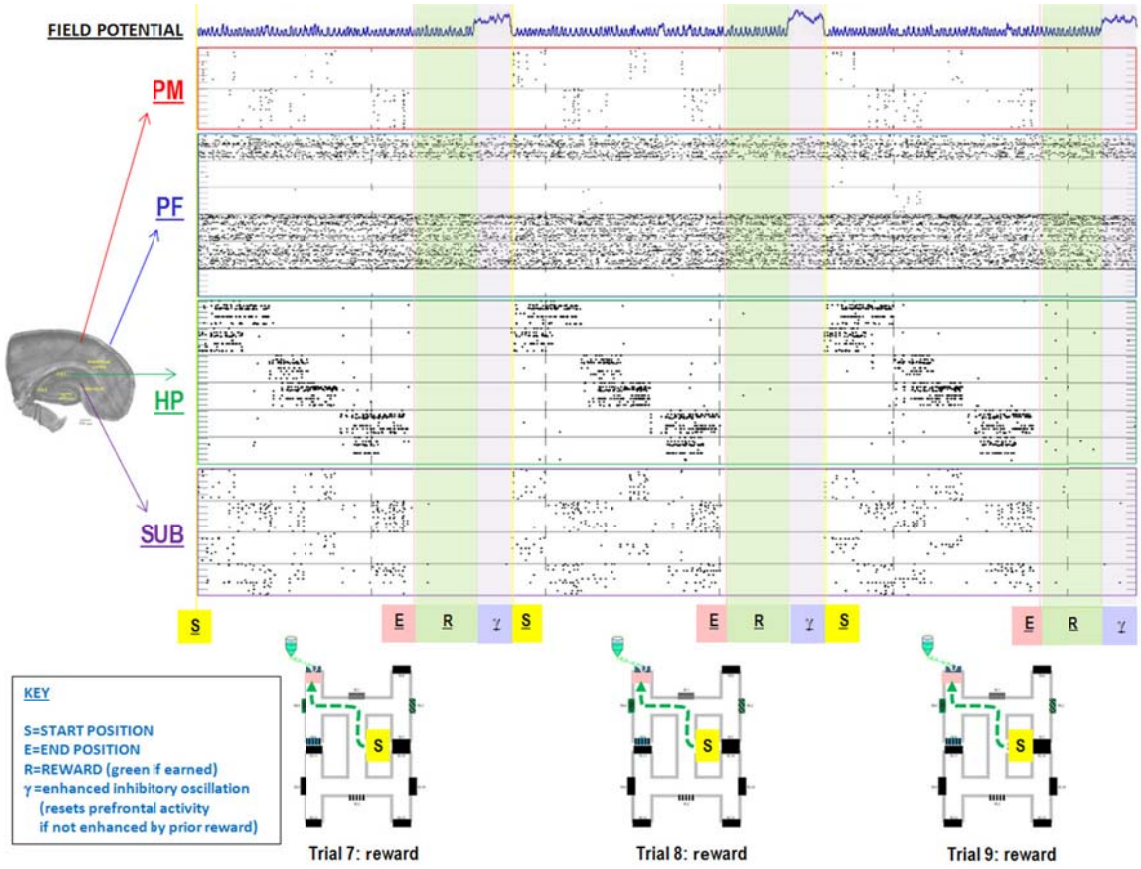

Figure 4.4c: **Brain Loop Dynamics.** Trials 7-9.

The firing pattern of each brain region used in our model during nine consecutive runs through the maze is presented in Figures 4.5 a-c. However, in these results, STDP was used such that prefrontal firing remained active accordingly with hippocampal activity and the position of the animal in the maze. STDP had positive fractional changes in synaptic strength ($+W$) of 0.0055 and negative fractional changes in synaptic strength ($-W$) of 0.003, with positive window ($+A$) of 50 ms and negative window ($-A$) of 90 ms, and with positive decay constant ($+\tau$) of 15 ms and negative decay constant ($-\tau$) of 30 ms.

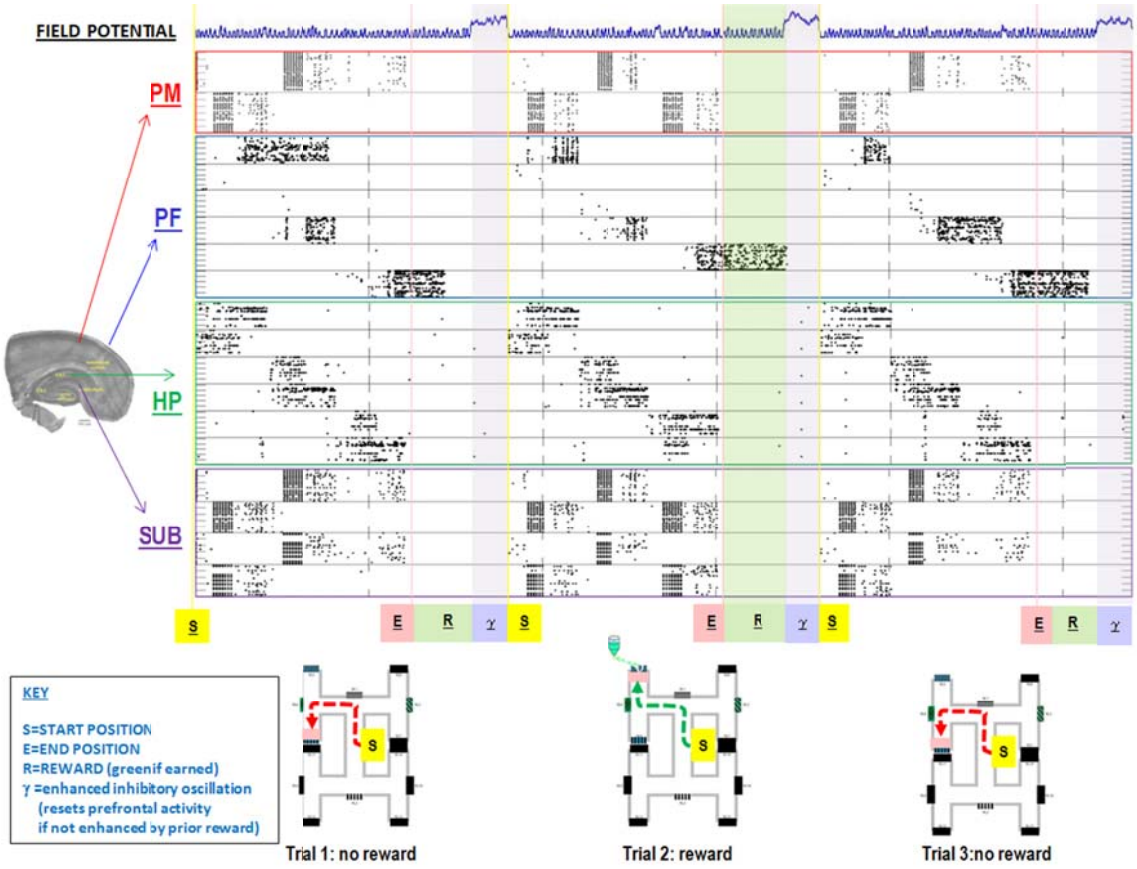

Figure 4.5a: **Brain Loop Dynamics.** Trials 1-3.

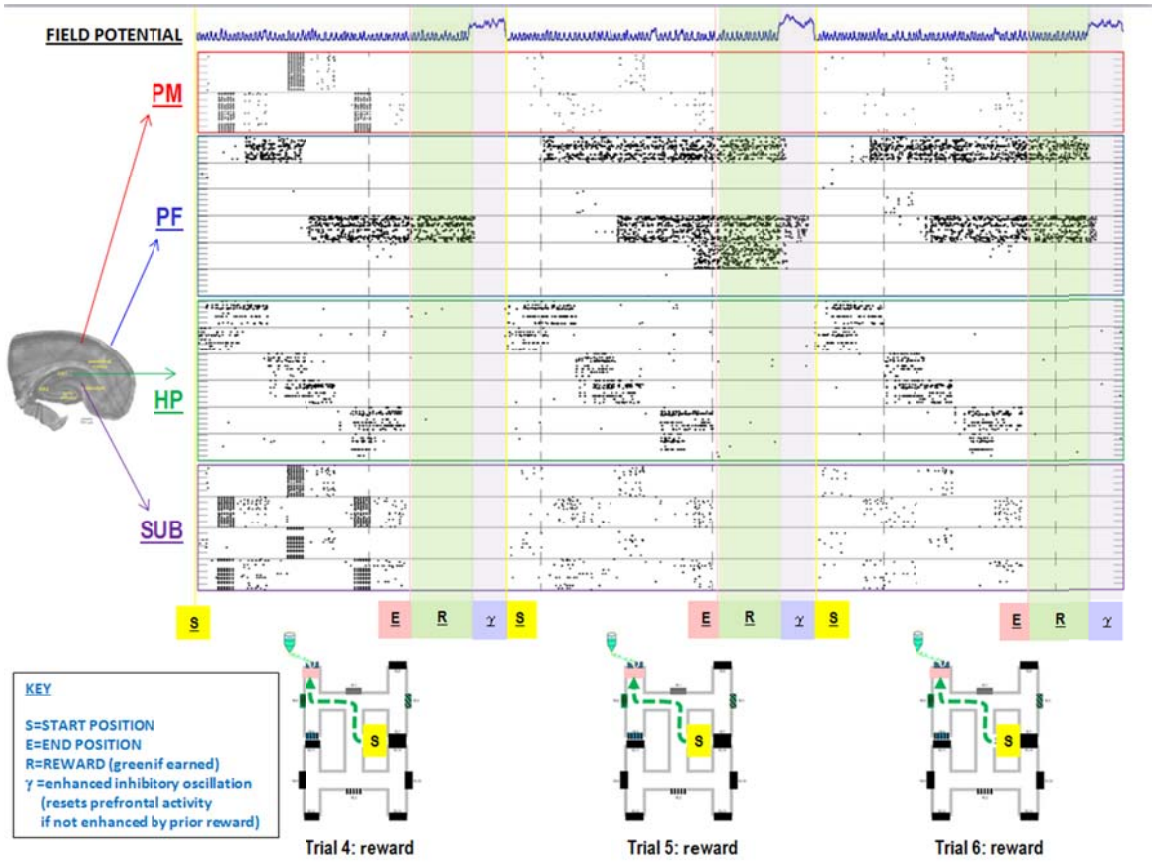

Figure 4.5b: **Brain Loop Dynamics.** Trials 4-6.

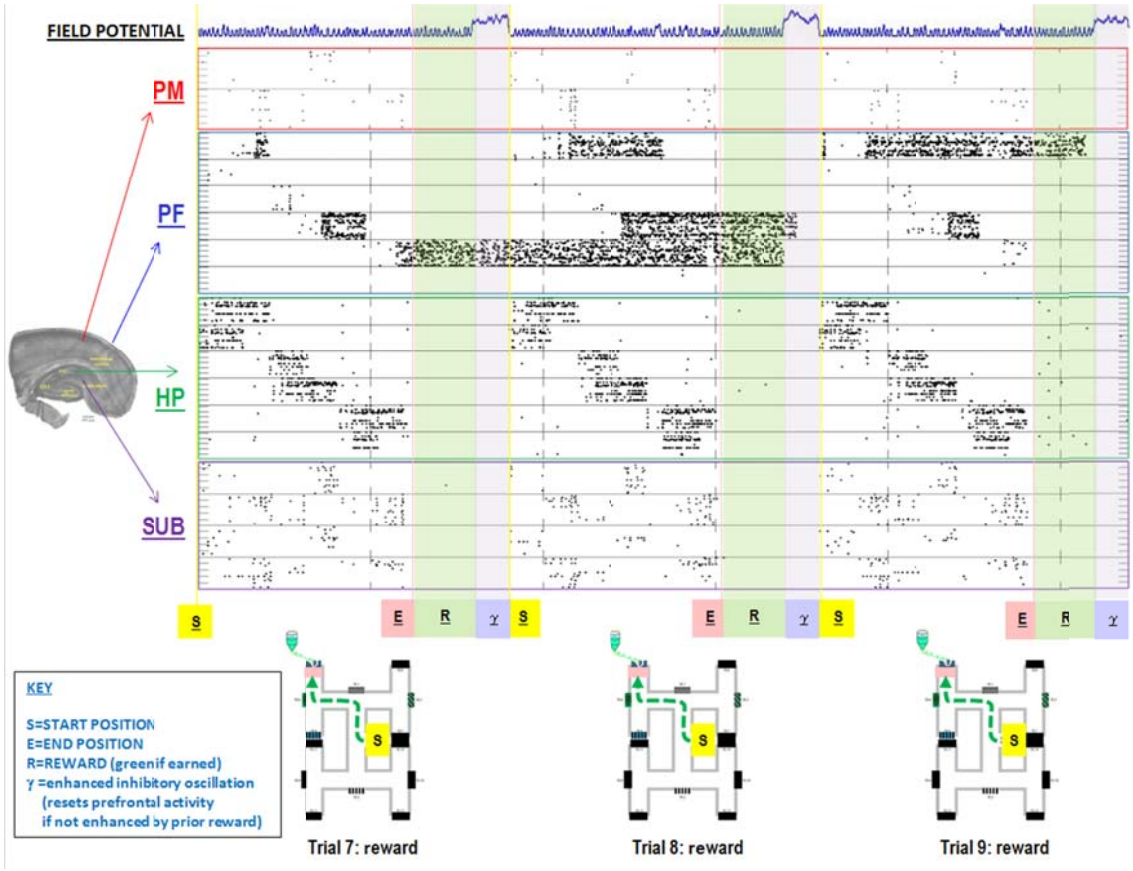

Figure 4.5c: **Brain Loop Dynamics.** Trials 7-9.

When each prefrontal column underwent SFD when the animal got a reward, the firing pattern of the prefrontal cortex, and consequently the subiculum and the premotor cortex was not representative of the sequential and navigational learning.

Hippocampal and Prefrontal Coherence

After trying different learning settings within the prefrontal cortex, we decided to look at the coherence between hippocampal and prefrontal oscillations. When STDP was higher, the coherence between the two regions was not significant (<0.5). Figure 4.6 A and B show the power of hippocampal (top) and prefrontal (middle) LFPs, and the coherence between the two as a function of frequency (bottom) for trial 3 and trial 9,

respectively. Figure 4.6 C and D represent the spectrograms of hippocampal and prefrontal LFPs (top and middle) and the coherogram during two representative trials (3 and 9 respectively). In this scenario, band coherence did not peak at the maze choice point, where hippocampal and prefrontal amplitudes are not maximal. Figure 4.6 E shows the overall coherence as less than 0.5 between trial 3 (red) and trial 9 (black) as a function of frequency.

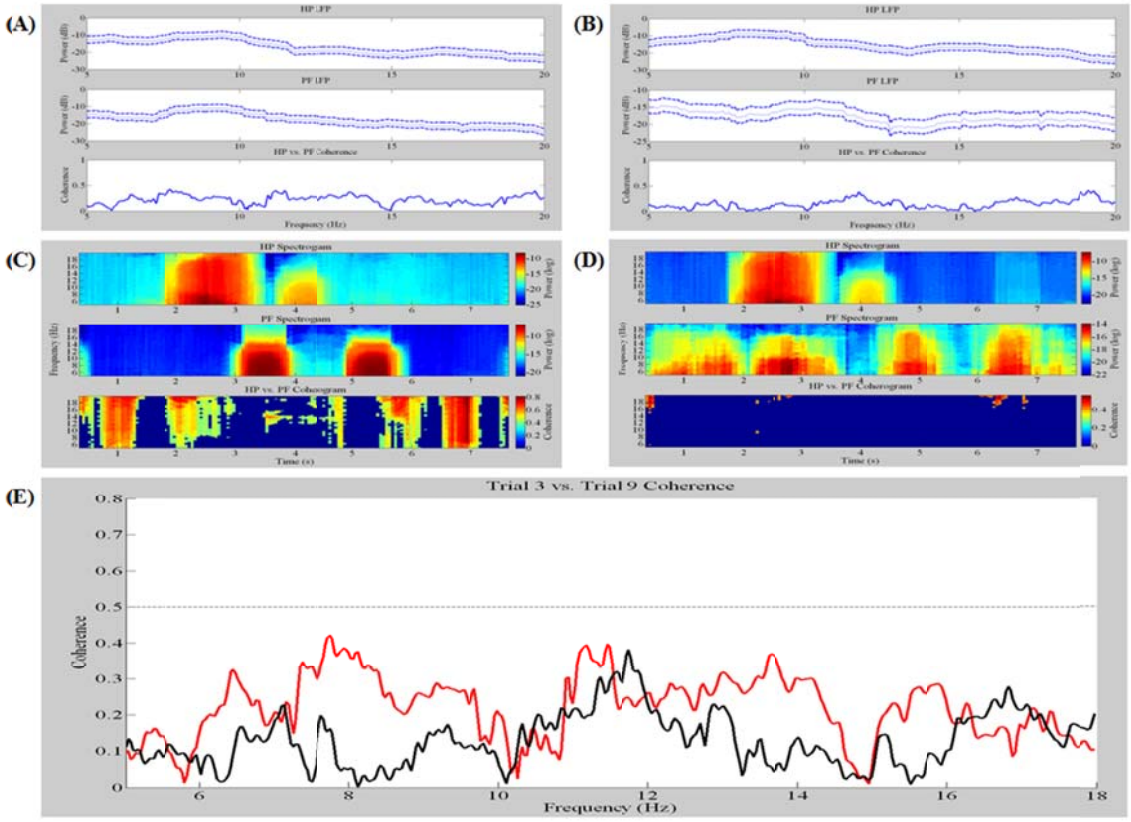

Figure 4.6: Characterization of Hippocampal-Prefrontal Coherence

When STDP was lower, the coherence between the two regions was significant (>0.5). Figure 4.7 A and B show the power of hippocampal (top) and prefrontal (middle) LFPs, and the coherence between the two as a function of frequency (bottom) for trial 3

and trial 9, respectively. Figure 4.7 C and D represent the spectrograms of hippocampal and prefrontal LFPs (top and middle) and the coherogram during two representative trials (3 and 9 respectively). In this scenario, band coherence peaks at the maze decision point. Figure 4.7 E shows the overall coherence as a function of frequency. It is above 0.5, which is significant between trial 3 (red) and trial 9 (black), upon learning.

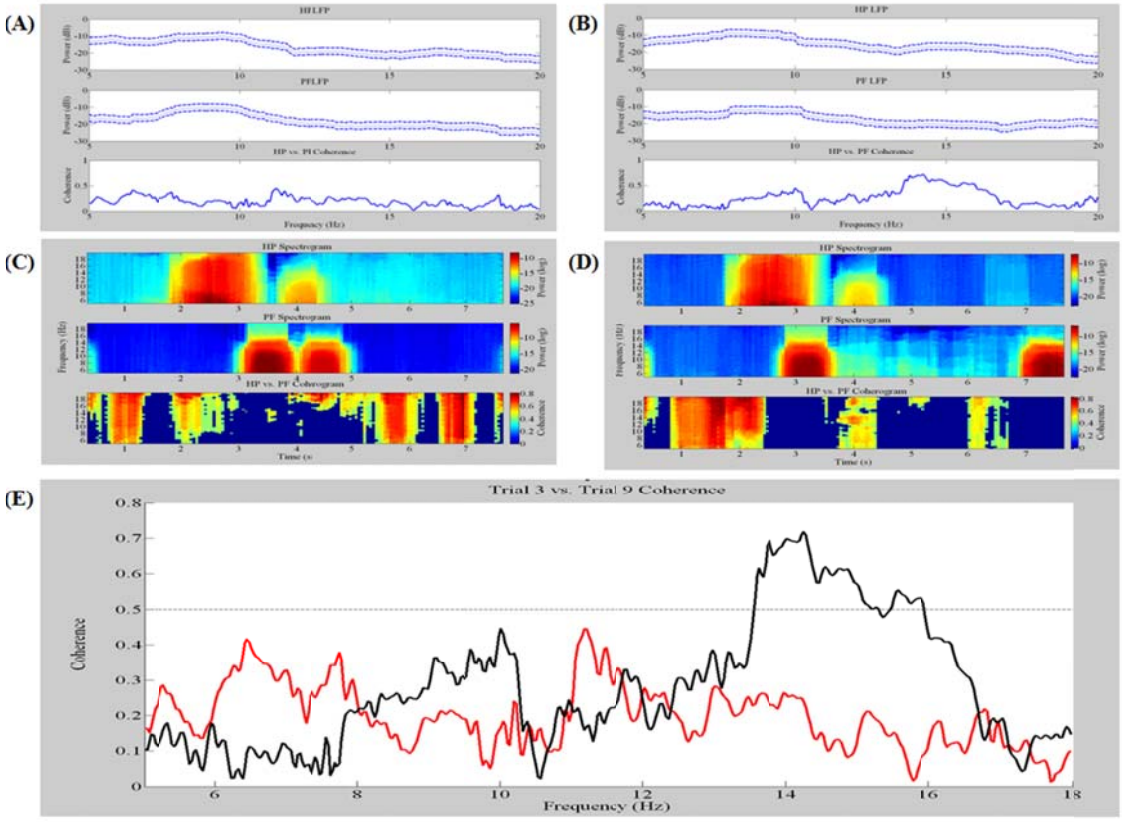

Figure 4.7: Characterization of Hippocampal-Prefrontal Coherence

4.3. Discussion

In addition to the findings of our previous model [85] regarding hippocampal-entorhinal dynamics, we report two unique circuit-level network features that can explain a closed loop with the prefrontal cortex during spatial working memory: (1) Hebbian

plasticity in the prefrontal areas and (2) winner-take-all behavior within the subiculum using K_{AHP} and HVA / LVA channels. STDP provided long-term learning from the hippocampus and also delivered appropriate learning in the prefrontal cortex to reinforce memory back to the hippocampus.

Both K_{AHP} and HVA / LVA channels helped reproduce three subicular dynamics, whose interconnectivity favored one decision over two conflicting choices. The intrinsic connections within the structure represented a winner-take-all scenario that helped the animal make a decision, which was reinforced by the prefrontal cortex. This subiculum deciding role supported the conflicting goal processing theory described by Mc Naughton *et al.* (2006) [123] and Naber *et al.* (2000) [134].

Our incorporation of STDP in the excitatory connections within the place cell networks and within prefrontal networks resulted in the cooperativity between the hippocampus and the prefrontal cortex in synaptic plasticity [40, 94]. These findings demonstrated how learning and consolidation could work between the two structures during spatial working memory. It also showed the importance of synaptic strengths within and among structures during navigational sequences, decision making, and learning reinforcement. However, defining STDP parameters precisely within the prefrontal area was crucial to have appropriate learning.

Our findings demonstrated that STDP positive fractional changes in synaptic strength had to be a little lower than 0.006 for hippocampal place cells to have a positive impact on the prefrontal cortex. Based on this parameter, the coherence, including both phase and frequency of the prefrontal cells to hippocampal oscillations during performing a task was consistent with biological findings of Sigurdsson *et al.* (2010) [159] and

Benchenane *el al.* (2010) [9]. Hippocampal-prefrontal coherence increased as the animal at the decision point in the maze, in particular after learning acquisition when reward occurred.

This first hippocampal-entorhinal-prefrontal circuit-level model demonstrated some important dynamics between the hippocampus, the entorhinal cortex, and the prefrontal cortex. Both the extrinsic and intrinsic connectivity of these structures gave a good representation of every region dynamics during spatial working memory. It also learning within both the hippocampus and the prefrontal cortex is crucial for a higher coherence between the two structures.

We speculate that transient activation of neural architectures consistent with RAIN-like networks may subserve hippocampal CA place field and prefrontal dynamics. This insight is important to better understand not only mammalian navigation but more complex episodic and semantic short-term memory, working memory and mechanisms of long-term memory consolidation and reconsolidation.

CHAPTER 5: BRAIN SLICE EXPERIMENTS

Brain slice experiments require precise, rapid, and accurate techniques to obtain best results. In these experiments, C57BL/6 mice (Figure 5.1) were used in accordance with National Institutes of Health (NIH) guidelines, and all procedures were reviewed and approved by the Downstate Medical Center Animal Care and Use Committee.

Figure 5.1: A Mouse Prior to Experiments

5.1. Materials and Methods

5.1.1. Brain Removal

The animal was anesthetized with 5% halothane and decapitated, as shown in Figure 5.2.

Figure 5.2: Head Decapitation

The outside layer (fur, skin…) was cut with scissors along the sagital axis from the caudal (posterior) to the rostral (anterior) part (Figure 5.3 A). The skull was then cut along the same axis (Figure 5.3 B) to access the brain. Using a curved spatula, the brain was carefully removed from the skull, as seen in Figure 5.3 C.

(A) **(B)** **(C)**

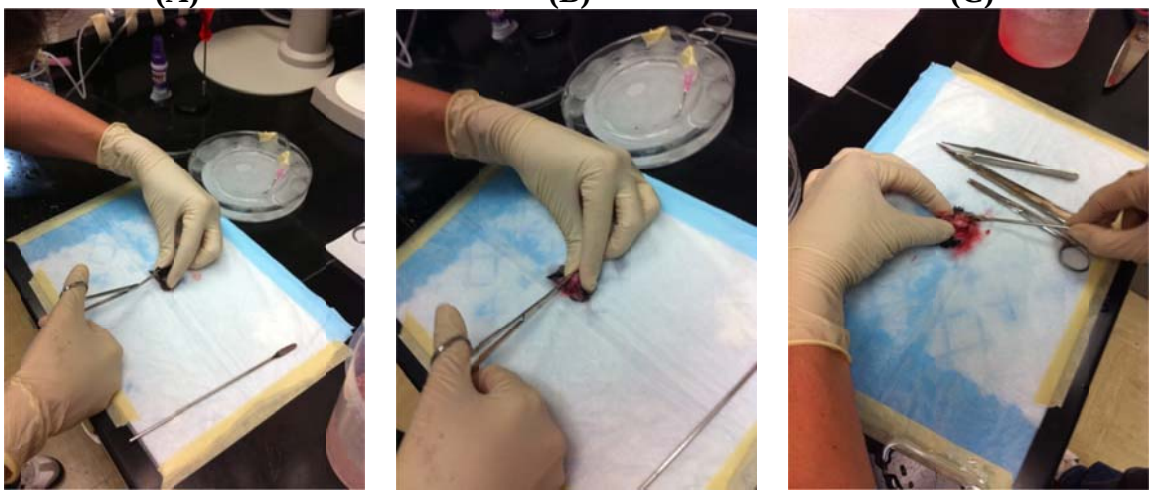

Figure 5.3: Brain Removal Steps

After removal (Figure 5.4 A), the brain was put in ice-cold ACSF cutting solution (in mM: NaCl 126, KCl 2.5, $CaCl_2$ 2, $MgCl_2$ 1, KH_2PO_4 1.25, $NaHCO_3$ 25, and glucose

20; pH 7.4, when exposed to 95% O_2 / 5% CO_2) and was allowed to sit for a few minutes before slicing (Figure 5.4 B, C).

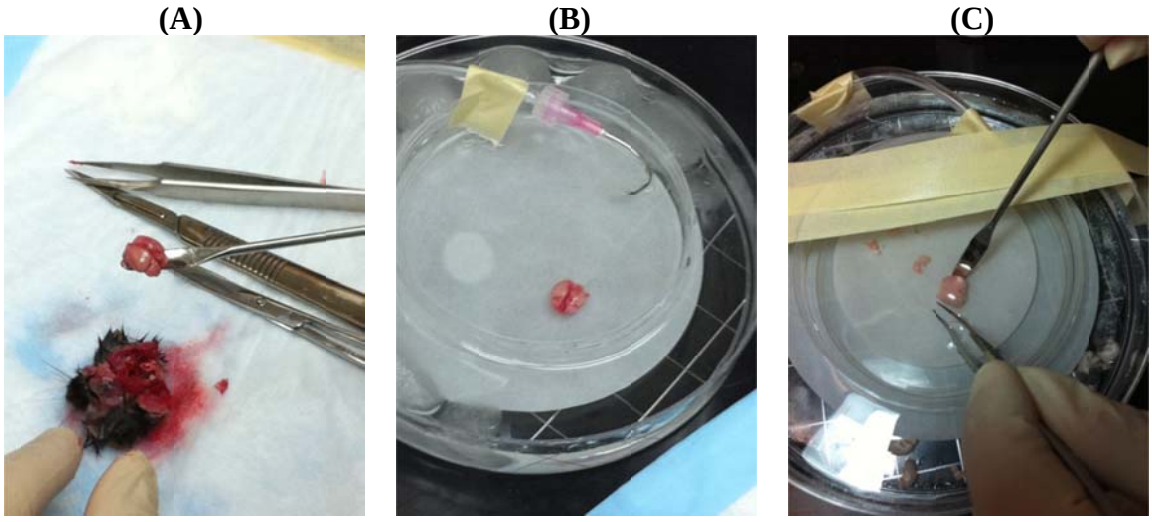

Figure 5.4: After Brain Removal

5.1.2. Brain Slice

The cerebellum and rostral pole of the brain were slightly dissected away. The whole brain was then mounted to a vibratome chuck using glue (Figure 5.5 A, B). Thin slices (400 µm) were cut using a Leica VT 1200 S sectioning system, which included portions of the hippocampus and parahippocampal areas, as shown in Figure 5.5 C). Slices were then transferred into a holding chamber that contained ACSF perfusing solution. Slices were incubated for one hour at room temperature until final transfer to the recording setup.

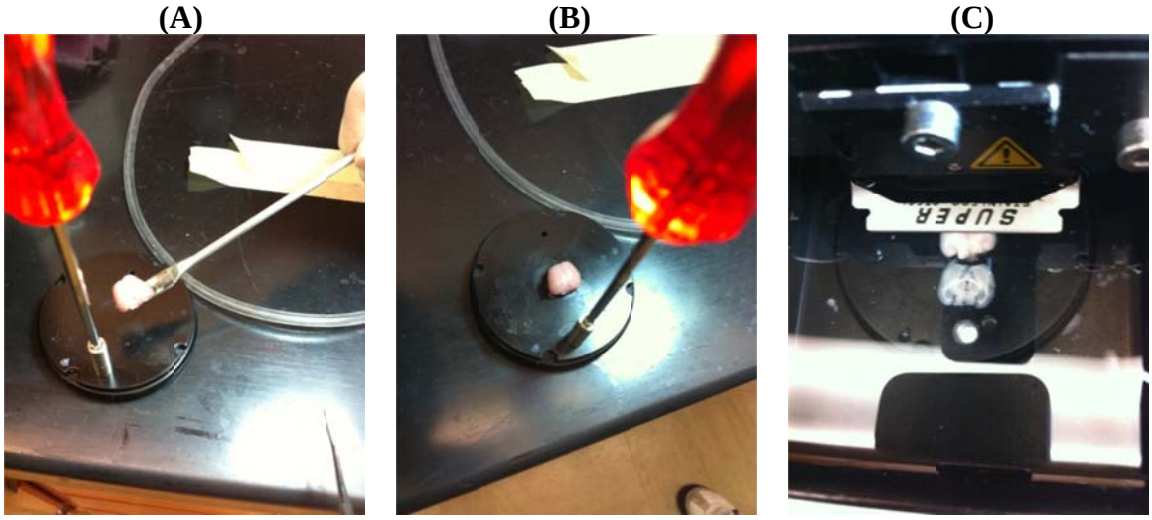

Figure 5.5: Slice Procedures

From the holding chamber, single slices were placed on a nylon mesh support in the recording chamber in the set-up shown in Figure 5.6 A, B.

Figure 5.6: Recording Set-up

5.2. Results

To obtain the desired slices of hippocampus and parahippocampal areas, important factors have to be set effectively and accurately. The vibration frequency was set at 85 Hz and the slicing speed of the blade was adjusted to 0.24 mm/s to prevent the tissue being pushed while cutting the slices. The amplitude was 0.95 µm.

The angle is critical to obtain the right brain regions that are important to the study. The brain was glued on its base with the rostral part facing forward, and slightly tilted upward at approximately 10º-15º angle. The vibratome blade was also set at an angle of 15º-21º, slicing from the top of the rostral portion to the bottom of the caudal portion, shown in Figure 5.7.

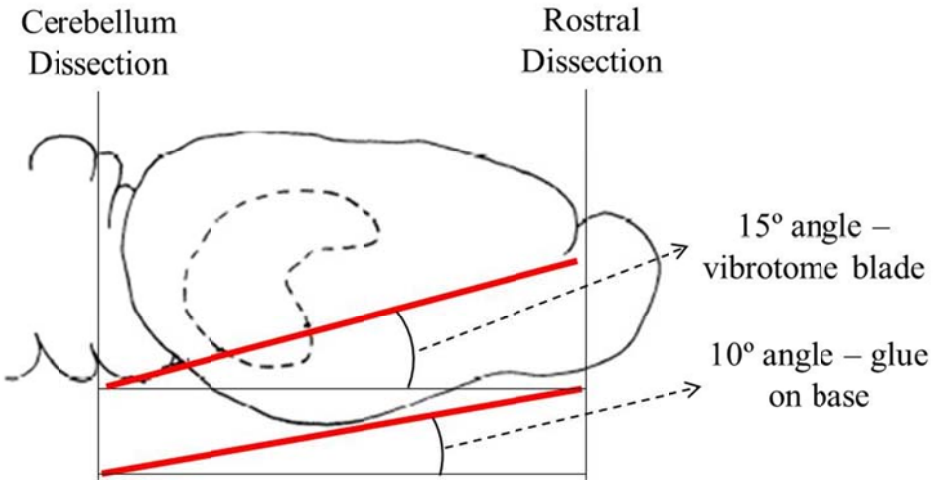

Figure 5.7: Slicing Angle (Modified from [89])

Figure 5.7 shows the regions of interest obtained from the slicing, portions of hippocampus (Figure 5.8 A), and both hippocampus and entorhinal cortex (Figure 5.8 B).

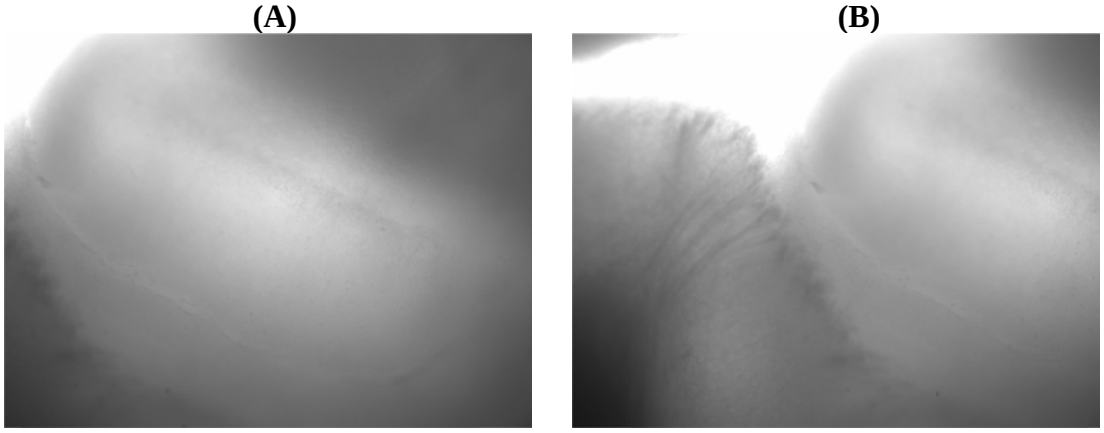

Figure 5.8: Slice Images

Recording experiments will be conducted in future work, and they are described in Section 6.3.2.

5.3. Discussion

To obtain optimal hippocampal – entorhinal slices with minimal damage of the neurons, we developed a fast, easy, and successful technique. Working with the size of mice brains has been a challenge in comparison to rat brains that are much bigger. However, in the long term, recordings on mice's neurons will be beneficial because of the recent increases in the use of genetically defined mouse lines, which have made mice an important animal model for research.

After rapidly removing the brain from the skull, slicing speed, frequency, and angle are crucial to a successful hippocampal – entorhinal study. The speed has to be close to maximal and the frequency has to be optimal to avoid trauma to the tissue. Last but not least, we found accurate angles to optimize the visualization of both the hippocampus and the entorhinal cortex on a same slice. Positioning the brain at an approximately 10º angle on its caudal base, where the rostral portion faced up was important as the first step of slicing. Then, slicing at a 15º angle from an upper position down to the caudal portion of the brain was the second key step of slicing. Once the hippocampal – entorhinal slices are obtained recording experiments can be done and are presented as future work (See Section 6.3.2).

CHAPTER 6: CONCLUSIONS AND FUTURE WORK

6.1. Conclusions

Computational neural modeling and *in vivo / in vitro* experiments should exchange findings to not only investigate complex brain dynamics that underlie behavior, memory, and learning, but also understand and treat neurologic disorders. Computational models lead to theoretical advances in the field of neuroscience so that some of the predictions can be biologically represented and experimentally tested.

In this study, we not only present two neural models, but also suggest relevant biological experiments that could lead to interesting findings in brain dynamics during navigational learning. The first model described unique circuit-level network features that could explain both intracellular and extracellular CA place field dynamics observed while navigating on a linear track. Our RAIN networks, combined with entorhinal excitatory and inhibitory cells groups provided hippocampal dynamic results similar to *in vivo* studies. In particular, RAIN networks that incorporated K_{AHP} channels, which provided a mechanism for the *in vivo* asymmetry of intracellular place field ramp of depolarization. Additionally, these dynamics explain the apparent population-rate discordance and the role of entorhinal cortex in stabilizing hippocampal place field activity.

The second model described hippocampal-entorhinal-prefrontal circuit-level dynamics during sequential learning. It demonstrated how important learning is within the prefrontal areas and how the subiculum acts as a winner-take-all using K_{AHP}, HVA and LVA channels. STDP provided both short-term learning within the hippocampus and delivered long-term consolidation to reinforce working memory back to the hippocampus, especially the subiculum. Additionally, coherence, including both the

phase and the frequency of the prefrontal cells to hippocampal oscillations increased at the decision point and upon learning, which was consistent with biological findings.

Last, experimental slicing techniques provided important protocols to obtain viable hippocampal–entorhinal slices. Hippocampal recordings following entorhinal cortex stimulation could lead to important findings on extrinsic connectivity between the two structures. Multiple electrode arrays are something interesting to consider, but they come with their own set of challenges, compared with intracellular single cell studies. In some experiments, recording field EPSPs and IPSPs can help to get population, rather than single neuron responses, but it depends on the experimental question. Patch clamping recording alternatives are described in Section 6.3.2.

6.2. Contributions to Neuroscience

Computational modeling is an approach to understanding the information content of neural signals by simulating some parts of the nervous system at many different structural scales, including the biophysical, the circuit, and the systems levels. Computer simulations of neurons and neural networks are complementary to traditional techniques in neuroscience, and lead to important hypotheses that could be tested experimentally. Here, we have demonstrated beyond the shape of pyramidal cells, some of their synaptic connectivity, and the network they impact in the temporal and frontal lobes. Specifically, the two models presented in this study have yielded crucial information on hippocampal, entorhinal, and prefrontal dynamics in relation to memory and learning, but there are still a lot to discover on a complex organ like the brain.

6.3. Future Work

Despite these fundamental findings in this dissertation, there are many discoveries that can still be made, both computationally and experimentally.

6.3.1. Computationally

Our updated model already contains many important biological-like features replicating dynamics in several areas of the brain, but additional important information can be simulated to make it even more realistic. For instance, more channel types and synapses should be further used because of their responsibility for most essential neuronal processes.

The hippocampus is modeled as two regions, CA and subiculum, but since the dentate gyrus seems to play a role in place sensitivity, especially in novel environments, it should also be included. The dentate gyrus is considered to be the main input region of the hippocampus, where entorhinal grid cells (layer II) provide monosynaptic projections to the granule cells [31], which are necessary for normal spatial-learning [121]. Also, the dissociation between grid cells and place cells was shown to arise in the entorhinal-dentate projection [70].

The entorhinal cortex should also be modeled as its own structure instead of just an input source because of its importance in spatiotemporal representation. Phase-coding between entorhinal and hippocampal theta activity has been found to influence memory formation in a theoretical model [183], and the two oscillations have been shown to be independent in humans *in vivo* studies [128]. Therefore, the hippocampus and the entorhinal cortex should have two way connections as a feedback loop. Also, in a freely

moving rodents study, both the intrinsic firing frequency of grid cells and theta frequency increased with running speed [86], which showed that the entorhinal cortex plays a significant role in spatial navigation.

Phase precession is a phenomenon present not only in the hippocampus, but also in the entorhinal and prefrontal cortices. Related to theta phase synchrony seen between the hippocampus and the prefrontal, phase precession in the prefrontal cortex is relative to the one in the hippocampus [87] during working memory tasks. However, phase precession in the entorhinal cortex seems to be independent from the hippocampus [62]. These phenomena are important and must also be considered in our future simulations as well.

Other cortices play important roles in memory, especially navigational learning. For instance, the parietal cortex seems to be involved in many different aspects of spatial information processing [154]. Ultimately, humans have shown to have different functions in the left and right hemispheres of the brain, also seen in the hippocampus [117]. Despite the limitations of computer hardware for larger simulations, further models should include most known brain areas involved in spatial navigation, and differentiate the two sides of the brain for multiple function purposes.

Our lab and collaborators are working on improving our computer hardware and software to simulate large-scale neural networks. The goal is to integrate 10^6 neurons and 10^{10} synapses into the architecture, which would lead to a million-cell model. Finally, a virtual environment was created to test the functionality of our models. It will be used in further studies for real-time simulations in combination with our new computer technology.

6.3.2. Experimentally

Now that the fundamental slicing procedure has been described, we discuss recording techniques that can be used. One alternative to consider is multiple electrode arrays, also known as multielectrode arrays contain plates through which neural signals are obtained. Their main advantage is to simultaneously receive data from multiple sites, which would be optimal when recording between two regions with a probability of connection is as low as 5%. However, they come with their own set of challenges, such as low spatial resolution. On the other hand, intracellular single cell recording gives more detail on one individual neuron by measuring voltage and/or current across the membrane to measure its resting potential and action potential.

Our results suggest further biological experiments to test our proposed mechanistic explanation in our first model. First, stimulation of subsets of entorhinal perforant path axons should result in enhanced tonic inhibition of CA pyramidal cells. Then, knock-out or knock-in experiments (potentially with rhodopsin optical modulation or monitoring) will test the role of specific CA interneurons. Finally, pharmacologic blockade or agonists of K_{AHP} channels [165] should modulate theta field activity of *ex vivo* hippocampal preparation [59]. In our second model, single-cell intracellular recording experiments within the subiculum could test the interconnectivity between RS, SB and FS neurons. Finally, multiple electrode recording experiments to verify synaptic strengths in between and within the hippocampus and the prefrontal cortex.

Therefore, when the connectivity between two regions is very sparse, such as the one between the hippocampus and the entorhinal cortex, single-cell intracellular recording would not be optimal, especially if EPSPs and/or IPSPs from the hippocampus

after stimulating the entorhinal cortex have to be identified. In some cases though, such as recording within the subiculum to identify the interconnectivity between SB, RS and FS neurons, this recording may be a better option. In other cases, such as recording connections between two major areas, such as the hippocampus and the prefrontal cortex, multielectrode arrays could be a better choice. As a further research project, these recording techniques will be tried and used for improving model parameters.

REFERENCES

[1] Albasser, M. M., Poirier, G. L., and Aggleton, J. P., "Qualitatively different modes of perirhinal-hippocampal engagement when rats explore novel vs. Familiar objects as revealed by c-fos imaging," *European Journal of Neuroscience,* vol. 31, pp. 134-147, 2010.

[2] Alger, B. E. and Nicoll, R. A., "Epileptiform burst afterhyperpolarization - calcium-dependent potassium potential in hippocampal ca1-pyramidal cells," *Science,* vol. 210, pp. 1122-1124, 1980.

[3] Amaral, D. G. and Witter, M. P., "The 3-dimensional organization of the hippocampal-formation - a review of anatomical data," *Neuroscience,* vol. 31, pp. 571-591, 1989.

[4] Andersen, P. M., R. Amaral, D. Bliss, T. O'keefe, J., *The hippocampus book*. New York, NY: Oxford University Press, 2006.

[5] Baeg, E. H., Kim, Y. B., Kim, J., Ghim, J. W., Kim, J. J., and Jung, M. W., "Learning-induced enduring changes in functional connectivity among prefrontal cortical neurons," *Journal of Neuroscience,* vol. 27, pp. 909-918, 2007.

[6] Balter, M., "Did working memory spark creative culture?," *Science,* vol. 328, pp. 160-163, 2010.

[7] Bast, T., Wilson, I. A., Witter, M. P., and Morris, R. G. M., "From rapid place learning to behavioral performance: A key role for the intermediate hippocampus," *Plos Biology,* vol. 7, pp. 730-746, 2009.

[8] Bear, J., Fountain, N. B., and Lothman, E. W., "Responses of the superficial entorhinal cortex in vitro in slices from naive and chronically epileptic rats," *Journal of Neurophysiology,* vol. 76, pp. 2928-2940, 1996.

[9] Benchenane, K., Peyrache, A., Khamassi, M., Tierney, P. L., Gioanni, Y., Battaglia, F. P., and Wiener, S. I., "Coherent theta oscillations and reorganization of spike timing in the hippocampal-prefrontal network upon learning," *Neuron,* vol. 66, pp. 921-936, 2010.

[10] Bi, G. Q., "Spatiotemporal specificity of synaptic plasticity: Cellular rules and mechanisms," *Biological Cybernetics,* vol. 87, pp. 319-332, 2002.

[11] Blair, H. T., Welday, A. C., and Zhang, K. C., "Scale-invariant memory representations emerge from moire interference between grid fields that produce theta oscillations: A computational model," *Journal of Neuroscience,* vol. 27, pp. 3211-3229, 2007.

[12] Bliss, T. V. P. and Collingridge, G. L., "A synaptic model of memory - long-term potentiation in the hippocampus," *Nature,* vol. 361, pp. 31-39, 1993.

[13] Bower, J. M. and Beeman, D., *The book of genesis: Exploring realistic neural models with the general neural simulation system*, 2nd ed. New York, NY: Springer, 1998.

[14] Brette, R., Rudolph, M., Carnevale, T., Hines, M., Beeman, D., Bower, J. M., Diesmann, M., Morrison, A., Goodman, P. H., Harris, F. C., Zirpe, M., Natschlager, T., Pecevski, D., Ermentrout, B., Djurfeldt, M., Lansner, A., Rochel, O., Vieville, T., Muller, E., Davison, A. P., El Boustani, S., and Destexhe, A., "Simulation of networks of spiking neurons: A review of tools and strategies," *Journal of Computational Neuroscience,* vol. 23, pp. 349-398, 2007.

[15] Brun, V. H., Leutgeb, S., Wu, H. Q., Schwarcz, R., Witter, M. P., Moser, E. I., and Moser, M. B., "Impaired spatial representation in ca1 after lesion of direct input from entorhinal cortex," *Neuron,* vol. 57, pp. 290-302, 2008.

[16] Brun, V. H., Otnaess, M. K., Molden, S., Steffenach, H. A., Witter, M. P., Moser, M. B., and Moser, E. I., "Place cells and place recognition maintained by direct entorhinal-hippocampal circuitry," *Science,* vol. 296, pp. 2243-2246, 2002.

[17] Brunel, N., "Dynamics of sparsely connected networks of excitatory and inhibitory spiking neurons," *Journal of Computational Neuroscience,* vol. 8, pp. 183-208, 2000.

[18] Burgess, N., Maguire, E. A., and O'keefe, J., "The human hippocampus and spatial and episodic memory," *Neuron,* vol. 35, pp. 625-641, 2002.

[19] Burton, B. G., Hok, V., Save, E., and Poucet, B., "Lesion of the ventral and intermediate hippocampus abolishes anticipatory activity in the medial prefrontal cortex of the rat," *Behavioural Brain Research,* vol. 199, pp. 222-234, 2009.

[20] Buzsaki, G., "2-stage model of memory trace formation - a role for noisy brain states," *Neuroscience,* vol. 31, pp. 551-570, 1989.

[21] Buzsaki, G., "Theta oscillations in the hippocampus," *Neuron,* vol. 33, pp. 325-340, 2002.

[22] Buzsaki, G., "Theta rhythm of navigation: Link between path integration and landmark navigation, episodic and semantic memory," *Hippocampus,* vol. 15, pp. 827-840, 2005.

[23] Buzsaki, G., Buhl, D. L., Harris, K. D., Csicsvari, J., Czeh, B., and Morozov, A., "Hippocampal network patterns of activity in the mouse," *Neuroscience,* vol. 116, pp. 201-211, 2003.

[24] Caporale, N. and Dan, Y., "Spike timing-dependent plasticity: A hebbian learning rule," *Annual Review of Neuroscience,* vol. 31, pp. 25-46, 2008.

[25] Churchwell, J. C., Morris, A. M., Musso, N. D., and Kesner, R. P., "Prefrontal and hippocampal contributions to encoding and retrieval of spatial memory," *Neurobiology of Learning and Memory,* vol. 93, pp. 415-421, 2010.

[26] Cohen, M. X., Elger, C. E., and Fell, J., "Oscillatory activity and phase-amplitude coupling in the human medial frontal cortex during decision making," *Journal of Cognitive Neuroscience,* vol. 21, pp. 390-402, 2009.

[27] Compte, A., Brunel, N., Goldman-Rakic, P. S., and Wang, X. J., "Synaptic mechanisms and network dynamics underlying spatial working memory in a cortical network model," *Cerebral Cortex,* vol. 10, pp. 910-923, 2000.

[28] Crill, W. E., "Persistent sodium current in mammalian central neurons," *Annual Review of Physiology,* vol. 58, pp. 349-362, 1996.

[29] Cutsuridis, V. and Wennekers, T., "Hippocampus, microcircuits and associative memory," *Neural Networks,* vol. 22, pp. 1120-1128, 2009.

[30] Dan, Y. and Poo, M. M., "Spike timing-dependent plasticity of neural circuits," *Neuron,* vol. 44, pp. 23-30, 2004.

[31] De Almeida, L., Idiart, M., and Lisman, J. E., "The input-output transformation of the hippocampal granule cells: From grid cells to place fields," *Journal of Neuroscience,* vol. 29, pp. 7504-7512, 2009.

[32] De Saint Blanquat, P., Hok, V., Alvernhe, A., Save, E., and Poucet, B., "Tagging items in spatial working memory: A unit-recording study in the rat medial prefrontal cortex," *Behavioural Brain Research,* vol. 209, pp. 267-273, 2010.

[33] Deco, G., Jirsa, V. K., Robinson, P. A., Breakspear, M., and Friston, K., "The dynamic brain: From spiking neurons to neural masses and cortical fields," *Plos Computational Biology,* vol. 4, pp. 1-36, 2008.

[34] Derdikman, D., Whitlock, J. R., Tsao, A., Fyhn, M., Hafting, T., Moser, M. B., and Moser, E. I., "Fragmentation of grid cell maps in a multicompartment environment," *Nature Neuroscience,* vol. 12, pp. 1325-1332, 2009.

[35] Diesmann, M., Gewaltig, M. D., Morrison, A., and Plesser, H. E., "Large scale simulations of cortical neuronal networks," *Neuroscience Research,* vol. 58, pp. S9-S9, 2007.

[36] Diesmann, M., Gewaltig, M. O., and Aertsen, A., "Stable propagation of synchronous spiking in cortical neural networks," *Nature,* vol. 402, pp. 529-533, 1999.

[37] Doeller, C. F., Barry, C., and Burgess, N., "Evidence for grid cells in a human memory network," *Nature,* vol. 463, pp. 657-663, 2010.

[38] Doherty, A. (2010). *Neural pathways*. Available: http://www.bristol.ac.uk/synaptic/pathways/

[39] Doughty, J. M., Barnes-Davies, M., Rusznak, Z., Harasztosi, C., and Forsythe, I. D., "Contrasting ca2+ channel subtypes at cell bodies and synaptic terminals of rat anterioventral cochlear bushy neurones," *Journal of Physiology-London,* vol. 512, pp. 365-376, 1998.

[40] Doyere, V., Burette, F., Redinidelnegro, C., and Laroche, S., "Long-term potentiation of hippocampal afferents and efferents to prefrontal cortex - implications for associative learning," *Neuropsychologia,* vol. 31, pp. 1031-1053, 1993.

[41] Dragoi, G. and Buzsaki, G., "Temporal encoding of place sequences by hippocampal cell assemblies," *Neuron,* vol. 50, pp. 145-157, 2006.

[42] Dragoi, G., Harris, K. D., and Buzsaki, G., "Place representation within hippocampal networks is modified by long-term potentiation," *Neuron,* vol. 39, pp. 843-853, 2003.

[43] Drewes, R., Zou, Q., and Goodman, P. H., "Brainlab: A python toolkit to aid in the design, simulation, and analysis of spiking neural networks with the neocortical simulator," *Frontiers in Neuroinformatics,* vol. 3, 2009.

[44] Duncan, J. and Owen, A. M., "Common regions of the human frontal lobe recruited by diverse cognitive demands," *Trends in Neurosciences,* vol. 23, pp. 475-483, 2000.

[45] Eichenbaum, H., "A cortical-hippocampal system for declarative memory," *Nature Reviews Neuroscience,* vol. 1, pp. 41-50, 2000.

[46] Fleischer, J. G., Gally, J. A., Edelman, G. M., and Krichmar, J. L., "Retrospective and prospective responses arising in a modeled hippocampus during maze navigation by a brain-based device," *Proceedings of the National Academy of Sciences of the United States of America,* vol. 104, pp. 3556-3561, 2007.

[47] Fox, C. and Humphries, M., "Technical integration of hippocampus, basal ganglia and physical models for spatial navigation," vol. 3, ed. Frontiers in Neuroinformatics, 2009.

[48] Frank, L. M., Stanley, G. B., and Brown, E. N., "Hippocampal plasticity across multiple days of exposure to novel environments," *Journal of Neuroscience,* vol. 24, pp. 7681-7689, 2004.

[49] Fries, P., "A mechanism for cognitive dynamics: Neuronal communication through neuronal coherence," *Trends in Cognitive Sciences,* vol. 9, pp. 474-480, 2005.

[50] Fuster, J. M., *The prefrontal cortex*, 4th ed. San Diego, CA: Elsevier, 2008.

[51] Fyhn, M., Hafting, T., Witter, M. P., Moser, E. I., and Moser, M. B., "Grid cells in mice," *Hippocampus,* vol. 18, pp. 1230-1238, 2008.

[52] Fyhn, M., Molden, S., Witter, M. P., Moser, E. I., and Moser, M. B., "Spatial representation in the entorhinal cortex," *Science,* vol. 305, pp. 1258-1264, 2004.

[53] Gabbott, P. L. A., Warner, T. A., Jays, P. R. L., Salway, P., and Busby, S. J., "Prefrontal cortex in the rat: Projections to subcortical autonomic, motor, and limbic centers," *Journal of Comparative Neurology,* vol. 492, pp. 145-177, 2005.

[54] Gasparini, S. and Magee, J. C., "State-dependent dendritic computation in hippocampal ca1 pyramidal neurons," *Journal of Neuroscience,* vol. 26, pp. 2088-2100, 2006.

[55] Gaussier, P., Banquet, J. P., Sargolini, F., Giovannangeli, C., Save, E., and Poucet, B., "A model of grid cells involving extra hippocampal path integration, and the hippocampal loop," *Journal of Integrative Neuroscience,* vol. 6, pp. 447-476, 2007.

[56] Gewaltig, M., "Self-sustained activity in networks of integrate and fire neurons without external noise," presented at the *Bernstein Conference on Computational Neuroscience*, Frankfurt, Germany, 2009.

[57] Giocomo, L. M. and Hasselmo, M. E., "Computation by oscillations: Implications of experimental data for theoretical models of grid cells," *Hippocampus,* vol. 18, pp. 1186-1199, 2008.

[58] Giocomo, L. M., Zilli, E. A., Fransen, E., and Hasselmo, M. E., "Temporal frequency of subthreshold oscillations scales with entorhinal grid cell field spacing," *Science,* vol. 315, pp. 1719-1722, 2007.

[59] Goutagny, R., Jackson, J., and Williams, S., "Self-generated theta oscillations in the hippocampus," *Nature Neuroscience,* vol. 12, pp. 1491-1493, 2009.

[60] Gray, J. R., Braver, T. S., and Raichle, M. E., "Integration of emotion and cognition in the lateral prefrontal cortex," *Proceedings of the National Academy of Sciences of the United States of America,* vol. 99, pp. 4115-4120, 2002.

[61] Griffin, A. L., Eichenbaum, H., and Hasselmo, M. E., "Spatial representations of hippocampal ca1 neurons are modulated by behavioral context in a hippocampus-dependent memory task," *Journal of Neuroscience,* vol. 27, pp. 2416-2423, 2007.

[62] Hafting, T., Fyhn, M., Bonnevie, T., Moser, M. B., and Moser, E. I., "Hippocampus-independent phase precession in entorhinal grid cells," *Nature,* vol. 453, pp. 1248-U50, 2008.

[63] Hafting, T., Fyhn, M., Molden, S., Moser, M. B., and Moser, E. I., "Microstructure of a spatial map in the entorhinal cortex," *Nature,* vol. 436, pp. 801-806, 2005.

[64] Harris, K. D., Csicsvari, J., Hirase, H., Dragoi, G., and Buzsaki, G., "Organization of cell assemblies in the hippocampus," *Nature,* vol. 424, pp. 552-556, 2003.

[65] Harris, K. D., Henze, D. A., Hirase, H., Leinekugel, X., Dragoi, G., Czurko, A., and Buzsaki, G., "Spike train dynamics predicts theta-related phase precession in hippocampal pyramidal cells," *Nature,* vol. 417, pp. 738-741, 2002.

[66] Harvey, C. D., Collman, F., Dombeck, D. A., and Tank, D. W., "Intracellular dynamics of hippocampal place cells during virtual navigation," *Nature,* vol. 461, pp. 941-946, 2009.

[67] Hassabis, D., Kumaran, D., and Maguire, E. A., "Using imagination to understand the neural basis of episodic memory," *Journal of Neuroscience,* vol. 27, pp. 14365-14374, 2007.

[68] Hasselmo, M. E., "Grid cell mechanisms and function: Contributions of entorhinal persistent spiking and phase resetting," *Hippocampus,* vol. 18, pp. 1213-1229, 2008.

[69] Hasselmo, M. E., Hay, J., Ilyn, M., and Gorchetchnikov, A., "Neuromodulation, theta rhythm and rat spatial navigation," *Neural Networks,* vol. 15, pp. 689-707, 2002.

[70] Hayman, R. M. and Jeffery, K. J., "How heterogeneous place cell responding arises from homogeneous grids-a contextual gating hypothesis," *Hippocampus,* vol. 18, pp. 1301-1313, 2008.

[71] Hebb, D. O., *The organization of behavior*. New York, NY: Wiley, 1949.

[72] Hille, B., *Ion channels in excitable membranes*, 3rd ed. Sunderland, MA: Sinauer Associates, Inc., 2001.

[73] Hines, M. and Moore, J. W., "Neuron, a computer program specialized for simulating nerve function," *Society for Neuroscience Abstracts,* vol. 19, p. 1759, 1993.

[74] Hines, M. L. and Carnevale, N. T., "The neuron simulation environment," *Neural Computation,* vol. 9, pp. 1179-1209, 1997.

[75] Hoang, L. T. and Kesner, R. P., "Dorsal hippocampus, ca3, and ca1 lesions disrupt temporal sequence completion," *Behavioral Neuroscience,* vol. 122, pp. 9-15, 2008.

[76] Hodgkin, A. L. and Huxley, A. F., "Currents carried by sodium and potassium ions through the membrane of the giant axon of loligo," *Journal of Physiology-London,* vol. 116, pp. 449-472, 1952.

[77] Hok, V., Lenck-Santini, P. P., Roux, S., Save, E., Muller, R. U., and Poucet, B., "Goal-related activity in hippocampal place cells," *Journal of Neuroscience,* vol. 27, pp. 472-482, 2007.

[78] Hotson, J. R. and Prince, D. A., "Calcium-activated hyperpolarization follows repetitive firing in hippocampal-neurons," *Journal of Neurophysiology,* vol. 43, pp. 409-419, 1980.

[79] Huxter, J., Burgess, N., and O'keefe, J., "Independent rate and temporal coding in hippocampal pyramidal cells," *Nature,* vol. 425, pp. 828-832, 2003.

[80] Isaac, J. T. R., Buchanan, K. A., Muller, R. U., and Mellor, J. R., "Hippocampal place cell firing patterns can induce long-term synaptic plasticity in vitro," *Journal of Neuroscience,* vol. 29, pp. 6840-6850, 2009.

[81] Izaki, Y., Takita, M., and Akema, T., "Specific role of the posterior dorsal hippocampus-prefrontal cortex in short-term working memory," *European Journal of Neuroscience,* vol. 27, pp. 3029-3034, 2008.

[82] Izhikevich, E. M., Gally, J. A., and Edelman, G. M., "Spike-timing dynamics of neuronal groups," *Cerebral Cortex,* vol. 14, pp. 933-944, 2004.

[83] Jay, T. M., Glowinski, J., and Thierry, A. M., "Selectivity of the hippocampal projection to the prelimbic area of the prefrontal cortex in the rat," *Brain Research,* vol. 505, pp. 337-340, 1989.

[84] Jay, T. M. and Witter, M. P., "Distribution of hippocampal ca1 and subicular efferents in the prefrontal cortex of the rat studied by means of anterograde transport of phaseolus-vulgaris-leukoagglutinin," *Journal of Comparative Neurology,* vol. 313, pp. 574-586, 1991.

[85] Jayet Bray, L. C., Quoy, M., Harris, F. C., and Goodman, P. H., "Hippocampal place field dynamics modulated by entorhinal grid and suppression-generating cells," *Frontiers in Neural Circuits,* vol. 4, 2010.

[86] Jeewajee, A., Barry, C., O'keefe, J., and Burgess, N., "Grid cells and theta as oscillatory interference: Electrophysiological data from freely moving rats," *Hippocampus,* vol. 18, pp. 1175-1185, 2008.

[87] Jones, M. W. and Wilson, M. A., "Phase precession of medial prefrontal cortical activity relative to the hippocampal theta rhythm," *Hippocampus,* vol. 15, pp. 867-873, 2005.

[88] Jones, M. W. and Wilson, M. A., "Theta rhythms coordinate hippocampal-prefrontal interactions in a spatial memory task," *Plos Biology,* vol. 3, pp. 2187-2199, 2005.

[89] Jones, R. S. G. and Heinemann, U., "Synaptic and intrinsic responses of medial entorhinal cortical-cells in normal and magnesium-free medium invitro," *Journal of Neurophysiology,* vol. 59, pp. 1476-1496, 1988.

[90] Jung, H. Y., Staff, N. P., and Spruston, N., "Action potential bursting in subicular pyramidal neurons is driven by a calcium tail current," *Journal of Neuroscience,* vol. 21, pp. 3312-3321, 2001.

[91] Jung, M. W. and Mcnaughton, B. L., "Spatial selectivity of unit-activity in the hippocampal granular layer," *Hippocampus,* vol. 3, pp. 165-182, 1993.

[92] Kamondi, A., Acsady, L., Wang, X. J., and Buzsaki, G., "Theta oscillations in somata and dendrites of hippocampal pyramidal cells in vivo: Activity-dependent phase-precession of action potentials," *Hippocampus,* vol. 8, pp. 244-261, 1998.

[93] Kandel, E. R., Schwartz, J. H., and And Jessell, T. M., *Principles of neural science*, 4th ed. New-York, NY: McGraw-Hill, 2000.

[94] Kawashima, H., Izaki, Y., Grace, A. A., and Takita, M., "Cooperativity between hippocampal-prefrontal short-term plasticity through associative long-term potentiation," *Brain Research,* vol. 1109, pp. 37-44, 2006.

[95] King, J., "Brain communication server: A dynamic data transferal system for a parallel brain simulator " Master's thesis, Computer Science, University of Nevada, Reno, NV, 2005.

[96] Klausberger, T., "Gabaergic interneurons targeting dendrites of pyramidal cells in the ca1 area of the hippocampus," *European Journal of Neuroscience,* vol. 30, pp. 947-957, 2009.

[97] Klausberger, T., Marton, L. F., Baude, A., Roberts, J. D. B., Magill, P. J., and Somogyi, P., "Spike timing of dendrite-targeting bistratified cells during hippocampal network oscillations in vivo," *Nature Neuroscience,* vol. 7, pp. 41-47, 2004.

[98] Knierim, J. J. and Mcnaughton, B. L., "Hippocampal place-cell firing during movement in three-dimensional space," *Journal of Neurophysiology,* vol. 85, pp. 105-116, 2001.

[99] Kobayashi, K. and Poo, M. M., "Spike train timing-dependent associative modification of hippocampal ca3 recurrent synapses by mossy fibers," *Neuron,* vol. 41, pp. 445-454, 2004.

[100] Koene, R. A. and Hasselmo, M. E., "Consequences of parameter differences in a model of short-term persistent spiking buffers provided by pyramidal cells in entorhinal cortex," 2008, pp. 54-67.

[101] Konkel, A., Warren, D. E., Duff, M. C., Tranel, D. N., and Cohen, N. J., "Hippocampal amnesia impairs all manner of relational memory," *Frontiers in Human Neuroscience,* vol. 2, 2008.

[102] Kumar, A., Schrader, S., Rotter, S., and Aertsen, A., "Dynamics of random networks of spiking neurons with conductance-based synapses," in *Cosyne*, Slat Lake City, UT, 2005.

[103] Kunec, S., Hasselmo, M. E., and Kopell, N., "Encoding and retrieval in the ca3 region of the hippocampus: A model of theta-phase separation," *Journal of Neurophysiology,* vol. 94, pp. 70-82, 2005.

[104] Kunitake, A., Kunitake, T., and Stewart, M., "Differential modulation by carbachol of four separate excitatory afferent systems to the rat subiculum in vitro," *Hippocampus,* vol. 14, pp. 986-999, 2004.

[105] Kwag, J. and Paulsen, O., "The timing of external input controls the sign of plasticity at local synapses," *Nature Neuroscience,* vol. 12, pp. 1219-1221, 2009.

[106] Kyd, R. J. and Bilkey, D. K., "Hippocampal place cells show increased sensitivity to changes in the local environment following prefrontal cortex lesions," *Cerebral Cortex,* vol. 15, pp. 720-731, 2005.

[107] Laroche, S., Davis, S., and Jay, T. M., "Plasticity at hippocampal to prefrontal cortex synapses: Dual roles in working memory and consolidation," *Hippocampus,* vol. 10, pp. 438-446, 2000.

[108] Laroche, S., Jay, T. M., and Thierry, A. M., "Long-term potentiation in the prefrontal cortex following stimulation of the hippocampal ca1/subicular region," *Neuroscience Letters,* vol. 114, pp. 184-190, 1990.

[109] Lee, I. and Kesner, R. P., "Differential roles of dorsal hippocampal subregions in spatial working memory with short versus intermediate delay," *Behavioral Neuroscience,* vol. 117, pp. 1044-1053, 2003.

[110] Lee, I. and Kesner, R. P., "Time-dependent relationship between the dorsal hippocampus and the prefrontal cortex in spatial memory," *Journal of Neuroscience,* vol. 23, pp. 1517-1523, 2003.

[111] Lee, I. and Solivan, F., "The roles of the medical prefrontal cortex and hippocampus in a spatial paired-association task," *Learning & Memory,* vol. 15, pp. 357-367, 2008.

[112] Lisman, J., "The theta/gamma discrete phase code occuring during the hippocampal phase precession may be a more general brain coding scheme," *Hippocampus,* vol. 15, pp. 913-922, 2005.

[113] Lubenov, E. V. and Siapas, A. G., "Hippocampal theta oscillations are travelling waves," *Nature,* vol. 459, pp. 534-539, 2009.

[114] Luczak, A., Bartho, P., Marguet, S. L., Buzsaki, G., and Harris, K. D., "Sequential structure of neocortical spontaneous activity in vivo," *Proceedings of the National Academy of Sciences of the United States of America,* vol. 104, pp. 347-352, 2007.

[115] Maccaferri, G., "Stratum oriens horizontal interneurone diversity and hippocampal network dynamics," *Journal of Physiology-London,* vol. 562, pp. 73-80, 2005.

[116] Magee, J. C., "Dendritic mechanisms of phase precession in hippocampal ca1 pyramidal neurons," *Journal of Neurophysiology,* vol. 86, pp. 528-532, 2001.

[117] Maguire, E. A., "The retrosplenial contribution to human navigation: A review of lesion and neuroimaging findings," *Scandinavian Journal of Psychology,* vol. 42, pp. 225-238, 2001.

[118] Malleret, G., Alarcon, J. M., Martel, G., Takizawa, S., Vronskaya, S., Yin, D. Q., Chen, I. Z., Kandel, E. R., and Shumyatsky, G. P., "Bidirectional regulation of hippocampal long-term synaptic plasticity and its influence on opposing forms of memory," *Journal of Neuroscience,* vol. 30, pp. 3813-3825, 2010.

[119] Manns, J. R., Howard, M. W., and Eichenbaum, H., "Gradual changes in hippocampal activity support remembering the order of events," *Neuron,* vol. 56, pp. 530-540, 2007.

[120] Manns, J. R., Zilli, E. A., Ong, K. C., Hasselmo, M. E., and Eichenbaum, H., "Hippocampal ca1 spiking during encoding and retrieval: Relation to theta phase," *Neurobiology of Learning and Memory,* vol. 87, pp. 9-20, 2007.

[121] Mcnaughton, B. L., Barnes, C. A., Meltzer, J., and Sutherland, R. J., "Hippocampal granule cells are necessary for normal spatial-learning but not for spatially-selective pyramidal cell discharge," *Experimental Brain Research,* vol. 76, pp. 485-496, 1989.

[122] Mcnaughton, B. L., Battaglia, F. P., Jensen, O., Moser, E. I., and Moser, M. B., "Path integration and the neural basis of the 'cognitive map'," *Nature Reviews Neuroscience,* vol. 7, pp. 663-678, 2006.

[123] Mcnaughton, N., "The role of the subiculum within the behavioural inhibition system," *Behavioural Brain Research,* vol. 174, pp. 232-250, 2006.

[124] Menendez De La Prida, L., "Control of bursting by local inhibition in the rat subiculum in vitro," *Journal of Physiology (Cambridge),* vol. 549, pp. 219-230, 2003.

[125] Menschik, E. D. and Finkel, L. H., "Neuromodulatory control of hippocampal function: Towards a model of alzheimer's disease," *Artificial Intelligence in Medicine,* vol. 13, pp. 99-121, 1998.

[126] Mitchell, D. J., Mcnaughton, N., Flanagan, D., and Kirk, I. J., "Frontal-midline theta from the perspective of hippocampal "theta"," *Progress in Neurobiology,* vol. 86, pp. 156-185, 2008.

[127] Mormann, F., Kornblith, S., Quiroga, R. Q., Kraskov, A., Cerf, M., Fried, I., and Koch, C., "Latency and selectivity of single neurons indicate hierarchical processing in the human medial temporal lobe," *Journal of Neuroscience,* vol. 28, pp. 8865-8872, 2008.

[128] Mormann, F., Osterhage, H., Andrzejak, R. G., Weber, B., Fernandez, G., Fell, J., Elger, C. E., and Lehnertz, K., "Independent delta/theta rhythms in the human hippocampus and entorhinal cortex," *Frontiers in Human Neuroscience,* vol. 2, 2008.

[129] Moscovitch, M., Rosenbaum, R. S., Gilboa, A., Addis, D. R., Westmacott, R., Grady, C., Mcandrews, M. P., Levine, B., Black, S., Winocur, G., and Nadel, L., "Functional neuroanatomy of remote episodic, semantic and spatial memory: A unified account based on multiple trace theory," *Journal of Anatomy,* vol. 207, pp. 35-66, 2005.

[130] Moser, E. I., Kropff, E., and Moser, M. B., "Place cells, grid cells, and the brain's spatial representation system," *Annual Review of Neuroscience,* vol. 31, pp. 69-89, 2008.

[131] Moser, E. I. and Moser, M. B., "A metric for space," *Hippocampus,* vol. 18, pp. 1142-1156, 2008.

[132] Muir, G. M. and Bilkey, D. K., "Instability in the place field location of hippocampal place cells after lesions centered on the perirhinal cortex," *Journal of Neuroscience,* vol. 21, pp. 4016-4025, 2001.

[133] Mysid. (2006). *Lobes of the brain nl*. Available: http://en.wikipedia.org/wiki/File:Lobes_of_the_brain_NL.svg

[134] Naber, P. A., Witter, M. P., and Da Silva, F. H. L., "Networks of the hippocampal memory system of the rat - the pivotal role of the subiculum," *Parahippocampal Region,* vol. 911, pp. 392-403, 2000.

[135] Nitz, D. and Mcnaughton, B., "Differential modulation of ca1 and dentate gyrus interneurons during exploration of novel environments," *Journal of Neurophysiology,* vol. 91, pp. 863-872, 2004.

[136] Nordlie, E., Gewaltig, M. O., and Plesser, H. E., "Towards reproducible descriptions of neuronal network models," *Plos Computational Biology,* vol. 5, 2009.

[137] Nyhus, E. and Curran, T., "Functional role of gamma and theta oscillations in episodic memory," *Neuroscience and Biobehavioral Reviews,* vol. 34, pp. 1023-1035, 2010.

[138] O'keefe, J., "Review of the hippocampal place cells," *Progress in Neurobiology,* vol. 13, pp. 419-439, 1979.

[139] O'keefe, J. and Burgess, N., "Dual phase and rate coding in hippocampal place cells: Theoretical significance and relationship to entorhinal grid cells," *Hippocampus,* vol. 15, pp. 853-866, 2005.

[140] O'keefe, J. and Dostrovski, J., "Hippocampus as a spatial map - preliminary evidence from unit activity in freely moving rats," *Brain Research,* vol. 34, pp. 171-175, 1971.

[141] O'keefe, J. and Nadel, L., *The hippocampus as a cognitive map*. Oxford, New York: Clarendon Press, 1978.

[142] O'keefe, J. and Recce, M. L., "Phase relationship between hippocampal place units and the eeg theta rhythm," *Hippocampus,* vol. 3, pp. 317-330, 1993.

[143] O'mara, S., "The subiculum: What it does, what it might do, and what neuroanatomy has yet to tell us," *Journal of Anatomy,* vol. 207, pp. 271-282, 2005.

[144] Paz, R., Bauer, E. P., and Pare, D., "Theta synchronizes the activity of medial prefrontal neurons during learning," *Learning & Memory,* vol. 15, pp. 524-531, 2008.

[145] Pineda, J. C., Waters, R. S., and Foehring, R. C., "Specificity in the interaction of hva ca2+ channel types with ca2+-dependent ahps and firing behavior in

neocortical pyramidal neurons," *Journal of Neurophysiology,* vol. 79, pp. 2522-2534, 1998.

[146] Poucet, B., "Object exploration, habituation, and response to a spatial change in rats following septal or medial frontal cortical damage," *Behavioral Neuroscience,* vol. 103, pp. 1009-1016, 1989.

[147] Purves, D., Augustine, G. J., Fitzpatrick, D., Hall, W. C., Lamantia, A. S., Mcnamara, J. O., and Williams, S. M., *Neuroscience*, 3rd ed. Sunderland, MA: Sinauer Associates, Inc, 2004.

[148] Rafiq, A., Zhang, Y. F., Delorenzo, R. J., and Coulter, D. A., "Long-duration self-sustained epileptiform activity in the hippocampal parahippocampal slice - a model of status epilepticus," *Journal of Neurophysiology,* vol. 74, pp. 2028-2042, 1995.

[149] Remondes, M. and Schuman, E. M., "Role for a cortical input to hippocampal area ca1 in the consolidation of a long-term memory," *Nature,* vol. 431, pp. 699-703, 2004.

[150] Rolls, E. T., "Memory systems in the brain," *Annual Review of Psychology,* vol. 51, pp. 599-630, 2000.

[151] Samsonovich, A. V. and Ascoli, G. A., "A simple neural network model of the hippocampus suggesting its pathfinding role in episodic memory retrieval," *Learning & Memory,* vol. 12, pp. 193-208, 2005.

[152] Samu, D., Eros, P., Ujfalussy, B., and Kiss, T., "Robust path integration in the entorhinal grid cell system with hippocampal feed-back," *Biological Cybernetics,* vol. 101, pp. 19-34, 2009.

[153] Sargolini, F., Fyhn, M., Hafting, T., Mcnaughton, B. L., Witter, M. P., Moser, M. B., and Moser, E. I., "Conjunctive representation of position, direction, and velocity in entorhinal cortex," *Science,* vol. 312, pp. 758-762, 2006.

[154] Save, E. and Poucet, B., "Role of the parietal cortex in long-term representation of spatial information in the rat," *Neurobiology of Learning and Memory,* vol. 91, pp. 172-178, 2009.

[155] Schwartzkroin, P. A. and Stafstrom, C. E., "Effects of egta on the calcium-activated afterhyperpolarization in hippocampal ca3-pyramidal cells," *Science,* vol. 210, pp. 1125-1126, 1980.

[156] Sehatpour, P., Molholm, S., Schwartz, T. H., Mahoney, J. R., Mehta, A. D., Javitt, D. C., Stanton, P. K., and Foxe, J. J., "A human intracranial study of long-range oscillatory coherence across a frontal-occipital-hippocampal brain network during

visual object processing," *Proceedings of the National Academy of Sciences of the United States of America,* vol. 105, pp. 4399-4404, 2008.

[157] Shankaranarayana Rao, B. S. and Raju, T. R., "The brain slice technique," in *Brain and behavior*, Raju, T. R., Kutty, B. M., Sathyaprabha, T. N., and Shankaranarayana Rao, B. S., Eds., ed Bangalore, India, 2004.

[158] Siapas, A. G., Lubenov, E. V., and Wilson, M. A., "Prefrontal phase locking to hippocampal theta oscillations," *Neuron,* vol. 46, pp. 141-151, 2005.

[159] Sigurdsson, T., Stark, K. L., Karayiorgou, M., Gogos, J. A., and Gordon, J. A., "Impaired hippocampal-prefrontal synchrony in a genetic mouse model of schizophrenia," *Nature,* vol. 464, pp. 763-U139, 2010.

[160] Skaggs, W. E., Mcnaughton, B. L., Wilson, M. A., and Barnes, C. A., "Theta phase precession in hippocampal neuronal populations and the compression of temporal sequences," *Hippocampus,* vol. 6, pp. 149-172, 1996.

[161] Slawinska, U. and Kasicki, S., "The frequency of rat's hippocampal theta rhythm is related to the speed of locomotion," *Brain Research,* vol. 796, pp. 327-331, 1998.

[162] Squire, L. R., Stark, C. E. L., and Clark, R. E., "The medial temporal lobe," *Annual Review of Neuroscience,* vol. 27, pp. 279-306, 2004.

[163] Stanton, P. K., Jones, R. S. G., Mody, I., and Heinemann, U., "Epileptiform activity induced by lowering extracellular mg-2+ in combined hippocampal-entorhinal cortex slices - modulation by receptors for norepinephrine and n-methyl-d-aspartate," *Epilepsy Research,* vol. 1, pp. 53-62, 1987.

[164] Sticker, C., "Slices of brain tissue," in *Neuroscience methods*, martin, R., Ed., ed Australia: Harwood Academic, 1997.

[165] Stocker, M., "Ca2+-activated k+ channels: Molecular determinants and function of the sk family," *Nature Reviews Neuroscience,* vol. 5, pp. 758-770, 2004.

[166] Stringer, J. L. and Lothman, E. W., "Epileptiform discharges induced by altering extracellular potassium and calcium in the rat hippocampal slice," *Experimental Neurology,* vol. 101, pp. 147-157, 1988.

[167] Stringer, J. L. and Lothman, E. W., "Hippocampal slices from kindled rats show an increased sensitivity for induction of epileptiform activity by changes in extracellular ion concentrations," *Neuroscience Letters,* vol. 89, pp. 43-48, 1988.

[168] Takita, M., Izaki, Y., Kuramochi, M., Yokoi, H., and Ohtomi, M., "Synaptic plasticity dynamics in the hippocampal-prefrontal pathway in vivo," *Neuroreport,* vol. 21, pp. 68-72, 2010.

[169] Tsodyks, M. V., Skaggs, W. E., Sejnowski, T. J., and Mcnaughton, B. L., "Population dynamics and theta rhythm phase precession of hippocampal place cell firing: A spiking neuron model," *Hippocampus,* vol. 6, pp. 271-280, 1996.

[170] Van Cauter, T., Poucet, B., and Save, E., "Unstable ca1 place cell representation in rats with entorhinal cortex lesions," *European Journal of Neuroscience,* vol. 27, pp. 1933-1946, 2008.

[171] Van Strien, N. M., Cappaert, N. L. M., and Witter, M. P., "The anatomy of memory: An interactive overview of the parahippocampal-hippocampal network," *Nature Reviews Neuroscience,* vol. 10, pp. 272-282, 2009.

[172] Van Vreeswijk, C. and Sompolinsky, H., "Chaotic balanced state in a model of cortical circuits," *Neural Computation,* vol. 10, pp. 1321-1371, 1998.

[173] Varga, V., Losonczy, A., Zemelman, B. V., Borhegyi, Z., Nyiri, G., Domonkos, A., Hangya, B., Holderith, N., Magee, J. C., and Freund, T. F., "Fast synaptic subcortical control of hippocampal circuits," *Science,* vol. 326, pp. 449-453, 2009.

[174] Vogels, T. P. and Abbott, L. F., "Signal propagation and logic gating in networks of integrate-and-fire neurons," *Journal of Neuroscience,* vol. 25, pp. 10786-10795, 2005.

[175] Walther, H., Lambert, J. D. C., Jones, R. S. G., Heinemann, U., and Hamon, B., "Epileptiform activity in combined slices of the hippocampus, subiculum and entorhinal cortex during perfusion with low magnesium medium," *Neuroscience Letters,* vol. 69, pp. 156-161, 1986.

[176] Wang, G. W. and Cai, J. X., "Disconnection of the hippocampal-prefrontal cortical circuits impairs spatial working memory performance in rats," *Behavioural Brain Research,* vol. 175, pp. 329-336, 2006.

[177] Watanabe, H., Aihara, T., and Tsukada, M., "Phase shift of subthreshold theta oscillation hippocampal ca1 pyramidal by excitatory synaptic inputs," *Neuroscience,* vol. 140, pp. 1189-1199, 2006.

[178] Whishaw, I. Q. and Vanderwo.Ch, "Hippocampal eeg and behavior - changes in amplitude and frequency of rsa (theta rhythm) associated with spontaneous and learned movement patterns in rats and cats," *Behavioral Biology,* vol. 8, pp. 461-484, 1973.

[179] Wills, T. J., Lever, C., Cacucci, F., Burgess, N., and O'keefe, J., "Attractor dynamics in the hippocampal representation of the local environment," *Science,* vol. 308, pp. 873-876, 2005.

[180] Wilson, C. E., Goodman, P. H., and Harris, F. C., Jr., "Implementation of a biologically realistic parallel neocortical-neural network simulator," in *Tenth SIAM conference on parallel processing*, Portsmouth, VA, 2001.

[181] Wilson, M. A. and Mcnaughton, B. L., "Dynamics of the hippocampal ensemble code for space," *Science,* vol. 261, pp. 1055-1058, 1993.

[182] Wu, Z. H. and Yamaguchi, Y., "Independence of the unimodal tuning of firing rate from theta phase precession in hippocampal place cells," *Biological Cybernetics,* vol. 102, pp. 95-107, 2010.

[183] Yamaguchi, Y., Sato, N., Wagatsuma, H., Wu, Z. H., Molter, C., and Aota, Y., "A unified view of theta-phase coding in the entorhinal-hippocampal system," *Current Opinion in Neurobiology,* vol. 17, pp. 197-204, 2007.

[184] Zirpe, M. A., "Rain and ncs5 benchmarks " Master's thesis, Computer Science, University of Nevada, Reno, NV, 2007.

APPENDICES

APPENDIX A: MODEL ONE – BRAIN INPUT FILE

```
################################ Define BRAIN ############################

%-- Model Main Brain Object --%

BRAIN
        TYPE            Brain_Navigation        %-- Name of brain configuration
        JOB             ./output/Brain_Navigation   %-- Name of any files generated
        FSV             1e3                     %-- Frequency of sampling value
        DURATION        8                       %-- Duration of simulation (sec)
        SEED            -20                     %-- Random number generator

################################## COLUMN TYPE ##########################

%-- Columns within Brain --%

COLUMN_TYPE             CA3_COLUMN

COLUMN_TYPE             column_VL1
COLUMN_TYPE             column_VL2
COLUMN_TYPE             column_VL3
COLUMN_TYPE             column_VL4
COLUMN_TYPE             column_VL5

COLUMN_TYPE             RAIN2_HP_COLUMN
COLUMN_TYPE             RAIN_ahp_HP_COLUMN

################################## STIM INJECT ##########################

%-- RAIN2_HP stimulation inject to jump start --%

STIMULUS_INJECT         RAIN2_HP_inj_stimE1
…
STIMULUS_INJECT         RAIN2_HP_inj_stimE13

%-- PCR GC stimulation inject to jump start --%%

STIMULUS_INJECT         PCR1_GCstim
…
STIMULUS_INJECT         PCR5_GCstim
```

```
%-- Visual landmark input --%

STIMULUS_INJECT          stiminj_VL1
…
STIMULUS_INJECT          stiminj_VL5

%-- Added current to OLM neurons --%

STIMULUS_INJECT          stiminj_OLM

%-- Added current to suppress the PCR-E cells --%

STIMULUS_INJECT          PCR1_E_GCsuppress
…
STIMULUS_INJECT          PCR5_E_GCsuppress

%-- Added current to suppress the PCR-I cells --%

STIMULUS_INJECT          PCR1_I_GCsuppress
…
STIMULUS_INJECT          PCR5_I_GCsuppress

%-- Hippocampal random activity --%

STIMULUS_INJECT          PCR1_random
…
STIMULUS_INJECT          PCR5_random


################################## REPORTS ##################################

%-- Sample of 1 RAIN voltage report (E1 group) --%

REPORT                   EC_II_Voltage_RAIN2_HP_E1

 %-- Sample of 1 PCR voltage report (PCR1 E group) --%

REPORT                   Voltage_PCR1_E

%-- Sample of 1 PCR synaptic strength report (PCR1 E group) --%

REPORT                   PCR1_EE_USE

%-- Reports can be obtained on any cell or group of cells used in the model --%
```

```
################################ CONNECTIONS ##########################

%-- Example of a connection from RAIN2 to RAIN_ahp  (Basket cells - theta) --%

CONNECT                 %-- From --%
                        RAIN2_HP_COLUMN
                        layer_RAIN2_HP
                        RAIN2_HP_E1
                        somaE_RAIN2

                        %-- To --% (Basket cells)
                        RAIN_ahp_HP_COLUMN
                        layer_RAIN_ahp_HP
                        RAIN_ahp_HP_E1
                        somaE_RAIN_ahp

                        synEE_R2C_RC    %-- Synapse used --%
                        0.03            %-- Probability of connection --%

%-- Many connections were used between each column and/or cell group --%
Please see Table 3.1 and 3.2.

END_BRAIN


################################ INCLUDE FILES ##########################

%-- ANATOMY --%

INCLUDE ./input/INCLUDE_ANATOMY_PCRAIN.inc
INCLUDE ./input/INCLUDE_ANATOMY_VL.inc
INCLUDE ./input/INCLUDE_ANATOMY_RAIN_ahp_HP.inc
INCLUDE ./input/INCLUDE_ANATOMY_RAIN2_HP.inc

%-- STIMULUS --%

INCLUDE ./input/INCLUDE_STIMULUS_PCRAIN.inc
INCLUDE ./input/INCLUDE_STIMULUS_VL.inc
INCLUDE ./input/INCLUDE_STIMULUS_GCsupp.inc
INCLUDE ./input/INCLUDE_STIMULUS_PCR_Random.inc
INCLUDE ./input/INCLUDE_STIMULUS_OLM.inc
INCLUDE ./input/INCLUDE_STIMULUS_RAIN_ahp_HP.inc
INCLUDE ./input/INCLUDE_STIMULUS_RAIN2_HP.inc
INCLUDE ./input/INCLUDE_STIMULUS_RAIN_ahp_PF.inc
INCLUDE ./input/INCLUDE_STIMULUS_RAIN2_PF.inc
```

%-- SYNAPSES --%

INCLUDE ./input/INCLUDE_SYNAPSES_PCRAIN.inc
INCLUDE ./input/INCLUDE_SYNAPSES_OLM.inc
INCLUDE ./input/INCLUDE_SYNAPSES_VL_PC.inc
INCLUDE ./input/INCLUDE_SYNAPSES_RAIN_ahp_HP_PF.inc
INCLUDE ./input/INCLUDE_SYNAPSES_RAIN2_HP_PF.inc
INCLUDE ./input/INCLUDE_SYNAPSES_RAIN_ahp_HP_PCRAIN.inc

%-- REPORTS --%

INCLUDE ./input/INCLUDE_REPORTS_VOLTAGES_PCRAIN.inc
INCLUDE ./input/INCLUDE_REPORTS_VL.inc
INCLUDE ./input/INCLUDE_REPORTS_OLM.inc
INCLUDE ./input/INCLUDE_REPORTS_USE_PCRAIN.inc
INCLUDE ./input/INCLUDE_REPORTS_VOLTAGES_RAIN_ahp_HP.inc
INCLUDE ./input/INCLUDE_REPORTS_VOLTAGES_RAIN2_HP.inc

%-- INCLUDE FILES have all data and parameters used in the model: ANATOMY of brain areas, STIMULUS, SYNAPSES for each connection, and REPORTS --%

APPENDIX B: MODEL TWO – BRAIN INPUT FILE

```
################################ Define BRAIN ##############################

%-- Model Main Brain Object (See Appendix A for detail) --%

BRAIN
        TYPE            Brain_Navigation_loop
        JOB             ./output/Brain_Navigation_loop
        FSV             1e3
        DURATION        54
        SEED            -21


################################## COLUMN TYPE ##########################

%-- Columns within Brain --%

COLUMN_TYPE         PM_LEFT_COLUMN
COLUMN_TYPE         PM_RIGHT_COLUMN

COLUMN_TYPE         PF_LEFT2_COLUMN
COLUMN_TYPE         PF_LEFT4_COLUMN
COLUMN_TYPE         PF_LEFT6_COLUMN
COLUMN_TYPE         PF_RIGHT1_COLUMN
COLUMN_TYPE         PF_RIGHT3_COLUMN
COLUMN_TYPE         PF_RIGHT5_COLUMN

COLUMN_TYPE         SUB_LEFT_COLUMN
COLUMN_TYPE         SUB_RIGHT_COLUMN

COLUMN_TYPE         CA_COLUMN

COLUMN_TYPE         column_VL1
COLUMN_TYPE         column_VL2
COLUMN_TYPE         column_VL3
COLUMN_TYPE         column_VL4
COLUMN_TYPE         column_VL5
COLUMN_TYPE         column_VL6
COLUMN_TYPE         column_VL7
COLUMN_TYPE         column_VL8
COLUMN_TYPE         column_VL9
COLUMN_TYPE         column_VL10
COLUMN_TYPE         column_VL11
```

```
COLUMN_TYPE          column_VL12
COLUMN_TYPE          column_VL13
COLUMN_TYPE          column_VL14


COLUMN_TYPE          RAIN2_HP_COLUMN
COLUMN_TYPE          RAIN_ahp_HP_COLUMN
COLUMN_TYPE          RAIN2_PF_COLUMN
COLUMN_TYPE          RAIN_ahp_PF_COLUMN


################################## STIM INJECT############################

%-- RAIN2_HP stimulation inject to jump start  (see appendix A) --%

%-- RAIN2_PF stimulation inject to jump start --%

STIMULUS_INJECT      RAIN2_PF_inj_stimE1
…
STIMULUS_INJECT      RAIN2_PF_inj_stimE13

%-- PCR GC stimulation inject to jump start --%%

STIMULUS_INJECT      PCR1_GCstim
…
STIMULUS_INJECT      PCR14_GCstim

%-- Visual landmark input --%

STIMULUS_INJECT      stiminj_VL1
…
STIMULUS_INJECT      stiminj_VL14

%-- Added current to OLM neurons --%

STIMULUS_INJECT      stiminj_OLM

%-- Added current to suppress the PCR-E cells --%

STIMULUS_INJECT      PCR1_E_GCsuppress
…
STIMULUS_INJECT      PCR14_E_GCsuppress

%-- Added current to suppress the PCR-I cells --%
```

```
STIMULUS_INJECT          PCR1_I_GCsuppress
…
STIMULUS_INJECT          PCR14_I_GCsuppress

%-- Added positive current to PF theta (E) to suppress PF networks when no reward --%

STIMULUS_INJECT          PF_theta_suppress

%-- Added positive current to subiculum for only the first run (biased decision) --%

STIMULUS_INJECT          SUB_LEFT2
STIMULUS_INJECT          SUB_LEFT4
STIMULUS_INJECT          SUB_LEFT6
STIMULUS_INJECT          SUB_RIGHT1
STIMULUS_INJECT          SUB_RIGHT3
STIMULUS_INJECT          SUB_RIGHT5

%-- PCR ongoing activity --%

STIMULUS_INJECT PCR1_activity
…
STIMULUS_INJECT PCR14_activity

%-- PF ongoing activity --%

STIMULUS_INJECT PF_LEFT2_E1_activity
…
STIMULUS_INJECT PF_LEFT2_E13_activity

STIMULUS_INJECT PF_LEFT4_E1_activity
…
STIMULUS_INJECT PF_LEFT4_E13_activity

STIMULUS_INJECT PF_LEFT6_E1_activity
…
STIMULUS_INJECT PF_LEFT6_E13_activity

STIMULUS_INJECT PF_RIGHT1_E1_activity
…
STIMULUS_INJECT PF_RIGHT1_E13_activity

STIMULUS_INJECT PF_RIGHT3_E1_activity
…
STIMULUS_INJECT PF_RIGHT3_E13_activity
```

```
STIMULUS_INJECT PF_RIGHT5_E1_activity
…
STIMULUS_INJECT PF_RIGHT5_E13_activity

################################## REPORTS ################################

%-- Reports can be obtained on any cell or group of cells used in the model --%
Please see Appendix A for an example

################################## CONNECTIONS ############################

%-- Many connections were used between each column and/or cell group --%
Please see Appendix A for an example
Please see Table 4.1 and 4.2

END_BRAIN

################################## INCLUDE FILES ##########################

%-- ANATOMY --%

INCLUDE ./input/INCLUDE_ANATOMY_PCRAIN.inc
INCLUDE ./input/INCLUDE_ANATOMY_VL.inc
INCLUDE ./input/INCLUDE_ANATOMY_RAIN_ahp_HP.inc
INCLUDE ./input/INCLUDE_ANATOMY_RAIN2_HP.inc
INCLUDE ./input/INCLUDE_ANATOMY_RAIN_ahp_PF.inc
INCLUDE ./input/INCLUDE_ANATOMY_RAIN2_PF.inc
INCLUDE ./input/INCLUDE_ANATOMY_PF_LEFT2.inc
INCLUDE ./input/INCLUDE_ANATOMY_PF_LEFT4.inc
INCLUDE ./input/INCLUDE_ANATOMY_PF_LEFT6.inc
INCLUDE ./input/INCLUDE_ANATOMY_PF_RIGHT1.inc
INCLUDE ./input/INCLUDE_ANATOMY_PF_RIGHT3.inc
INCLUDE ./input/INCLUDE_ANATOMY_PF_RIGHT5.inc
INCLUDE ./input/INCLUDE_ANATOMY_SUB_LEFT.inc
INCLUDE ./input/INCLUDE_ANATOMY_SUB_RIGHT.inc
INCLUDE ./input/INCLUDE_ANATOMY_PM.inc

%-- STIMULUS --%

INCLUDE ./input/INCLUDE_STIMULUS_PCRAIN.inc
INCLUDE ./input/INCLUDE_STIMULUS_VL.inc
INCLUDE ./input/INCLUDE_STIMULUS_GCsupp.inc
```

```
INCLUDE ./input/INCLUDE_STIMULUS_PFsupp.inc
INCLUDE ./input/INCLUDE_STIMULUS_PCR_Random.inc
INCLUDE ./input/INCLUDE_STIMULUS_OLM.inc
INCLUDE ./input/INCLUDE_STIMULUS_RAIN_ahp_HP.inc
INCLUDE ./input/INCLUDE_STIMULUS_RAIN2_HP.inc
INCLUDE ./input/INCLUDE_STIMULUS_RAIN_ahp_PF.inc
INCLUDE ./input/INCLUDE_STIMULUS_RAIN2_PF.inc
INCLUDE ./input/INCLUDE_STIMULUS_activity_PCR_PF.inc
INCLUDE ./input/INCLUDE_STIMULUS_SUB.inc

%-- SYNAPSES --%

INCLUDE ./input/INCLUDE_SYNAPSES_PCRAIN.inc
INCLUDE ./input/INCLUDE_SYNAPSES_OLM.inc
INCLUDE ./input/INCLUDE_SYNAPSES_VL_PC.inc
INCLUDE ./input/INCLUDE_SYNAPSES_RAIN_ahp_HP_PF.inc
INCLUDE ./input/INCLUDE_SYNAPSES_RAIN2_HP_PF.inc
INCLUDE ./input/INCLUDE_SYNAPSES_RAIN_ahp_HP_PCRAIN.inc
INCLUDE ./input/INCLUDE_SYNAPSES_RAIN_ahp_PF_PF.inc
INCLUDE ./input/INCLUDE_SYNAPSES_RAIN_ahp_HP_SUB.inc
INCLUDE ./input/INCLUDE_SYNAPSES_HP_PF_ahp.inc
INCLUDE ./input/INCLUDE_SYNAPSES_PF.inc
INCLUDE ./input/INCLUDE_SYNAPSES_PCR_PF.inc
INCLUDE ./input/INCLUDE_SYNAPSES_SUB.inc
INCLUDE ./input/INCLUDE_SYNAPSES_PF_SUB.inc
INCLUDE ./input/INCLUDE_SYNAPSES_PCR_SUB.inc
INCLUDE ./input/INCLUDE_SYNAPSES_SUB_PM.inc
INCLUDE ./input/INCLUDE_SYNAPSES_probe.inc

%-- REPORTS --%

INCLUDE ./input/INCLUDE_REPORTS_VOLTAGES_PCRAIN.inc
INCLUDE ./input/INCLUDE_REPORTS_VL.inc
INCLUDE ./input/INCLUDE_REPORTS_OLM.inc
INCLUDE ./input/INCLUDE_REPORTS_USE_PCRAIN.inc
INCLUDE ./input/INCLUDE_REPORTS_USE_PF.inc
INCLUDE ./input/INCLUDE_REPORTS_VOLTAGES_RAIN_ahp_HP.inc
INCLUDE ./input/INCLUDE_REPORTS_VOLTAGES_RAIN2_HP.inc
INCLUDE ./input/INCLUDE_REPORTS_VOLTAGES_RAIN_ahp_PF.inc
INCLUDE ./input/INCLUDE_REPORTS_VOLTAGES_RAIN2_PF.inc
INCLUDE ./input/INCLUDE_REPORTS_VOLTAGES_PF.inc
INCLUDE ./input/INCLUDE_REPORTS_VOLTAGES_PM.inc
INCLUDE ./input/INCLUDE_REPORTS_SUB.inc
INCLUDE ./input/INCLUDE_REPORTS_VOLTAGE_probe.inc
```

APPENDIX C: INCLUDE FILES

%-- ANATOMY --% (Example of premotor cell group anatomy)

```
#########################
## Define Column Shells
#########################

COLUMN_SHELL
   TYPE                columnshell_PM
   WIDTH               300
   HEIGHT              800
END_COLUMN_SHELL

#########################
## Define Columns
#########################

COLUMN
        TYPE            PM_LEFT_COLUMN
        COLUMN_SHELL    columnshell_PM
        LAYER_TYPE      layershell_PM_LEFT
END_COLUMN

COLUMN
        TYPE            PM_RIGHT_COLUMN
        COLUMN_SHELL    columnshell_PM
        LAYER_TYPE      layershell_PM_RIGHT
END_COLUMN

#########################
## Define Layer Shells
#########################

LAYER_SHELL
        TYPE            layershell_PM_LEFT
        UPPER           100
        LOWER           0
END_LAYER_SHELL

LAYER_SHELL
        TYPE            layershell_PM_RIGHT
        UPPER           100
        LOWER           0
END_LAYER_SHELL
```

```
#########################
## Define Layers
#########################

LAYER
        TYPE                layer_PM_LEFT
        LAYER_SHELL         layershell_PM_LEFT
        CELL_TYPE           LEFT_E_PM           100
END_LAYER

LAYER
        TYPE                layer_PM_RIGHT
        LAYER_SHELL         layershell_PM_RIGHT
        CELL_TYPE           RIGHT_E_PM          100
END_LAYER

#########################
## Define Cells
#########################

CELL
        TYPE                LEFT_E_PM
        COMPARTMENT         soma_exc_PM     soma_E_PM     0  0        0
END_CELL

CELL
        TYPE                RIGHT_E_PM
        COMPARTMENT         soma_exc_PM     soma_E_PM     0  0        0
END_CELL

#########################
## Define Compartments
#########################

COMPARTMENT
   TYPE                     soma_exc_PM
   SPIKESHAPE               spikeshape_1k_default
   TAU_MEMBRANE             0.020           0.0
   R_MEMBRANE               200             0
   THRESHOLD                -50             0
   VMREST                   -60    0
END_COMPARTMENT
```

```
%-- STIMULUS --% (Example of subiculum stimulus)

STIMULUS_INJECT
   TYPE                 SUB_LEFT2
   STIM_TYPE            realstim_SUB_LEFT2
   INJECT               SUB_LEFT_COLUMN
                        layer_SUB_LEFT
                        SUB_LEFT_E_SB
                        somaE          0.50
END_STIMULUS_INJECT

STIMULUS
        TYPE            realstim_SUB_LEFT2
        MODE            CURRENT
        PATTERN         PULSE
        TIME_INCREMENT  0.01
        FREQ_COLS       100
        CELLS_PER_FREQ  1
        DYN_RANGE       0       400
        TIMING          EXACT
        SAMESEED        NO
        AMP_START       2
        WIDTH           0.001
        TIME_START      .5
        TIME_END        1
END_STIMULUS

%-- SYNAPSES --% (Example of subiculum synapses)

SYNAPSE
   TYPE                 synIE_SUB
   SFD_LABEL            NO_SFD
   LEARN_LABEL          NO_LEARN
   SYN_PSG              PSGinhib
   MAX_CONDUCT          0.008   0.0
   DELAY                0.001  0.005
   SYN_REVERSAL         -80    0
   ABSOLUTE_USE         0.5    0.05
END_SYNAPSE

SYNAPSE
   TYPE                 synEI_SUB
   SFD_LABEL            NO_SFD
   LEARN_LABEL          NO_LEARN
   SYN_PSG              PSGexcit
```

```
   MAX_CONDUCT          0.006  0.0
   DELAY                0.005  0.01
   ABSOLUTE_USE         0.25    0.1
END_SYNAPSE

SYNAPSE
   TYPE                 synEE_SUB
   SFD_LABEL            NO_SFD
   LEARN_LABEL          NO_LEARN
   SYN_PSG              PSGexcit
   MAX_CONDUCT          0.006  0.0
   DELAY                0.005  0.01
   ABSOLUTE_USE         0.25    0.1
END_SYNAPSE

%-- REPORTS --% (Example of premotor cell group reports)

REPORT
   TYPE                 LEFT_PM_VOLTAGE_E
   CELLS                PM_LEFT_COLUMN
                        layer_PM_LEFT
                        LEFT_E_PM
                        soma_E_PM
   PROB                 0.3
   REPORT_ON            VOLTAGE
   FILENAME             LEFT_PM_VOLTAGE_E.txt
   FREQUENCY            1
   TIME_START           0
   TIME_END             100
END_REPORT

REPORT
   TYPE                 RIGHT_PM_VOLTAGE_E
   CELLS                PM_RIGHT_COLUMN
                        layer_PM_RIGHT
                        RIGHT_E_PM
                        soma_E_PM
   PROB                 0.3
   REPORT_ON            VOLTAGE
   FILENAME             RIGHT_PM_VOLTAGE_E.txt
   FREQUENCY            1
   TIME_START           0
   TIME_END             100
END_REPORT
```